THE UNIVERSITY OF CHICAGO

THE ROLE OF CUX1 IN THERAPY-RELATED MYELOID NEOPLASMS

A DISSERTATION SUBMITTED TO

THE FACULTY OF THE DIVISION OF THE BIOLOGICAL SCIENCES

AND THE PRITZKER SCHOOL OF MEDICINE

IN CANDIDACY FOR THE DEGREE OF

DOCTOR OF PHILOSOPHY

INTERDISCIPLINARY SCIENTIST TRAINING PROGRAM: CANCER BIOLOGY

BY

MOLLY KATHLEEN IMGRUET

CHICAGO, ILLINOIS

DECEMBER 2020

Copyright © 2020 by Molly Kathleen Imgruet

All rights reserved

This thesis is dedicated to my family, Joe Imgruet, Katie Imgruet, Megan Imgruet and Curtis Eisen

TABLE OF CONTENTS

LIST OF FIGURES ..... **v**

LIST OF TABLES ..... **vii**

ACKNOWLEDGEMENTS ..... **viii**

ABSTRACT ..... **xii**

INTRODUCTION **1**

Therapy-related myeloid neoplasms 1
Clonal Hematopoiesis 5
-7/del(7q) and myeloid neoplasms 7
CUX1 in hematopoiesis 10
DNA damage response in hematopoietic cells 14
Epigenetic regulation of DNA damage repair 20
Aims of this thesis: Critical gaps in knowledge that will be addressed 24

MATERIALS AND METHODS **27**

RESULTS: THE ROLE OF CUX1 IN THERAPY-RELATED MYELOID NEOPLAMS **42**

Introduction 42
CUX1 loss impairs EHMT2 recruitment to DNA breaks and disrupts DNA damage-induced histone methylation 45
CUX1 is necessary for DNA repair and foci formation 52
CUX1-deficient cells upregulate expression of genes involved in proliferation and DNA repair 63
$Cux1^{low}$ cells aberrantly proliferate and expand following DNA-damaging alkylating agents 66
CUX1-deficient mice develop therapy-related myeloid neoplasms after alkylator chemotherapy exposure 67
Discussion 81

DISCUSSION **88**

Overview 88
CUX1 plays a non-transcriptional role in the local DNA damage response 89
CUX1 promotes H3K9 and H3K27 methylation 93
CUX1-deficient clones expand following cytotoxic therapy 95
CHIP in non-hematopoietic tissues 97
CUX1 loss predisposes mice to t-MN 99
Conclusions 103
Future Directions 104

REFERENCES **107**

LIST OF FIGURES

Figure 1. CUX1 rapidly colocalizes to DSBs following irradiation. 47

Figure 2. CUX1 promotes EHMT2 recruitment to DSBs. 49

Figure 3. CUX1 promotes H3K27 and H3K9 methylation following IR. 53

Figure 4. Methyltransferase and demethylase transcript levels are not decreased in CUX1-deficient cells. 56

Figure 5. CUX1 knockdown leads to reduced H3K9 methylation at foci. 57

Figure 6. CUX1 loss inhibits H3K27 methylation at foci. 58

Figure 7. CUX1 loss impairs DNA damage recognition and foci formation 61

Figure 8. CUX1-deficient HSPCs have an impaired DDR and unrepaired DNA damage *in vivo*. 64

Figure 9. CUX1-deficient cells upregulate expression of genes involved in proliferation and DNA repair 68

Figure 10. CUX1 does not transcriptionally regulate H3K27 methyltransferases and demethylases in murine HSCs. 69

Figure 11. CUX1-deficient human K562 cells aberrantly proliferate following irradiation. 70

Figure 12. $Cux1^{low}$ cells aberrantly proliferate and expand following DNA-damaging alkylating agents 71

Figure 13. CUX1-deficient cells aberrantly proliferate following alkylator chemotherapy. 73

Figure 14. CUX1 deficiency prior to chemotherapy predisposes mice to t-MN 76

Figure 15. CUX1 deficiency leads to an expansion of myeloid cells.....77
Figure 16. CUX1-deficient mice develop t-MN after alkylator chemotherapy. 78
Figure 17. CUX1-deficient mice develop erythroleukemia following alkylator chemotherapy.....79
Figure 18. Erythroblasts infiltrate non-hematopoietic tissues in CUX1-deficient mice following alkylator chemotherapy. 80
Figure 19. Model for CUX1 loss in therapy-related myeloid neoplasms 86

LIST OF TABLES

Table 1. ChIP-seq and RNA-seq Sequencing Reads Table 55

ACKNOWLEDGEMENTS

This work would not have been possible without the support, encouragement and patience of my family, friends, lab members and my incredible mentor, Dr. Megan McNerney. Dr. McNerney has been a part of my journey since my first days at the University of Chicago, when she interviewed me for admission to the MSTP. Her passion for science, incredible knowledge of the field and true dedication to mentorship made my experience in graduate school an incredibly positive one. I have never had a mentor give more prompt and helpful feedback on presentations, grant proposals and abstracts. She takes the time to carefully read everything that I send to her, and I have drastically improved my scientific writing and presentation skills with her guidance. Dr. McNerney has been an exemplary role model as a mentor and a scientist, and I learned so much through our weekly meetings. Dr. McNerney is truly committed to advancing the careers and well-being of all of the students she works with, whether they are members of her lab, students in her classes or graduate trainees in the Committee on Cancer Biology, and I truly could not have accomplished any of this work without her steadfast guidance. It was an honor to be your first graduate student.

The entire McNerney Lab has been such a joy to work with, and I would like to personally thank Dr. Ningfei An, Saira Khan, Stephanie Konecki, Dr. Jeff Kurkewich, Manisha Krishnan, Weihan Liu, Julian Lutze, Dr. Jeremy Baeten, Bonnie Hu, Matt Jotte, Lia Jueng, Henna Nam, Isabelle Preddy, Dhivyaa Anandan and Madhavi Senagolage for being such wonderful teammates and always being willing to help with experiments, chat about project ideas and walk to the food trucks. I will forever be indebted to Ningfei and Saira for training me, and it has been so fun seeing the lab grow from the three of

us to fourteen lab members. Bonnie made invaluable contributions to the data presented here, and over the past two years it has been incredible to see her pick up techniques and skills that put her on a par with graduate students. I could not have completed the project without her. During my last year of graduate school, I had the pleasure of partnering with Julian to accomplish the DNA damage repair imaging, and I am so thankful for his effort and collaboration. Dhivyaa Anandan and Isabelle Preddy were always willing to go above and beyond to help with mouse work, genomics experiments and peppermint mocha preparation. To my fellow graduate students, Manisha, Stephanie, Weihan and Matt, thank you so much for always being willing to chat about experiments and life and for telling me when our program meetings were happening. Jeff, Madhavi and Jeremy provided such great mentorship and advice throughout these past four years. Thank you for always being willing to read my first drafts.

I would especially like to thank the members of my thesis committee for their time, patience and incredibly helpful contributions to my project. Dr. Ivan Moskowitz, Dr. Michelle Le Beau and Dr. Amittha Wickrema are all extraordinary scientists, and I was honored to benefit from their expertise. Their unique perspectives helped shape the direction of this project and challenged me to think about these scientific questions in new ways. All of their labs were also very helpful in providing advice on experimental design, with a special thanks to Dr. Rajiv Nadadur, Dr. Alex Guzzetta, Dr. Sriram Sundaravel, Dr. Angela Stoddart and Anthony Fernald.

Several collaborations were vital to the success of this project. First, I would like to thank Dr. Michelle Le Beau, Dr. Angela Stoddart and the entire Le Beau lab for their

thoughtful comments and insightful discussions of my project and presentations these past four years. Much of the growth that I experienced in professional presentation and as a scientist began in those meetings. I would like to thank Dr. Stephen Kron and the Kron lab for all of their guidance in entering the world of DNA damage repair, your knowledge and technical expertise were essential and much appreciated. I would like to thank Claudia Wing and Eileen Dolan's lab for their help in guidance in developing our experimental setup for cisplatin treatment and their advice on studying drug resistance. Stephen Arnovitz was very helpful in discussing techniques related to studying therapy-related myeloid neoplasms, antibody panels and DNA damage repair, and thank you for taking the time to answer my many questions. I would like to thank Mandel Davis, Robert "Bert" Ladd, David Leclerc, and Mike Olsen for their assistance in cell sorting. I would also like to thank the incredible members of the Animal Resources Center, Genomics Core Facility and Integrated Light Microscopy Core for all of their help in training and gathering data for this project.

It has been an honor to be a part of the University of Chicago Medical Scientist Training Program, and I would like to thank you all for letting me in five years ago. I would especially like to thank Dr. Marcus Clark, Dr. Kristin McCann, Dr. Lucia Rothman-Denes, Marisa Davis, Hafsah Mohammed, Dr. Alison Anastasio, Sarah Blum and Shay McAllister. I would also like to thank the entire Committee on Cancer Biology, especially Dr. Kay Macleod and Laura Negrete. I would also like to thank my fellow cohort members and friends, Reem Elorbany, Will Wagstaff, Zaina Zayaad, Christine Miller, Wenli Dai, Dustin Shaw, Michael Okoreeh and John Coukos. I couldn't imagine a better group to spend eight years with.

I have been blessed to have such wonderful friends to share the highs and lows of graduate school with, and I truly cannot thank you enough for being by my side these past four years. To Elise Bicek, Tess Madden, Danielle Rankovich, Jaclyn Pavilonis, Mike Gilbert, Emily Skarda, Cori Walker, Alicia Cañas, Claire Dugan, Sarah Peters Lorraine Mascarenhas, Colleen Clarke and Paige Szymanski, thank you for being such wonderful people and making my life so fun.

None of this could have been possible without my amazing, loving and caring family. To my mom and dad, Katie and Joe Imgruet, thank you so much for always supporting my dreams and being the best parents. I wouldn't have made it to medical school without you. To my sister, Megan, thank you for being the best little sister and my best friend and always making sure I don't forget to have some fun. I am so honored to be joining the Eisen family after this pandemic is over, and I would like to thank Rita, Gary, Hannah, Jay, Ian, Sarah, Conrad and Rachel for being so kind and welcoming me to the Eisen family. Being a part of a big extended family shaped my childhood and who I am today, and I would like to thank the Harper family, the Boers family, the Imgruet family, the Brown family, the Mysz family, the Rosenbaum family, the Jacksonville Walshes, the Tampa Walshes and the Denver Walshes for all of their love. I'm so happy to be a part of your family. Finally, I would like to thank my incredible grandparents, Grandpa Lou, Grandma Mary Kay, Grandma Rita and Grandpa Joe for being wonderful role models and building such loving families.

Finally, I would like to thank my partner and fiancé, Curtis Eisen. Your love and support has made this all possible and made my journey through graduate school such a joy.

ABSTRACT

Therapy-related myeloid neoplasms (t-MN) are high-risk, late effects in cancer survivors with poorly understood pathogenesis. It has been postulated that, in some cases, hematopoietic stem and progenitor cells (HSPCs) harboring mutations are selected for by cytotoxic exposures and transform. Here, we evaluate this model in the context of deficiency of CUX1, a transcription factor encoded on chromosome 7q and deleted in half of t-MN cases. We report that CUX1 has a critical, early role in the DNA repair process in HSPCs. Mechanistically, CUX1 recruits the histone methyltransferase EHMT2 to DNA breaks to promote downstream H3K9 and H3K27 methylation, phospho-ATM retention, subsequent γH2AX foci formation and propagation and, ultimately, 53BP1 recruitment. Despite significant unrepaired DNA damage sustained in CUX1-deficient murine HSPCs after cytotoxic exposures, they continue to proliferate and expand, mimicking clonal hematopoiesis in patients post-chemotherapy. As a consequence, preexisting CUX1 deficiency predisposes mice to highly penetrant and rapidly fatal therapy-related erythroleukemias. These findings establish the importance of epigenetic regulation of HSPC DNA repair and position CUX1 as a gatekeeper in myeloid transformation.

INTRODUCTION

Therapy-related myeloid neoplasms

A serious side effect of the chemotherapy and radiation therapy used to treat cancer is the development of therapy-related myeloid neoplasms (t-MN). t-MN are blood cancers that arise in myeloid lineage cells, and the classification includes acute myeloid leukemia (AML), myelodysplastic syndrome (MDS), and myelodysplastic syndrome/myeloproliferative neoplasms (MDS/MPN) that occur after cytotoxic therapy for a malignant or non-malignant primary condition. Although the development of t-MN is rare, occurring in 0.62 per 100,000 men and women, this comprises approximately 10-20% of newly-diagnosed AML/MDS[1,2], and the incidence is expected to rise as the efficacy of cancer treatments improves and the number of cancer survivors continues to rise[3]. The median survival for t-MN is poor, at just 14.6 months[4,5]. A high-risk karyotype, chemoresistance and comorbidities are found more often in t-MN than *de novo* AML patients, all of which contribute to this poor prognosis[4,5].

The primary tumor type and the type of therapy used to treat the tumor both affect t-MN risk. The most common primary cancers preceding t-MN are breast cancer and hematologic malignancies[6–9]. Topoisomerase II inhibitors and alkylating agents are especially linked to the development of t-MN, and these two cytotoxic therapies are associated with two distinct t-MN subtypes. Topoisomerase II inhibitors, which function by inducing DNA double-strand breaks (DSBs) during DNA replication, are associated with a short latency to disease after therapy (less than two years), overt leukemia and balanced chromosomal translocations, often involving the KMT2A/MLL gene on 11q23[10]. Patients treated with alkylating agents form the second, and most common,

subtype of t-MN. Alkylating agents function as a chemotherapeutic agent by transferring an alkyl group to the DNA, which then often leads to single- and double-strand DNA breaks[11,12]. t-MN following treatment with alkylating agents typically arises 4-7 years after therapy[13] and is associated with the partial loss of chromosome 5 [del(5q)] and/or the loss of all or part of chromosome [-7/del(7q)]. Approximately 70% of t-MN patients present with this subtype[9].

A pressing problem in the field has been determining what differentiates the subset of patients that develop a t-MN after cytotoxic therapy. Previously, it was thought that the DNA damage sustained during chemotherapy and irradiation led to a large number of somatic mutations, and that these mutations drove the pathogenesis of t-MN[14]. However, whole genome sequencing of t-MN and *de novo* AML patients revealed that t-MN patients do not carry a greater number of acquired mutations[14,15]. Furthermore, the percentage of transversion-type mutations, a signature of chemotherapy, was not increased in t-MN compared to *de novo* AML[14]. Thus, therapy-induced mutations, although they may contribute to pathogenesis, do not appear to be the primary driver of t-MN development. Several additional factors have recently been proposed to contribute to the development of t-MN, including inherited risk, clonal selection of hematopoietic stem and progenitor cells (HSPCs) with mutations conferring a fitness advantage, and a dysfunctional bone marrow niche. These factors, possibly in combination with a small number of mutations induced by cytotoxic therapy, could lead to t-MN in certain patients.

Up to 21% of cancer survivors that develop a t-MN have been reported to have one or more inherited germline mutations associated with increased cancer

suceptibility[16–18]. Germline mutations in DNA damage response (DDR) genes, including *BRCA1/2*, *TP53* and Fanconi anemia genes, are particularly enriched in t-MN patients[16–18]. It is likely that the percentage of patients with an inherited risk for t-MN will increase as more candidate susceptibility genes are identified, and as more widespread sequencing is done in these patients.

In addition to germline mutations, it has also been appreciated the past 10 years that patients may harbor HSPCs with somatic mutations prior to cytotoxic therapy. While most somatic mutations are inconsequential, certain mutations may confer elevated risk for t-MN. Healthy individuals have been found to have clonal expansions of HSPCs with somatic mutations in their blood, termed clonal hematopoiesis of indeterminate potential (CHIP)[19–22]. Individuals with CHIP have up to 10 times greater risk of developing a hematologic malignancy than individuals without CHIP[19,23]. CHIP preceding cytotoxic therapy has also been linked to an increased risk of developing t-MN[14]. This leads to a model in which patients with CHIP prior to chemotherapy may develop t-MN after clones with a fitness advantage are selected for under the pressure of chemotherapy. Wong *et. al.* showed that in two t-MN patients, the same TP53 mutations found in the t-MN were present as CHIP mutations prior to chemotherapy[14]. CHIP presents a promising field of inquiry in determining individual t-MN risk for patients, and the field is discussed in more detail in the next section.

The bone marrow microenvironment has been appreciated to play a significant role in malignant myeloid transformation[24–27]. Damage to the niche may precede chemotherapy—induced by aging, inflammation or inherited genetic changes—or may be directly caused by cytotoxic therapy. Aging-associated senescence of mesenchymal

stromal cells has been linked to inflammation and cancer progression[28]. Genetic perturbations in mesenchymal stem cells and their progeny, including osteoblasts, have also been linked to malignant transformation. For example, increased WNT signaling in the niche has been reported in murine and human myeloid neoplasms, and has been reported to drive leukemogenesis[24,27]. Recently, Stoddart *et. al.* demonstrated that chemotherapy not only impacts HSPC survival and expansion, but also directly impacts the bone marrow microenvironment. Exposing mesenchymal stromal cells to an alkylating agent increased the incidence of myeloid disease compared to exposing only HSPCs, and this was found to be due to senescence of the mesenchymal stromal cells establishing a chronic inflammatory state[29]. Cytotoxic therapy is also known to induce release of inflammatory cytokines and inflammation, and inflammation of the bone marrow niche alone has been shown to induce myeloid transformation[30].

It is likely that these factors—therapy-induced mutations, inherited risk, CHIP and an altered bone marrow microenvironment—interact in complex ways that set the stage for t-MN. For example, inflammation has been linked to CHIP[31], and HSPCs with somatic or inherited mutations (i.e. in TP53) have been shown to directly compete with wildtype counterparts by altering expression of genes involved in HSPC-niche signaling[32]. Crosstalk between mesenchymal stem cells and hematopoietic cells is crucial for both initiating and sustaining transformation to malignant disease[25]. Mutations in DNA damage repair genes have been observed in inherited t-MN risk[16], CHIP after cytotoxic therapy[33] and therapy-induced mutations[29]. These studies and others have helped to shift the field from seeing t-MN as solely a consequence of therapy-induced mutations to a complex disease arising from a convergence of cell-intrinsic and extrinsic

factors. Understanding these factors will allow for the prevention and treatment of this devastating side effect of cancer treatment.

Clonal Hematopoiesis

Over time, the process of aging and prolonged exposure to environmental mutagens leads to somatic mutations in stem cells[34]. With age, somatic mutations can be detected in almost all tissue types[35]. Although most mutations will not significantly impact stem cell function, certain mutations can give cells a fitness advantage that allows them to clonally expand. In fact, the clonal expansion of hematopoietic stem cells (HSCs) with a somatic mutation can be detected in up to 95% of healthy adults by age 60[36]. Clonal hematopoiesis with a mutation specifically in a cancer-associated gene at a variant allele frequency greater than 2% in an otherwise healthy individual has been termed clonal hematopoiesis of indeterminate potential, or CHIP, and it is associated with approximately 10-fold increased relative risk of developing malignancy[14,37–40].

Clonal hematopoiesis in patients without cancer was first reported following the observation of non-random X-chromosome inactivation. During female embryonic development, one X chromosome is randomly inactivated in each cell, leading to roughly half the cells in the body inactivating one allele, and half the other allele. The observation that in the blood of some women one allele was inactivated at a proportion greater than 50% pointed to the clonal expansion of certain HSCs[41]. Fifteen years after this first observation of clonal hematopoiesis, mutations in cancer-associated genes were detected in clonally expanded hematopoietic populations in healthy individuals, and it was presumed that these mutations were driving clonal hematopoiesis. In the

past ten years, large exome sequencing studies have determined that CHIP is common in healthy individuals with aging. Furthermore, certain mutational patterns were identified. Epigenetic regulators, including *DNTM3A*, *TET2* and *ASXL1,* are frequently mutated in CHIP. Mutations in genes involved in growth signaling, the DNA damage response and splicing were also commonly found[38–40]. In addition to base substitutions, insertions and deletions, large structural variations in chromosomes have also been detected in clonal hematopoiesis and increase in frequency with age[22,42,43]. It is likely that additional, as yet unreported mutations also drive clonal hematopoiesis, including mutations in noncoding regions.

The mechanisms of clonal expansion in CHIP are largely unknown. It is also unclear which CHIP genes will confer the greatest risk of transformation. However, some patterns have emerged. Mutations in *DNMT3A* and *TET2*, while frequent in CHIP[40,44,45], are less likely to progress to AML than clones with mutations in in splicing factors or clones with mutations in multiple genes[46]. While mouse models demonstrate increased self-renewal and a competitive advantage for HSCs with loss-of-function mutations in *Dnmt3a* and *Tet2*, the mechanism for this clonal advantage is unclear[44,47]. Mutations in genes encoding splicing factors, including *Sf3b1* and *U2af1* do not provide a competitive advantage to HSCs in mice*,* unlike in humans, making *in vivo* studies of mechanism difficult. Some models of clonal expansion have pointed to inflammation as both a cause and effect of CHIP. CHIP in *Tet2*-mutant mice is promoted by an inflammatory milieu driven by disruption of the small intestinal barrier and resulting IL-6 production[31]. Intriguingly, mutations in *TET2* and *DNMT3A* have also been shown to promote inflammation by increasing the inflammatory response of macrophages and

mast cells[48–50]. These extrahematopoietic effects of CHIP are associated with an increased risk of coronary heart disease and accelerated atherosclerosis[51,52].

CHIP at the time of cytotoxic therapy for cancer and non-malignant conditions has been linked to an increased risk of developing t-MN[53–56]. Clones with mutations in DDR genes have been shown to preferentially expand following therapy[33,56]. Mutations in two DDR genes, *Tp53* and a regulator of *Tp53*, *Ppm1d,* were shown to provide HSCs with a clonal advantage following chemotherapy by allowing cells to cycle despite the presence of unrepaired DNA damage, although it remains unclear whether PPM1D mutations drive transformation to t-MN after chemotherapy[57,58]. In addition to mutations, copy number alterations have been found in CHIP preceding chemotherapy and t-MN, including -7/del(7q) in rare cases, which is found in half of all t-MN[9,19,22,55]. Understanding the clonal advantage provided by these mutations will prove crucial in understanding patient risk for hematologic malignancies, and early evidence suggests that an altered DNA damage response plays an important role in CHIP and malignancy.

-7/del(7q) and myeloid neoplasms

Chromosomal abnormalities are a frequent occurrence in cancer cells. The first chromosomal translocation associated with the pathogenesis of cancer was identified in hematopoietic cells[59], and chromosomal duplications, deletions and translocations have frequently been reported in hematopoietic malignancies in the time since. Loss of all or part of chromosome 7 frequently occurs in a range of myeloid disorders and is the most common high-risk cytogenetic abnormality[60]. -7/del(7q) occurs in bone marrow failure, pediatric and adult myelodysplastic syndrome (MDS), aplastic anemia and AML[61–66]. It

is especially prevalent in myeloid neoplasms in the elderly[67] and t-MN, where it is found in a striking 49% of patients[9]. Unfortunately, this cytogenetic abnormality is associated with a poor response to treatment and a poor prognosis[66].

Although -7/del(7q) was first observed as a frequent cytogenetic abnormality in AML almost 50 years ago[68], it remains unclear which lost genes are responsible for driving the pathogenesis of -7/del(7q) disease. Early models suggested that both copies of a tumor suppressor gene must be lost in order to see disease initiation[69]. However, many tumor suppressor genes are now thought to be haploinsufficient[70,71], in that the loss of one copy of a gene, whether through mutation or chromosomal loss, is sufficient to drive disease. With the exception of *EZH2*[72,73], a "second hit" mutation is not recurrently seen in cases of -7/del(7q), suggesting that the crucial tumor suppressor gene(s) encoded on chromosome 7 are haploinsufficient. Furthermore, it is likely that the loss of multiple neighboring genes results in a combinatorial effect, in the form of a contiguous gene sydrome[74,75]. In this case, decreased expression of multiple genes in combination would be more pathogenic than the loss of a single gene within the segment. This is the case in another common cytogenetic abnormality in myeloid neoplasms, del(5q). Haploinsufficiency of both *Apc* and *Egr1*, encoded on 5q, is necessary to induce myeloid neoplasms in mice with reduced Trp53. Extensive research has gone into determining which genes on del(7q) play a similar role in a potential contiguous gene syndrome and in determining the pathogenesis of -7/del(7q) myeloid neoplasia.

Several groups have mapped the commonly deleted segments on 7q to uncover potential tumor suppressor genes. To date, three commonly deleted regions have been

reported: 7q35-36, 7q34 and 7q22[76–79]. Several candidate tumor suppressor genes are encoded in these regions. The 7q35-36 locus contains the haploinsufficient tumor suppressor gene *KMT2C* (also known as *MLL3*), an H3K4 methyltransferase that cooperates with reduction of *Trp53* and *Nf1* in the haploinsufficient state to accelerate leukemogenesis in mice. However, loss of *KMT2C* alone does not accelerate myeloid disease[80]. *EZH2*, localized at 7q36.1, encodes an H3K27 methyltransferase. EZH2 is a component of the Polycomb Repressive Complex 2 (PRC2) that is mutated in myeloid malignancies[73]. Loss of *Ezh2* accelerates MDS in *Runx1*-mutant mouse models[81], but loss of *Ezh2* alone does not lead to myeloid malignancies in mice[82]. *CUL1*, a core member of E3 ubiquitin ligase complex, is also contained in the MDR, at 7q36.1, and is mutated in myeloid neoplasms[83–85]. The 7q34 locus contains *LUC7L2* (LUC7 like 2), a pre-mRNA splicing factor component[85]. This is of potential interest, as splicing factor mutations are observed in more than 50% of MDS cases[86]. The 7q22 MDR contains *CUX1*, a homeobox-containing transcription factor with strong evidence supporting its role as a haploinsufficient tumor suppressor gene, which will be explored in greater detail in the next section. With monosomy 7 or large deletions of 7q, additional putative tumor suppressor genes are lost, including *SAMD9L* at 7q21.2, *KTM2E* at 7q22.3 and *DOCK4* at 7q31.1. Samd9L function has not been fully characterized, although it is potentially involved in cytokine receptor endocytosis and recycling. *Samd9L* homozygous and heterozygous knockout mice develop MDS with bone marrow failure and dysplasia[87]. Loss of *Kmt2e* (*Mll5*) results in dysfunctional hematopoiesis, however mice do not develop overt myeloid disease[88–90]. Finally, *DOCK4,* which encodes a guanine exchange factor, has been found to be disrupted in AML, MDS and cancer cell

lines[85,91,92]. Among these putative 7q tumor suppressor genes, *EZH2*, *CUX1* and *LUC7L2* mutations are associated with shorter survival. Low expression of *EZH2*, *CUX1* and *LUC7L2* is also associated with significantly shorter survival[85]. Intriguingly, these three mutations are not mutually exclusive, suggesting that they may cooperate, similar to the effect of -7 or long deletions of 7q[85]. In further support of contiguous gene syndrome on 7q, heterozygous deletion of a 2 Mb interval on 7q led to features of MDS in mice[75]. In summary, the pathogenesis of -7/del(7q) in myeloid neoplasms, and the relative importance of the loss of individual tumor suppressor genes remains to be elucidated.

CUX1 in hematopoiesis

CUX1 is a non-clustered HOX family transcription factor that is ubiquitously expressed and highly conserved, from *Drosophila* to humans. The full-length p200 CUX1 protein has one homeodomain and three CUT repeat DNA-binding domains[93]. CUX1 is encoded on chromosome 7q22.1, and it is frequently inactivated in myeloid neoplasms, through both -7/del(7q) and loss-of-function mutations[79]. McNerney *et. al.* performed transcriptome sequencing and SNP array analysis on *de novo* and therapy-related myeloid neoplasms with and without -7/del(7q) and identified a commonly deleted segment on 7q containing *CUX1.* Furthermore, they found that *CUX1* expression was the most significantly decreased among the genes encoded on the commonly deleted segment. They further showed that haploinsufficiency of the *CUX1* ortholog in *Drosophila, cut,* led to hemocyte overgrowth and tumor formation. Haploinsufficiency of *CUX1* in human hematopoietic cells led to a significant

engraftment advantage in xenograft models[79]. This breakthrough in identifying *CUX1* as haploinsufficient tumor suppressor gene sparked extensive work characterizing the molecular function of CUX1 in hematopoiesis.

CUX1 displays distinct genomic binding features in hematopoietic cells. ChIP-seq in K562 cells revealed that CUX1 preferentially binds distal enhancers, rather than promoters, compared to other transcription factors. A CUX1 DNA-binding motif has been identified (ATCRAT), however, this motif is only present in up to ~40% of CUX1 binding sites, and <4% of ATCRAT motifs within open chromatin contain a CUX1 peak. CUX1 frequently co-occupies sites with RNA polymerase II, the transcriptional activator EP300 and components of the cohesin complex, suggesting that CUX1 may be associated with DNA looping[94].

RNA-seq following CUX1-knockdown has revealed common features of CUX1-regulated genes. In K562 cells, CUX1 is both an activator and repressor[94], in agreement with microarray data in LOUCY T-ALL cells[95], although in other studies the full-length p200 CUX1 protein was reported to repress transcription[93]. In $CD34^+$ human HSPCs, RNA-sequencing analysis following CUX1-knockdown revealed 81% of the differentially expressed genes were downregulated, indicating that in this cell type CUX1 may act as primarily a transcriptional activator[96]. CUX1 has been reported to regulate pathways involved in cell cycle progression, proliferation, apoptosis, multilineage differentiation and quiescence[79,94,96–98]. Some genes have been validated as direct transcriptional targets of CUX1. CUX1 deficiency activates phosphoinositide 3-kinase (PI3K) signaling through direct transcriptional downregulation of the PI3K inhibitor *PIK3IP1* (phosphoinositide-3-kinase interacting protein 1), leading to tumor

growth[95]. In the MCF7 human breast cancer cell line and in mouse embryonic fibroblasts, CUX1 knockdown reduced transcription of several DDR genes, including *ATM*, *ATR*, *BRCA1*, *CHEK1* and *CHEK2 in vitro*[99]. CUX1 has also been linked to repression of *CDKN1A* through recruitment of the histone lysine methyltransferase EHMT2 to form H3K9me2 at the *CDKN1A* promoter[100]. However, following DNA damage, CUX1 is necessary for appropriate upregulation of CDKN1A[99]. The role of CUX1 in preferentially binding distal enhancers suggests that CUX1 plays disparate roles in different cell types; it is possible that CUX1 also plays different transcriptional roles under stress conditions as well.

Very little is known about the transcriptional regulation of CUX1. In lung fibroblasts, CUX1 protein levels are upregulated following TGF- β stimulation[101]. Activation of the PI3K-AKT signaling pathway by IGF1 or AKT2 overexpression has been reported to upregulate CUX1, while downregulation of PI3K signaling through an inhibitor downregulated CUX1 expression[102]. This suggests a possible negative feedback loop, wherein PI3K-AKT signaling upregulates CUX1, which in turn upregulates the PI3K inhibitor PIK3IP1[93]. As CUX1 regulation of transcription fits an analog model, allowing for dosage-sensitive regulation of a wide variety of cellular programs[94], uncovering the mechanisms that precisely control transcription of CUX1 itself will be crucial.

CUX1 has been reported to function in base excision repair (BER). BER is responsible for removing small, non-helix-distorting base lesions, which occur following deamination, oxidation or methylation, and they are typically the result of spontaneous decay of DNA[103]. DNA glycosylases recognize the lesion and cleave the altered base

from deoxyribose, leading to the formation of an abasic site. The abasic site is then processed by an endonuclease, an exonuclease, DNA polymerase and a ligase. Different types of lesions are recognized and processed by different DNA glycosylases. For example, the DNA glycosylase methyl purine DNA glycosylase (MPG) processes biproducts of alkylation, such as 3-Methyladenine[104]. CUX1 has been reported to localize to DNA damage within one minute of radiation damage[105]. This was attributed by one group to the role of CUX1 as an ancillary factor to the DNA glycosylase OGG1 in three non-hematopoietic human cell lines[105–107]. OGG1 recognizes 8-Oxoguanine lesions, which are formed by oxidation. This function of CUX1 was found to be oncogenic in these cell lines.

Developing a knockout mouse to study CUX1 function *in vivo* presented several challenges. *CUX1* is one of the largest genes in the genome, ranked in the top 2.1% of all mammalian genes by size. *Cux1* also shares exons with *Casp,* a gene encoding a Golgi-associated protein lacking the DNA binding motifs of CUX1[108]. Previous knockout of *CUX1* in mice led to hypomorphic protein expression, incomplete CUX1 knockout and perinatal lethality[109–112]. To circumvent these issues, our lab generated two doxycycline-inducible, shRNA knockdown mouse models. The two shRNA mouse lines led to mid (~54% residual protein) and low (~12% residual protein) levels of CUX1. CUX1 knockdown led to MDS and MDS/MPN, with anemia, trilineage dysplasia and a myeloid expansion. RNA-seq analysis revealed that CUX1-deficient cells exhibit decreased quiescence and increased proliferation, decreased negative regulation of myeloid cell differentiation and increased PI3K/AKT/MTOR signaling. Furthermore, CUX1 deficiency drives a gene signature concordant with -7/del(7q)-driven MDS compared to normal

karyotype MDS[96]. CUX1 deficiency *in vivo* reduces transcription of *Pik3ip1*, in accordance with a previous report[95], and leads to decreased quiescence of LT-HSCs[96]. The data from human patients, *in vitro* studies and mouse modeling provides strong evidence for *CUX1* as a crucial myeloid tumor suppressor gene encoded on 7q.

DNA damage response in hematopoietic cells

Throughout the lifespan of an organism, both exogenous and endogenous processes lead to DNA damage. Endogenous stressors include biproducts of metabolism and cell division, such as reactive oxygen species (ROS). Exogenous stressors range from sunlight to genotoxic therapies. In order to maintain and protect genomic integrity, cells have evolved mechanisms to recognize and repair DNA damage. The specific response to damage initiated by a cell depends on a variety of factors, including damage type, the extent of the damage and whether the cell is cycling or quiescent. In healthy cells, these pathways then lead to (1) DNA repair (2) senescence or (3) apoptosis[113].

DSBs are the most dangerous form of DNA damage. Inefficient DSB repair can result in mutations, chromosomal translocations, genomic instability and cancer development[114]. DSBs can be introduced indirectly through propagated SSBs or stalled and collapsed replication forks, or directly through genotoxic therapy such as radiation[115,116]. After the initial break, ATM auto-phosphorylates to generate phospho-ATM (pATM). pATM is recruited to sites of DNA damage by the MRN complex (MRE11, RAD50 and NBS1) and Tip60. Tip60 then directly acetylates and activates ATM to promote phosphorylation of repair factors[117,118]. H2AX is phosphorylated at serine 139

to generate γH2AX immediately adjacent to DSBs. pATM and DNA-PK primarily phosphorylate H2AX in response to ionizing radiation, while this phosphorylation is primarily catalyzed by ATR following replication stress and UV irradiation. γH2AX then binds MDC1 (mediator of DNA damage checkpoint 1), and MDC1 is methylated by EHMT2 to amplify local activation of ATM[119]. The break site accumulates additional pATM and MDC1, resulting in additional phosphorylation of neighboring H2AX and the spreading of γH2AX to chromosomal regions surrounding the break. This γH2AX foci formation results in changes in chromatin structure and leads to the accumulation of downstream repair factors at the sites of DNA damage[120]. Continual ATM phosphorylation then leads to checkpoint activation and repair pathway choice. The two main DSB repair pathways, homologous recombination (HR) and end joining (EJ) are reviewed below.

Homologous Recombination (HR)

Homologous recombination constitutes one of the major pathways for repairing DSBs. HR is canonically associated with “error-free” repair, although the trade-off for this can be genomic instability. HR is able to achieve this fidelity by utilizing a homologous DNA sequence as a template for repair. The requirement for a sister homolog generally limits the use of this pathway to the S and G2 phases of the cell cycle. During S phase the activity of cyclin-dependent kinases (CDKs) rises, and this allows for phosphorylation of NBS1 and C-terminal binding protein interacting protein (CtIP). Phosphorylation of NBS1 and CtIP activates MRN endonuclease activity and initiates end resection, which then allows BRCA1 to bind CtIP, shuttling repair towards

HR. Further resection is carried out by DNA2/BLM and EXO1, creating extensive single-stranded DNA (ssDNA)[121]. The resulting ssDNA is first bound by RPA, and then BRCA1/2 promotes RAD51 binding to the ssDNA, replacing RPA. The RAD51 recombinase is central to the search for a homologous strand, strand invasion and DNA polymerization, all of which are essential to synthesize the sequence surrounding the break site. Following DNA synthesis based on the homologous template, DNA damage repair machinery is disassembled and cell cycling resumes[122].

End joining (EJ)

In addition to HR, DSBs can also be repaired through end-joining pathways, which include non-homologous end-joining (NHEJ) and alternative end-joining (alt-EJ). EJ pathways involve religating the DNA ends together with little or no processing, and no homologous template. Although historically NHEJ is considered “error-prone”, recent evidence has brought to light that NHEJ is likely accurate in the majority of cases[123,124]. EJ pathways are involved in repair throughout interphase but are inhibited during mitosis. NHEJ is the predominant pathway for DSB in quiescent cells, such as HSCs[125]. During phases where NHEJ will be used, the Ku70-Ku80 heterodimer rapidly binds to the DSB, and DNA-PK is recruited to the site and activated. DNA-PK maintains the proximity of the broken DNA ends and assists in recruiting end-processing factors. DNA ligase complex promotes the relegation of the break[126]. 53BP1 is recruited to the break, where it prevents end resection at DSBs and channels repair away from HR and towards EJ. End joining then proceeds through NHEJ, utilizing DNA ligase IV and Ku, or through alt-EJ. The most well-characterized alt-EJ pathway is theta-mediated end

joining (TMEJ), and utilizes PARP1, LigI/III and DNA polymerase θ (POLθ, encoded by *POLQ*)[123]. There is evidence that alt-EJ is a second line of defense for both NHEJ and HR, as loss of *POLQ* is lethal in cells that have mutations in both *KU/53BP1* and *BRCA1/2*, and presents a possible vulnerability in cancer cells[127–129].

Other repair pathways

Single-strand DNA lesions induced by replication errors or UV-induced pyrimidine dimers can be repaired by employing mismatch repair (MMR) or nucleotide excision repair (NER), respectively. Unlike NHEJ and HR, these mechanisms for repair are available to cells at all stages of the cell cycle[130]. Deficiency for DNA mismatch repair does not appear to have major effects on hematopoiesis under normal conditions, but impairs the capacity of HSCs to reconstitute irradiated mice[131]. NER removes bulky, helix-distorting nucleotide lesions, such as those induced by UV damage, environmental mutagens and cisplatin[132,133]. Loss of *xeroderma pigmentosum (Xpc)*, a gene essential for global genomic nucleotide excision repair, similarly led to minor phenotypes in unstressed HSCs, however $Xpc^{-/-}$ mice were more sensitive to the alkylating agent carboplatin[134,135].

Checkpoint Activation

In response to DNA damage, cells activate checkpoints that halt the cell cycle to allow for DNA damage repair, or in the case of excessive damage, initiate apoptosis or senescence[136–138]. The primary drivers of cell cycle progression are CDKs. These kinases are inactive until they are bound by cyclin subunits, which are regulated in a

cell-cycle dependent manner through control of their synthesis and degradation. Following DNA damage, common checkpoint pathways are activated that prevent CDK activation until repair is complete. These checkpoint pathways can be categorized as CHEK1-dependent or p53-dependent. Following damage, ATM signaling leads to end resection, allowing RPA loading on single-stranded, resected DNA. RPA loading then promotes ATR activation, and ATR phosphorylates CHEK1, activating CHEK1 kinase activity[139,140]. CHEK2 is phosphorylated by ATM[141]. During the G2/M transition, CHEK1 and CHEK2 cooperate to phosphorylate kinases and phosphatases in order to prevent the dephosphorylation, and activation, of cyclin-dependent kinases. The two most crucial cyclin-dependent kinases at this stage are cyclin-dependent kinases 1 and 2 (CDK1 and CDK2)[142–144]. CHEK1 phosphorylates WEE1, which in turn phosphorylates CDK1, preventing the G2/M transition[145]. CHEK1 also mediates phosphorylation of a phosphatase responsible for removing CDK1 phosphorylation, CDC25C, promoting cell cycle arrest in G2 during repair[146]. CHEK2, being downstream of ATM, is particularly important in checkpoint activation following DSBs, and phosphorylates CDC25 to prevent CDK dephosphorylation[147]. CHEK2 is also able to phosphorylate and stabilize p53[148].

p53 plays a critical role in both the G1/S and G2/M checkpoints. ATM and ATR kinase activity leads to phosphorylation and activation of p53. Stabilized p53 then inhibits cell cycle progression through upregulation of the cyclin-dependent kinase inhibitor p21[149]. p21 prevents cyclins from complexing with cyclin-dependent kinases and prevents the progression from G1 to S phase. Without this complex formation, cyclin-dependent kinases are unable to phosphorylate the retinoblastoma protein (Rb),

E2F remains bound to pRB and cell cycle arrest occurs[150]. The G1/S checkpoint is entirely p53-dependent, while the G2/M checkpoint results from a convergence of multiple pathways[151,152]. In the G2/M checkpoint, phosphorylated p53 transcriptionally represses cdc2C and cyclin B[153] and upregulates proteins that inhibit cyclin-B-CDK complex formation, including p21, 14-3-3 sigma proteins and GADD45[154–156]. Cells that have inactivated p53 will lose the G1/S checkpoint but maintain the G2/M checkpoint, although this checkpoint may decay over time.

DNA damage in HSCs

An effective DNA damage response is especially important in HSCs, which are responsible for maintaining lifelong hematopoiesis and generating progeny that produce approximately one trillion mature blood cells per day[157]. In contrast to more differentiated cells, HSCs are able to avoid some sources of endogenous DNA damage. HSCs are largely quiescent[158], and cell division and the reactive oxygen species (ROS) generated by division are a major source of endogenous DNA damage in cells. HSCs are also uniquely able to avoid ROS-induced damage by transporting ROS to adjacent mesenchymal stem cells via gap junctions[159]. If HSCs do sustain DNA damage, checkpoint activation leads to differentiation of these damaged HSCs, limiting their self-renewal[160,161]. However, despite these adaptations designed to protect the genomic integrity of HSCs, aged HSC still accumulate DNA damage[162–164].

In addition to evading DNA damage, HSCs have developed strategies to ensure a surviving pool of stem cells. In mice, HSCs are radioresistant compared to differentiated cells[130,165] and maintain elevated expression of pro-survival members of

the *Bcl2* family[125]. HSC pools also seem able to select for the "least damaged" cells in a non-autonomous manner, allowing for sustained production of blood cells. Cells with lower levels of p53 and checkpoint activation are able to outcompete HSCs with higher levels of p53, theoretically allowing healthier cells to survive to continue blood production, but also inadvertently selecting for HSCs with mutant or lost p53[32,166].

The DDR in HSCs sits at the interface of genomic fidelity and HSC survival. Inherited DDR deficiencies often manifest with hematologic defects, including bone marrow failure syndromes and increased leukemia risk[130,167,168]. Deficiency for proteins involved in HR leads to bone marrow failure in humans[169] and impairs hematopoiesis in mice as well[170,171]. As HSCs are largely quiescent, NHEJ is the predominant pathway for DSB repair[125]. Impaired NHEJ does not affect HSC frequency or hematopoiesis in normal young adult mice, but does reduce HSC function in response to stress[172] and aging[173]. Transgenic mice with knockout of DDR genes involved in HR, NHEJ, MMR and NER reveal that an intact DNA damage response is required for optimal HSC reconstitution potential and self-renewal[174]. DNA damage repair pathway choice plays an essential role in normal hematopoiesis and in leukemogenesis.

Epigenetic regulation of DNA damage repair

In eukaryotic cells, all DNA damage repair occurs in the context of chromatin. Chromatin is composed of DNA and protein, and the basic unit is the nucleosome. Each nucleosome is composed of eight histones, with two copies each of histones H2A, H2B, H3 and H4, or variants of these histones, wrapped with 146 bp of DNA. Modifications of these histones and histone variant exchanges at sites of DSBs impact break

recognition, repair efficiency, pathway choice and resolution. The chromatin structure dictates accessibility at sites of DNA repair, as well as recruitment of downstream factors. Repair factors are able to recognize histone variants, post-translational histone modifications and chromatin conformational changes introduced by ATP-dependent chromatin remodeling complexes and histone chaperones[175]. The importance of a wide variety of epigenetic modifications in local break repair has emerged within the last ten years, and their perturbation plays an important role in carcinogenesis.

Recognition of DSBs

Histone modifications are involved in the earliest stages of DNA repair. Tip60 binds H3K9me3 at breaks to activate its acyltransferase activity. Tip60 then acetylates pATM, which in turn phosphorylates the histone variant H2AX, to form γH2AX within minutes of break formation [117,176,177]. EHMT2 is recruited to breaks, where it methylates histone and non-histone targets. Methylation of H3K9 and H3K27 occurs around DSBs rapidly after break formation[177–179], and EHMT2 methylates MDC1 to promote interaction between MDC1 and pATM, which then promotes further local accumulation of pATM[119,120]. pATM accumulation promotes spreading of H2AX phosphorylation. In human cells, the phosphorylation of H2AX propagates over more than 1 Mb on both sides of the break. Although ATM, DNA-PK and ATR are all able to phosphorylate H2AX, only ATM is involved in promoting γH2AX spreading and maintaining γH2AX density[180]. γH2AX is not required for the initial recruitment of signaling and repair factors, but it is essential for the accumulation and retention of these factors at breaks, as well as propagation of the DNA damage repair signal[181–183].

Chromatin accessibility at DSB

Chromatin remodeling complexes localize to the break, including INO80, TIP60-p400 and SWI/SNF, and large gH2AX foci are thought to be platforms for cohesin binding to promote chromatin stability and retain end-to-end proximity[175]. CBP/p300 is recruited to sites of DNA damage to promote acetylation of H3 at lysine 18, as well as H4K5, H4K8, H4K12 and H4K16, which then promotes SWI/SNF localization to the break and chromatin relaxation[184]. Acetylation also leads to destabilization of the nucleosome to promote accessibility at the DSB. In areas of heterochromatin, stability is maintained by HP1 binding to H3K9me3. Upon the formation of a DSB, HP1 is phosphorylated and dissociates from H3K9me3, providing both chromatin relaxation and also allowing Tip60 to bind H3K9me3. Loss of H3K9me2/3 leads to diminished Tip60 acetyltransferase activity, pATM acetylation and foci formation[117,185].

Chromatin modifications in pathway choice at DSBs

Chromatin modifications influence repair factor binding and, as a consequence, DSB repair pathway choice between NHEJ and HR. Ku70-80 and NBS1, early DNA repair components involved in NHEJ, are recruited and stabilized by the dimethylation of H3K36 at DSBs[178]. The Ku heterodimer binds free DNA ends, and DNA-PK recruitment rapidly follows. 53BP1, which prevents end resection and promotes NHEJ, reads a histone code unique to DSBs that integrates ubiquitylation, methylation and acetylation[186]. 53BP1 has been reported to bind γH2AX, H4K20me1/2, H3K79me, H3K27me2/3 and ubiquitylated H2AK15 (H2AK15ub)[187–189]. Mutation of H3K79 or

H3K27me1/2 impairs 53BP1 foci formation[188,189], as do point mutations that impair 53BP1 binding to H4K20me1/2 or H2AKuB[190,191].

Components of HR both compete with NHEJ for these components and bind their own distinct histone code. It has been suggested that FANCD2, an HR-associated protein that also binds H4K20me2, competes with 53BP1 for H4K20me2 binding to promote HR and restrict NHEJ[187,192]. While components of NHEJ are stabilized by dimethylation of H3K36, trimethylation of H3K36 promotes CtIP binding, DSB resection and RPA loading to initiate HR[193]. Tip60 binding to H3K9me3 promotes HR, by activating Tip60 acetyltransferase activity. Tip60 acetylates H4K16, which hinders 53BP1 binding to neighboring H4K20me2. The displacement of HP1 that precedes Tip60 binding also promotes chromatin relaxation and facilitates end resection for HR[194,195]. H3K27 methylation also coordinates pathway choice between NHEJ and HR. Reduced H3K27me2/3 at sites of DNA damage leads to reduced 53BP1 binding and NHEJ, but increased binding of FANCD2[189]. DNA damage induces a dynamic set of epigenetic marks and chromatin conformational changes that are essential to recognizing and repairing breaks, and the interplay between epigenetic modifications and the DDR, both of which are perturbed in CHIP and myeloid malignancies, is an important area of study.

Aims of this thesis: Critical gaps in knowledge that will be addressed

As introduced above, critical gaps in knowledge remain in the relationship between clonal hematopoiesis, t-MN and -7/del(7q). Despite the high prevalence of -7/del(7q) in t-MN, no mouse model of -7/del(7q)-driven t-MN exists. This work aims to examine whether there is a mechanistic link between -7/del(7q), CHIP and t-MN. CUX1, encoded on 7q, is mutated in CHIP and myeloid malignancies, but it is unclear what role it plays in responding to cytotoxic therapy and protecting from t-MN. Finally, the importance of the DNA damage response in CHIP and t-MN following therapy is becoming clear, and it is unknown what role CUX1 plays in the DNA damage response in hematopoietic cells. Understanding the mechanism of t-MN pathogenesis will create opportunities for drug targeting, individualized t-MN prevention strategies and novel treatments for patients predisposed to develop a t-MN.

Prior work has indicated that clonally expanded populations of stem cells exist in most tissues and may present an increased risk for malignancy. Clonally-expanded stem cell populations were first observed in the hematopoietic system, and many efforts have been made to uncover mutations that both provide a clonal advantage to HSCs and prime for transformation. Furthermore, understanding which genes provide HSCs a fitness advantage under the pressure of cytotoxic therapy could provide a blueprint for uncovering other mutations that help stem cells preferentially survive similar mutagenic processes, such as sun exposure, aging and smoking. Given the high prevalence of -

7/del(7q), and the observation of both -7 and del(7q) in CHIP in patients[19,22,55], it is likely that 7q contains one or more such genes.

Loss of chromosome 7 has long been known to constitute a high-risk cytogenetic change in myeloid neoplasms, yet the gene(s) responsible for promoting malignancy remain unclear. Treatment of wild type mice of most mouse strains, including C57BL/6J mice, with alkylating agents does not induce t-MN[196], and reduction of multiple cooperating genes is required to induce t-MN[29,197]. Here, we aim to probe whether the loss of a single 7q gene, *CUX1,* is sufficient to predispose mice to t-MN. The finding that the loss of a single gene encoded on 7q is able to drive myeloid disease would alter the approach to developing treatments for t-MN with -7/del(7q), as well as generate a mouse model for testing these therapies.

There is strong evidence for CUX1 as a myeloid tumor suppressor gene. CUX1 mutations are found in CHIP and in a spectrum of myeloid malignancies, and they independently carry a poor prognosis[95,198,199]. Knockdown of CUX1 *in vivo* drives MDS and MDS/MPN, and CUX1 regulates cell cycle, proliferation and differentiation pathways. However, CUX1 is widely understood as transcription factor, and most previous work studying CUX1 loss has focused on its role as a transcriptional regulator of tumorigenesis. Given the association between the DNA damage response, CHIP and t-MN observed in patients, this work explores a non-transcriptional role for CUX1 in DNA damage repair. One group previously reported a non-transcriptional role for CUX1 acting in base excision repair, however, they found that CUX1 acts as an oncogene in these tissues. As CUX1 acts a tumor suppressor gene in hematopoietic cells, it is probable that CUX1 plays a distinct role in HSCs. The finding that CUX1 plays a role

(transcriptional or otherwise) in the DNA damage response would not only provide a novel insight into the function of CUX1, but also support the connection between CUX1 loss and t-MN.

Although the connections between the clonal expansion of stem cells and malignancy have been best-described in hematopoiesis, evidence is emerging to suggest that this paradigm may underlie malignant transformation more broadly. Cytotoxic therapy is only one example of a litany of mutational processes that impact every cell in the body throughout life, and the discovery that CUX1 is lost in CHIP, malignancy and involved in DNA damage repair would open new areas of investigation into similar genes and evolutionary processes in other tissues, as well as impact screening for CHIP preceding chemotherapy.

MATERIALS AND METHODS

Cell culture and transfections

K562 cells were maintained as described previously[79]. We generated gCUX1 and gHPRT cell lines using the RNP-based CRISPR/Cas9 delivery system[200,201]. The BROAD shRNA Genetic Perturbation Platform (GPP) sgRNA Designer[202] was used to identify potential guides targeting *CUX1*. Potential guides were verified using the Synthego Verify Guide Design tool, and a guide targeting exon 4 of *CUX1* (5'-UGCACUGAGUAAAAGAAGCA-3') was selected. A guide targeting intron 2 of *HPRT* (5'-GCAUUUCUCAGUCCUAAACA-3') was chosen to generate an isogenic control cell line. The sgRNAs and Cas9 were obtained from Synthego. RNPs were generated by incubating the sgRNA with Cas9 at a 9:1 ratio in Buffer R for 10 minutes at room temperature. After incubation, 2 x 10^5 cells were resuspended with the Cas9-sgRNA RNPs and electroporated with 3 pulses at 1450V for 10 ms using the Neon Transfection System (ThermoFisher). Single-cell clones were generated from the transfected pool, and the clonal populations were analyzed by Sanger sequencing and western blotting. Single-cell clones with deletion of *CUX1* and *HPRT* were used for experiments.

Western blot

K562 cells were lysed in protein lysis buffer and processed for immunoblotting as previously reported[96]. For protein detection, an antibody targeting CUX1 (B10, Santa Cruz, 1:300) followed by anti-mouse-HRP secondary antibody (Sigma, 1:5,000), and anti-β-actin-HRP (C4,Santa Cruz, 1:4,000) were used.

Histone sample preparation for LC-MS/MS

Briefly, 5 x 10^6 cells were harvested 1 hour after irradiation (6 Gy) or mock irradiation, and nuclei were isolated using NEB buffer (10 mM HEPES pH 7.9, 1 mM KCl, 1.5 mM $MgCl_2$, 1mM DTT). Histones were extracted from nuclei by treatment with 0.4 N H_2SO_4 for 30 minutes at room temperature and then precipitated from the supernatant by dropwise addition of ice-cold trichloroacetic acid. Precipitated protein was spun down and washed twice with ice-cold acetone. The pellet was then air dried and resuspended in double-distilled H_2O. For each sample set, 20 µg of protein was loaded and run in a gel for 6 minutes at 200 V. Gel sections were subjected to propionyl derivatization (protein level), trypsin digestion, then propionyl derivatization (peptide level), then C18 cleanup. For propionyl derivatization, propionic anhydride (Sigma) was mixed 1:3 with isopropanol pH 8.0 and reacted 37 °C for 15 minutes. Following protein derivatization treatment, gel sections were washed in deionized H_2O and de-stained using 100 mM NH_4HCO_3 pH 7.5 in 50% acetonitrile. A reduction step was performed by addition of 100 µl 50 mM NH_4HCO_3 pH 7.5 and 10 µl of 200 mM tris(2-carboxyethyl) phosphine HCl at 37 °C for 30 min. The proteins were alkylated by addition of 100 µl of 50 mM iodoacetamide prepared fresh in 50 mM NH_4HCO_3 pH 7.5 buffer, and allowed to react in the dark at 20 °C for 30 minutes. Gel sections were washed in water, then acetonitrile, and vacuum dried. Trypsin digestion was carried out overnight at 37 °C with 1:50-1:100 enzyme–protein ratio of sequencing grade-modified trypsin (Promega) in 50 mM NH_4HCO_3 pH 7.5, and 20 mM $CaCl_2$. Peptides were extracted with 5% formic acid and vacuum dried and sent to the Mayo Clinic Proteomics Core facility for HPLC and LC-MS/MS data acquisition. Post-digestion, peptides were derivatized with propionic

anhydride:IPA 1:3 at 37 °C for 15 min and repeated for a total of two times. Peptides were then cleaned up with C18 spin columns (Pierce).

LC-MS/MS and EpiProfile analysis

Three samples of K562 gHPRT and gCUX1 irradiated (6 Gy) and mock-irradiated cells were collected one hour after treatment. Peptide samples were re-suspended in Burdick & Jackson HPLC-grade water containing 0.2% formic acid (Fluka), 0.1% TFA (Pierce), and 0.002% Zwittergent 3–16 (Calbiochem), a sulfobetaine detergent that contributes the following distinct peaks at the end of chromatograms: MH^+ at 392, and in-source dimer [2 M + H^+] at 783, and some minor impurities of Zwittergent 3-12 seen as MH^+ at 336. The peptide samples were loaded to a 0.25 µl C_8 OptiPak trapping cartridge custom-packed with Michrom Magic (Optimize Technologies) C8, washed, then switched in-line with a 20 cm by 75 µm C_{18} packed spray tip nano column packed with Michrom Magic C18AQ, for a 2-step gradient. Mobile phase A was water/acetonitrile/formic acid (98/2/0.2) and mobile phase B was acetonitrile/isopropanol/water/formic acid (80/10/10/0.2). Using a flow rate of 350 nL/minute, a 90 min, 2-step LC gradient was run from 5% B to 50% B in 60 minutes, followed by 50%–95% B over the next 10 minutes, hold 10 minutes at 95% B, back to starting conditions and re-equilibrated.

Electrospray tandem mass spectrometry (LC-MS/MS) was performed at the Mayo Clinic Proteomics Core on a Thermo Q-Exactive Orbitrap mass spectrometer, using a 70,000 RP survey scan in profile mode, m/z 340–2000 Da, with lockmasses, followed by 20 MS/MS HCD fragmentation scans at 17,500 resolution on doubly and

triply charged precursors. Single charged ions were excluded, and ions selected for MS/MS were placed on an exclusion list for 60 seconds. An inclusion list (generated with in-house software) consisting of expected histone post-translational modifications was used during the LC-MS/MS runs.

Sample *.raw files were extracted with pXtract version 2.0 to obtain their MS1 and MS2 files[203]. These along with their *.raw files were analyzed in MATLAB[204] with the EpiProfile 2.0 script[205,206]. Downstream post-translational modifications analysis was performed in Perseus version 1.6.7.0[207] and formatted in Perseus, Excel (Microsoft) or R. All code is available upon request.

ChIP-Sequencing

ChIP-seq was performed as follows. Chromatin was fixed using 1% formaldehyde for 10 minutes at RT and stopped by the addition of 0.125M glycine. Fixed chromatin was then harvested from $100x10^6$ gHPRT or gCUX1 K562 cells and sonicated (Bioruptor) for 10 minutes in 30 second on/off pulses two times for a total of 20 minutes, vortexing in between. Immunoprecipitation was performed using Dynabead protein G magnetic beads (Thermo Fischer) and 10ug of anti-H3K27Me3 (Abcam, ab6002). Following elution, samples were treated with RNAseA and proteinase K before crosslink reversal. DNA was purified using a PCR purification kit (Qiagen). Libraries were prepped using the Ovation Ultralow Library Kit (NuGEN) and size selected using with SPRIselect beads (Beckman Coulter). Illumina HiSeq was used to perform 50 bp single-end sequencing on the libraries. Two biological replicates were performed for each sample. Sequencing data are available at GEO accession number GSE154674.

ChIP-sequencing analysis

Sequencing reads were aligned to the human hg19 genome using BWA (version 0.7.12)[208] and low quality reads were removed using the SAMtools q30 filter[209]. Peaks were called using MACS2[210] with a q value threshold of 0.05. For differential peak calling, DiffBind software[211] was applied using an FDR cutoff of 0.10. The average read density from two biological replicates was normalized by RPKM in 50 bp bins and visualized using the deepTools software[212]. Statistical differences in read density were calculated using the Wilcoxon signed-rank test.

Immunofluorescence antibodies

Antibodies used for immunofluorescence in this study are as follows: γH2AX (mouse monoclonal, clone JBW301, Millipore Sigma), H3K27me3 (rabbit, monoclonal, clone C36B11, CST), H3K27me2 (rabbit, polyclonal, Sigma), H3K27me1 (rabbit, polyclonal, Sigma), H3K9me1 (rabbit, polyclonal, Sigma), H3K9me2 (rabbit, polyclonal, Sigma), H3K9me3 (rabbit, polyclonal, Sigma), EHMT2 (rabbit, monoclonal, clone C6H3, CST), phospho-ATM (mouse, monoclonal, clone 10H11.E12, CST) and 53BP1 (rabbit, polyclonal, Novus Biological). Secondary antibodies were sheep anti-mouse, Alexa Fluor 488 and goat anti-rabbit, Alexa Fluor 594 and 647.

Generation of CUX1-specific antibody: Rabbit polyclonal antibodies that recognize a C-terminal peptide amino acids 1223-1242 (CEPPSVGTEYSQGASPQPQH) of CUX1

were generated by the Pocono Rabbit Farm and Laboratory (Canadensis, PA) and affinity purified.

Colocalization analysis

Colocalization between two channels was determined by in-house code written to implement the ICA method developed by Li *et. al*[213,214]. Briefly, regions of interest (ROIs) corresponding to individual nuclei were segmented and cropped and images were saved as intensity matrices. A custom R script was written to transform corresponding matrices into colocalization scores. Pixels were considered to be colocalized if the intensity in a given pixel was above the mean intensity for an image in both channels. We reported the fraction of pixels within a given nuclear ROI which were colocalized. This method is insensitive both to the amount of staining present in an image and also to variations in intensity between cells or regions of an image.

Ground State Depletion (GSD) superresolution imaging

For superresolution imaging, cells were adhered to coverslips and stained as above but not mounted. Instead, coverslips were washed 5 times with PBS to remove non-specifically bound fluorophores, inverted over depression slides containing 50 µl of freshly prepared 300 mM MEA oxygen scavenging medium, sealed with a two-part, quick-curing epoxy, and cured 5 minutes in a 50° C oven. For imaging, we utilized a Leica GSD 3D imaging system equipped with a 160 X/1.43 NA, 0.07 mm WD objective; Suppressed Motion (SuMo) stage; PiFoc precision focusing control system; blue (488

nm), green (532 nm) and red (642 nm) excitation lasers; fluorescein, rhodamine and far red emission filters and an iXon Ultra EMCCD camera. Slides were then imaged using standard GSD imaging protocols with at least 10,000 frames captured per channel per image. GSD data analysis and processing were carried out with a series of custom ImageJ macros. Identification of emission events was performed via ImageJ plugin ThunderSTORM[215]. Final images were then pseudo colored and compiled in ImageJ. Superresolution imaging macros are available upon request.

GSD Fluorescence Resonance Energy Transfer (FRET) imaging

We labeled target proteins or PTMs with primary antibodies and utilized fluorescent secondary antibodies to introduce either a donor fluorophore (AF 594) or an acceptor fluorophore (AF 647). Hereafter, the labeled protein targets will be referred to as the donor and the acceptor, respectively. We first imaged both donor and acceptor at their respective excitation maxima to obtain an image of donor and acceptor location. Next, we made use of the high-powered laser on the Leica GSD microscope to deplete or bleach the acceptor fluorophores. We then imaged both donor and acceptor at their respective excitation maxima again. The second acceptor image displayed no detectable signal indicating efficient bleaching on acceptor fluorophores. Before acceptor bleach, donor energy was transferred to the acceptor proportionately to the distance between donor and acceptor molecules. Bleached acceptor fluorophores can no longer accept donor energy, and all donor energy is thus observed when exciting donor fluorophores at donor excitation maxima. Any increase in the donor emission after acceptor bleaching is thus indicative of FRET and proportionate to the distance

between acceptor and donor molecules. To obtain a FRET image, the donor image before acceptor bleach is subtracted from the donor image after acceptor bleach. The resultant image intensity is proportional to FRET between acceptor and donor. GSD-FRET reports both the location and the degree of FRET interactions between two labeled antigens. GSD-FRET imaging was carried out in the sequence described above. Images were pseudo-colored and manipulated in ImageJ.

Immunofluorescence imaging and foci analysis

For all imaging, we used round #1.5 cover glass pretreated with 0.1% poly-L-Lys for 12 hours. Coverslips were placed in 24-well plates and approximately 250,000 K562 cells were seeded into each well and allowed to grow for 12-24 hours. Irradiation and/or treatment with indicated inhibitors were performed *in situ*. For slide preparation, plates were spun in a benchtop centrifuge at 500 G for 5 minutes to aid in cell adhesion. Subsequently, cells were fixed with 4% PFA in PBS for 10 minutes at the indicated time point, stained with 0.5 µg/mL DAPI, and mounted using ProLong Gold (Invitrogen). For immunofluorescence staining, cells were fixed as above, then permeabilized with 10% Triton-X 100 for 10 minutes. After blocking with 5% BSA in PBS for 1 hour, the indicated primary antibodies were added and coverslips were incubated overnight at 4°C. All antibodies were used at 1:1000 dilution. Following three 5 minute washes with 5% BSA in PBS supplemented with 0.1% TX-100 and 0.05% NP-40, fluorescent secondary antibodies (Jackson ImmunoResearch) were applied for 1 h at room temperature. All images were captured on an Olympus IX81 wide-field microscope with either 150X oil-immersion objective and pseudo colored using ImageJ. 2-3 biological replicates were

performed (as indicated in the legend) for each experiment and greater than 50 cells were imaged per replicate. Foci counting was performed with a custom ImageJ macro. Briefly, nuclei were thresholded and segmented and foci were counted within each nucleus via a thresholding and FindMaxima routine. Foci intensity analysis was performed by segmenting the foci as above and then measuring the MFI within each focus. Foci within each nucleus were grouped, and the mean Foci-MFI value was reported per nucleus. Foci size was determined by auto-local thresholding of the γH2AX channel followed by segmentation and measurement of segmented foci regions. All other image analysis was carried out in ImageJ via custom macros. All macros available upon request.

Inhibitors and Drug Treatment

For EHMT2 inhibitor treatment experiments, we used UNC0642 obtained from Selleck Chem. UNC0642 was dissolved in DMSO and used at a final concentration of 10 nM and added to cells in culture for the indicated length of time.

DNA Damage Treatment

DNA damage was induced by exposure to a ^{60}Co source. Cells were placed in an irradiator (MDS Nordion) and exposed to the indicated dose. Dosage rates varied between 10.5 and 9.1 cGy/s depending on the date of the experiment. Cells were allowed to recover in an incubator for the indicated time. Non-irradiated (NIR) samples were mock irradiated. N-Ethyl-N-nitrosourea (Sigma) was dissolved in 10% ethanol (95%) and 90% PBS and administered intraperitoneally (100 mg/kg).

Mouse models

All animal studies were approved by the University of Chicago Institutional Animal Care and Use Committee mice were housed in Association for Assessment and Accreditation of Laboratory Animal Care-accredited, specific pathogen-free animal care facilities at the University of Chicago. Both sexes of mice were used, and experimental mice were housed separately by sex with five mice per cage. Tail clips were performed for genotyping. Renilla, shCux1.581 ($Cux1^{mid}$) and shCux1.2812 ($Cux1^{low}$) mice were generated as previously described[96]. A second-generation reverse tet-transactivator (M2rtTA) is expressed from the endogenous *ROSA26* promoter, and an shRNA targeting Renilla luciferase or *Cux1* is expressed downstream of *Col1a1.* Resulting mice were rtTA-$M2^{tg/tg}$;$Col1a1^{Cux1/wt}$ (either $Cux1^{low}$ or $Cux1^{mid}$) or rtTA-$M2^{tg/tg}$;$Col1a1^{Ren/wt}$ (Ren) littermate controls, on a mixed C57BL/6 x 129/Sv background. The transgene was induced by maintaining the mice on continuous doxycycline-containing chow diet (TD.12006, 1 mg/kg, Envigo). For all experiments, adult mice (8-16 weeks) were used. ENU (Sigma) was administered intraperitoneally at 100 mg/kg at the times indicated in the legend.

Flow Cytometry

Peripheral blood was collected from the submandibular vein for complete blood counts and flow cytometry. Complete blood counts were performed using a Hemavet 950 counter (CDC Technologies, Oxford, CT). For flow cytometry, 50 uL of blood was blocked with an Fc receptor blocking reagent (clone 93, Fisher Scientific), split into two

aliquots and stained with CD45-BUV395 (30-F11, Fisher Scientific) and either CD3e-APC (145-2C11, BD Biosciences) and B220-PE (RA3-6B2, eBioscience), or Gr1-PE (RB6-8C5, Fisher Scientific) and CD11b-APC (M1/70, BD Biosciences). For competitive transplants and autopsy analysis, the peripheral blood, BM and spleen were stained with the following antibodies (BD Biosciences): PerCP-Cy5.5-CD45R/B220 (RA3-6B2), BUV737-CD3e (145-2C11), BUV395-Gr1 (1A8), APC-Cy7-CD11b (M1/70), PE-CD45.1 (A20), APC-CD45.2 (104). Cells were incubated for 30 minutes at room temperature and then lysed with ACK red blood cell lysis buffer prior to analysis.

For BM and spleen analysis, cells were lysed by ACK lysis buffer, FcR blocked and stained with the following biotin-conjugated lineage markers (BD Biosciences): CD3e (145-2C11), CD5 (53-7.3), CD19 (1D3), CD11b (M1/70), Gr-1 (RB6-8C5), Ter119 (Ter-119), and B220 (RA3-6B2) for 20 minutes on ice. For stem cell analysis, cells were washed with flow buffer and stained with the following (BD Biosciences): cKit-APC-Cy7 (2B8), Sca-1-PE-Cy7 (D7), Streptavidin-BUV737, CD45.1-BUV395 (A20), CD45.2-APC (104), CD48-Percp/Cy5.5 (HM48-1), CD150-PE (Q38-480). For myeloid progenitor cells, the following antibodies were used: cKit-APC-Cy7 (2B8, BD Biosciences), Sca-1-PE-Cy7 (D7, BD Biosciences), CD45.2-BUV737 (104, BD Biosciences), Streptavidin-BUV395 (BD Biosciences), CD34-eFluor-660 (RAM34, Invitrogen/eBioscience), CD16/32-PerCP-5/Cy5.5 (2.4G2, BD Biosciences), CD45.1-PE (A20, BD Biosciences). Cells were incubated for 30 minutes at room temperature. Staining for γH2AX, BrdU and cPARP were performed according to the manufacturer's protocol (BD Biosciences, 562253). Flow cytometry was performed on an LSR Fortessa (BD Biosciences), and data analyzed with FlowJo software (Tree Star, Inc., Ashland, OR).

For erythroblast analysis of the spleen and bone marrow, cells were FcR blocked and stained with the following antibodies from Fisher Scientific: Ter119-PE (Ter-119), and CD71-APC (C2). For Ter119 and CD71 erythroblast analysis, cells were analyzed without red cell lysis.

RNA-seq

Adult Ren and Cux1^{low} mice were treated with doxycycline for 5 days, and bone marrow cells were collected and lysed. BM cells were lineage depleted (Mouse Direct Lineage Cell Depletion kit, Miltenyi Biotec) and stained. HSCs (Lin$^-$, cKit$^+$, Sca1$^+$, CD135$^-$) were sorted on a FACSAria II (BD Biosciences) directly into Trizol. RNA was purified by RNeasy Kit (Qiagen), and >100 ng of RNA was used for library preparation. Three biological replicates were performed.

Barcoded RNA-seq libraries were generated with the TruSeq v2 kit (Illumina) and >23 million, single end, 50 bp reads were generated by Illumina sequencing (HiSeq 2000). Reads were aligned using STAR[216], and alignments with a mapping quality <30 were removed. Differential gene expression analysis was performed using DESeq2[217], and a negative binomial general linearized model fitting and Wald statistics were used to generate p values, with p values adjusted using the Benjamini Hochberg method. Sequencing data are available in the GEO Database (accession GSE154674).

Data Availability

The data discussed in this publication have been deposited in NCBI's Gene Expression Omnibus[218] and are accessible through GEO Series accession number GSE154674.

γH2AX Assay

Mice were treated with dox for 7 days, and bone marrow was collected. Whole bone marrow was cultured overnight in StemSpan SFEM medium (Stemcell Technologies) supplemented with β-mercaptoethanol (55 uM), doxycycline (1 μg/mL), murine stem cell factor (100 ng/mL), murine IL-3 (100 ng/mL), murine IL-6 (100 ng/mL) and FBS (10%) prior to treatments. Bone marrow was irradiated (2 Gy) or mock-irradiated, and cells were collected at the time points indicated. Lineage-negative cells and $Lin^-/cKit^+/Sca1^+$ (LSK) cells were gated.

Proliferation and Apoptosis assays

K562 cells were irradiated (6 Gy) and cultured for 24 hours. One hour before collection, BrdU was added to the culture for a final concentration of 10 μM. For *in vivo* experiments, mice were given continuous doxycycline for one week before injecting ENU (100 mg/kg) intraperitoneally (IP). A second dose of ENU was administered 9 days later, and BrdU was injected IP 6 hours after ENU. BM and spleen cells were collected 12 hours after BrdU. Murine cells were then stained for stem cell and progenitor markers, and BrdU and cPARP staining were performed according to the manufacturers protocol (BD Biosciences, 562253).

Bone Marrow Transplants

For competitive bone marrow transplants, 2 $x10^6$ RBC-depleted cells were transplanted, with 20% Ren, $Cux1^{mid}$ or $Cux1^{low}$ cells and 80% wildtype competitor (C57BL/6, CD45.1)

transplanted retro-orbitally into lethally irradiated (γ-irradiation, 8.5 Gy) C57BL/6 (CD45.1) recipient mice. Dox was given immediately after transplant, and ENU was administered (100mg/kg) IP at week 5, with a second dose following 9 days later.

Histology

Tissues were fixed in 10% formalin, embedded in paraffin, sectioned at 4 μm, and stained with hematoxylin and eosin or GATA1. Images were taken with a Zeiss Axioskop microscope.

Comet single cell electrophoresis assay

Ren, $Cux1^{mid}$ and $Cux1^{low}$ mice were treated with doxycycline for 7 days and irradiated (6 Gy). Bone marrow cells were collected at the indicated times following irradiation, and $cKit^{+}$ cells were selected (Mouse CD117 Microbead kit, Miltenyi Biotec). Cells were embedded in low-melting agarose (Trevigen). Comet assays were performed with a Trevigen Comet Kit according to manufacturer's directions with the following modifications. Cells were electrophoresed at 23 V for 60 min and stained with SYBR Green rather than SYBR Gold. Imaging of comet slides was carried out on a wide-field microscope with a 10 X air objective. Images were analyzed using ImageJ plugin OpenComet[219].

Statistical analysis and plotting

All statistical analysis was performed as indicated. Unless otherwise indicated, all replicates represent biological replicates. Test were carried out using GraphPad Prism

version 8.3.0 (328) or R[220] using the ggpubr package[221]. Significance testing was performed using the tests indicated in the figures. For all plots, significance values are as follows: ns $p>0.05$; * $p<0.05$; ** $p<0.01$; *** $p<0.001$; **** $p<0.0001$. Box plots show first and third quartiles of the data as well as the median. In scenarios where multiple testing was considered, p-values were transformed into FDR q-values by the qvalues package in R (Storey method)[222] unless otherwise indicated. Plots generated in R were generated using the ggplot[223], cowplot[224] and ggpubr packages. All R code, for data generation, analysis, and plotting is available upon request.

RESULTS: THE ROLE OF CUX1 IN THERAPY-RELATED MYELOID NEOPLAMS

Introduction

A devastating sequela of the use of chemotherapy and/or irradiation is the development of a secondary malignancy. Therapy-related myeloid neoplasms (t-MN) are blood cancers that develop as a consequence of genotoxic treatments for several conditions, most commonly cancer, but also autoimmune disease and solid organ transplantation. t-MN are associated with high-risk karyotypes and chemoresistance[9], hence the five-year survival rate is poor, at 14.6 months[5]. As cancer survivors are a growing population[3], the incidence of t-MN is also expected to rise. Treatment and prevention of this long-term side effect is of increasing importance.

Historically, t-MN was thought to be primarily driven by exposure to DNA-damaging agents and subsequent mutations in HSPCs. More recently, the etiology of this disease has been appreciated to also include inherited genetic predisposition, therapy-induced changes in the bone marrow microenvironment, and the selection of preexisting, somatically-mutated hematopoietic stem cells (HSCs)[15]. The latter phenomenon, termed clonal hematopoiesis of indeterminate potential (CHIP), is associated with an increased risk for developing a hematopoietic malignancy[14,37–40]. The presence of CHIP prior to cytotoxic therapy has been linked to an elevated risk of developing a t-MN, and the subsequent t-MN typically harbors the same mutations as the antecedent clone[53,225]. This leads to a model wherein clonal populations harboring certain mutations have a fitness advantage in the setting of chemotherapy and/or irradiation, outcompete wildtype counterparts, and transform. Somatic mutations have been found across a variety of genes and in a high percentage of healthy individuals[36],

yet only some progress to either *de novo* or therapy-related malignancy[34]. Epigenetic regulators, such as *DNMT3A* and *TET2*, are frequently found in CHIP in healthy older adults[38,40]. In contrast, DNA damage response (DDR) genes, such as *TP53,* are more common in CHIP following cytotoxic therapy[33]. Despite these patterns, which CHIP mutations confer the highest risk of transformation for either therapy-related or *de novo* disease is incompletely understood.

Monosomy 7 and del(7q), are adverse-risk cytogenetic abnormalities found in a variety of hematopoietic disorders, including bone marrow failure, pediatric and adult myelodysplastic syndrome (MDS) and acute myeloid leukemia (AML)[61–64]. In *de novo* AML, -7/del(7q) increases in prevalence with age, from 4% in patients younger than 30 years to 20% in patients 60 years of age or older[226]. Most striking is the prevalence of -7/del(7q) in t-MN, where it occurs in up to 49% of cases, and particularly those associated with exposure to alkylating agents[9]. -7 and del(7q) have also been detected in CHIP and can be an initiating event in transformation[19,22,55,227]. However, the pathogenesis of -7/del(7q) in t-MN remains unclear.

We identified *CUX1* as a haploinsufficient myeloid tumor suppressor gene encoded on 7q22.1[79,96]. In addition to *CUX1* loss through -7/del(7q), *CUX1* inactivating mutations have been found in CHIP, myeloid malignancies, and a variety of solid tumors[40,53,66,95,228,229]. Furthermore, *CUX1* inactivating mutations independently carry a poor prognosis in myeloid malignancies[95,198,199]. CUX1 is a non-clustered HOX family transcription factor that is ubiquitously expressed and regulates critical cellular processes such as proliferation and differentiation in disparate cell types[93,96,230]. To identify the role of CUX1 in the hematopoietic compartment, we generated two

doxycycline-inducible, shRNA-based transgenic CUX1-knockdown mouse lines. CUX1-knockdown in mice leads to MDS and MDS/MPN characterized by trilineage dysplasia, anemia, and myelomonocytic expansion[96]. Thus, loss of this single 7q gene is sufficient to cause *de novo* myeloid malignancies.

CUX1 has been reported to epigenetically regulate gene expression through the recruitment of the histone lysine methyltransferase EHMT2 (G9a) to the promoter of one reported locus, *CDKN1A*[100]. In addition to regulating transcription[100,231,232], the enzymatic activity of EHMT2 is required for the DNA damage response via the stabilization of activated ATM at sites of DNA damage, necessary for downstream repair factor recruitment[119,233]. Indeed, histone post-translational modifications are dynamic at sites of DNA damage[188,189,234–238]. For example, phosphorylation of the histone H2AX, to form γH2AX, occurs within minutes and is used as a marker of DNA double strand breaks (DSB)[176]. Other histone modifications, such as methylation, are recognized by DDR proteins to direct repair pathway choice and initiate the recruitment of DDR factors[189]. The interplay of epigenetic modifications and repair of DNA damage is still poorly understood, and the impact of deficiencies in these pathways will be crucial in understanding the cellular response to damage induced by cytotoxic therapy.

In this study, we investigated the relationship between a CHIP gene on 7q, *CUX1*, and the DDR to cytotoxic therapy in hematopoietic cells. We report that CUX1 localizes to sites of DNA damage in hematopoietic cells. Insufficient CUX1 disrupts EHMT2 recruitment and attenuates activated ATM accumulation and DNA damage foci formation, leading to defective DNA repair. Furthermore, CUX1-deficient cells exhibit elevated proliferation after chemotherapy, allowing cells with DNA damage to

outcompete their wildtype counterparts. Finally, we examine the impact of cytotoxic therapy on an *in vivo* mouse model and show that *Cux1* deficiency preceding chemotherapy predisposes mice to an aggressive t-MN, specifically a therapy-related acute erythroleukemia. This study reveals a novel role for CUX1 in regulating the local DDR at the epigenetic level, links CHIP preceding therapy to t-MN, and presents the first mouse model of -7/del(7q)-driven t-MN.

CUX1 loss impairs EHMT2 recruitment to DNA breaks and disrupts DNA damage-induced histone methylation

CUX1 has previously been shown to rapidly accumulate at sites of DNA damage in non-hematopoietic cells[105], suggesting a direct and localized effect on DNA damage repair. We first verified this recruitment following irradiation (6 Gy) in MCF7 human breast cancer cells using ground state depletion superresolution imaging for CUX1 and γH2AX. We confirmed that CUX1 is recruited to sites of DNA damage within one hour, as determined by γH2AX colocalization **(Figure 1A)**. We next assessed if this colocalization extended to hematopoietic cells using a human hematopoietic cell line, K562, derived from a patient with chronic myelogenous leukemia (CML) in blast crisis. One hour after irradiation, we assessed the colocalization of CUX1 and γH2AX. We again employed ground state depletion superresolution imaging, and we examined Förster resonance energy transfer (FRET) between γH2AX (donor) and CUX1 (acceptor) fluorophores (**Figure 1B).** FRET was observed between the fluorophores **(Figure 1C)**, indicating that CUX1 co-localizes with γH2AX and is recruited to sites of DNA damage in hematopoietic cells. We next assessed the transcriptional role for

CUX1 in the DDR. It has previously been reported that CUX1 transcriptionally upregulates expression of DDR genes, including *ATM* and *ATR* in MCF7 cells and mouse embryonic fibroblasts[99]. However, we did not observe this finding in our RNA-seq data from either K562 cells or human $CD34^+$ hematopoietic stem and progenitor cells (HSPCs) after shRNA knockdown of *CUX1* [94,96] **(Figure 1D)**. Absent an obvious transcriptional role for CUX1 in the DDR, and following the observation of CUX1 localization to sites of DNA damage, we explored other known functions of CUX1 that could impact the local DDR. As CUX1 has been reported to recruit EHMT2[100], we hypothesized that CUX1 may regulate DNA repair at the epigenetic level. To test this model, we used a CRISPR/Cas9 approach with guides targeting a safe harbor site, *HPRT* (gHPRT), or *CUX1* (gCUX1) in K562 cells. Single-cell clones were generated from the gHPRT- and gCUX1-transfected pools, and we verified the knockout by western blotting **(Figure 2A).** We assayed global histone post-translational modifications one hour following irradiation (6 Gy) or mock irradiation in gHPRT and gCUX1 K562 cells. To accomplish this, we employed the EpiProfile software for mass spectrometry-based post-translational modification analysis[206]. Histones were extracted and analyzed by liquid chromatography with tandem mass spectrometry according to published methods[205]. The resultant data consisted of quantifications of 120 histone post-translational modifications across all major histones. Histone post-translational modifications known to be induced following irradiation, such as dimethylation of H3K36 (fold-change 1.8, q=0.13)[178] and acetylation of H3K18 (fold-change=4.1, q=0.001)[184], were appropriately induced in HPRT cells following irradiation, indicating that we detected relevant irradiation-induced modifications. Principal component analysis of the

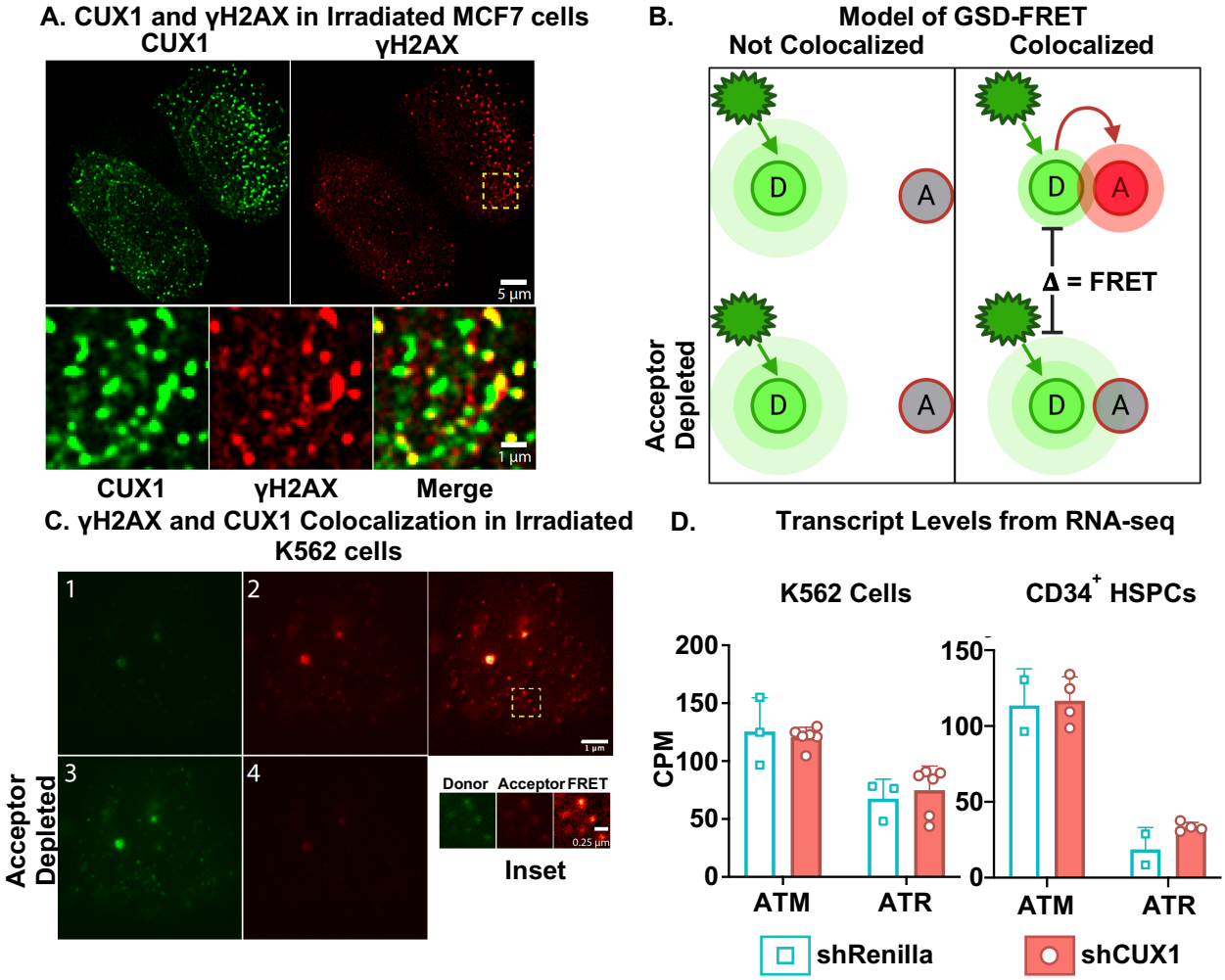


Figure 1. CUX1 rapidly colocalizes to DSBs following irradiation.
A, Superresolution imaging of irradiated MCF7 cells showing CUX1 (green) and γH2AX (red). Colocalization of CUX1 with γH2AX is shown in yellow. Cells were fixed 1 hour after irradiation (6 Gy) and imaged on a Leica GSD imaging system (n=3). **B,** Model of GSD-FRET. Target proteins are identified with antibodies tagged with either a donor (D) or acceptor (A) fluorophore. An image is taken using the donor excitation maxima. If the donor fluorophore is not near an acceptor fluorophore, the donor will emit all energy at the donor emission wavelength (left panel, top). If the donor is colocalizing with the acceptor fluorophore, some of the donor emission energy will be transferred to the acceptor, in proportion to the proximity to the acceptor (right panel, top). The samples are then bleached at the acceptor wavelength, and the bleached acceptors are no longer able to absorb energy. The samples are then reimaged at the donor excitation wavelength. Any increase in donor brightness in the second image compared to the first image is proportional to the energy that was previously transferred to the acceptor, or FRET (bottom right). If the molecules were not colocalizing, there will be no change in donor emission intensity, and no FRET (bottom left). **C,** GSD-FRET analysis of colocalization between γH2AX (donor) and CUX1 (acceptor) in K562 cells. Bottom row images are following depletion of the acceptor fluorophore. Inset shows representative FRET. Images shown are representative of results from three independent experiments. **D,** *ATM* and *ATR* transcripts measured by RNA-seq in shRenilla and shCUX1 cells in K562 cells (Arthur *et al.*, 2017) and human CD34 HSPCs (An *et al.*, 2018) (extracted from published RNA-seq data).

histone post-translational modification matrix showed that while irradiation induced changes in histone post-translational modifications in gHPRT cells (principle component 1, 31.8% of variance), these changes did not occur in gCUX1 cells, and gCUX1 samples clustered together, separately from gHPRT cells **(**principle component 2, 16.8% of variance), irrespective of radiation status **(Figure 2B)**. These results indicate that CUX1 is necessary for DNA damage-induced histone alterations following irradiation.

As CUX1 recruits the histone methyltransferase EHMT2 to the *CDNK1A* locus, we hypothesized that CUX1 might also be responsible for recruiting EHMT2 to sites of DNA damage. This function could then explain, in part, the altered epigenetic response in gCUX1 cells post-irradiation. We irradiated gHPRT and gCUX1 K562 cells and performed immunofluorescence imaging for EHMT2 and γH2AX. One hour after irradiation of gHPRT cells, EHMT2 colocalizes with γH2AX, consistent with prior reports in non-hematopoietic cells[239]. In gCUX1 cells, EHMT2 colocalization with γH2AX is significantly reduced **(Figure 2C).** To verify the importance of EHMT2 enzymatic activity in DSB repair, we treated cells with the selective EHMT2 inhibitor, UNC0642[240]. The addition of UNC0642 to gHPRT cells reduced EHMT2-γH2AX colocalization to the extent seen in gCUX1 cells. The addition of the inhibitor did not further decrease EHMT2-γH2AX colocalization in gCUX1 cells, suggesting that CUX1 acts upstream of EHMT2 recruitment **(Figure 2C).** We further confirmed the role of CUX1 in EHMT2 localization to DSBs by GSD-FRET**.** In agreement with the immunofluorescence data, we found significantly decreased EHMT2-γH2AX interaction in gCUX1 cells **(Figure 2D,E).** Overall, CUX1 is required for the recruitment of EHMT2 to sites of DNA damage.

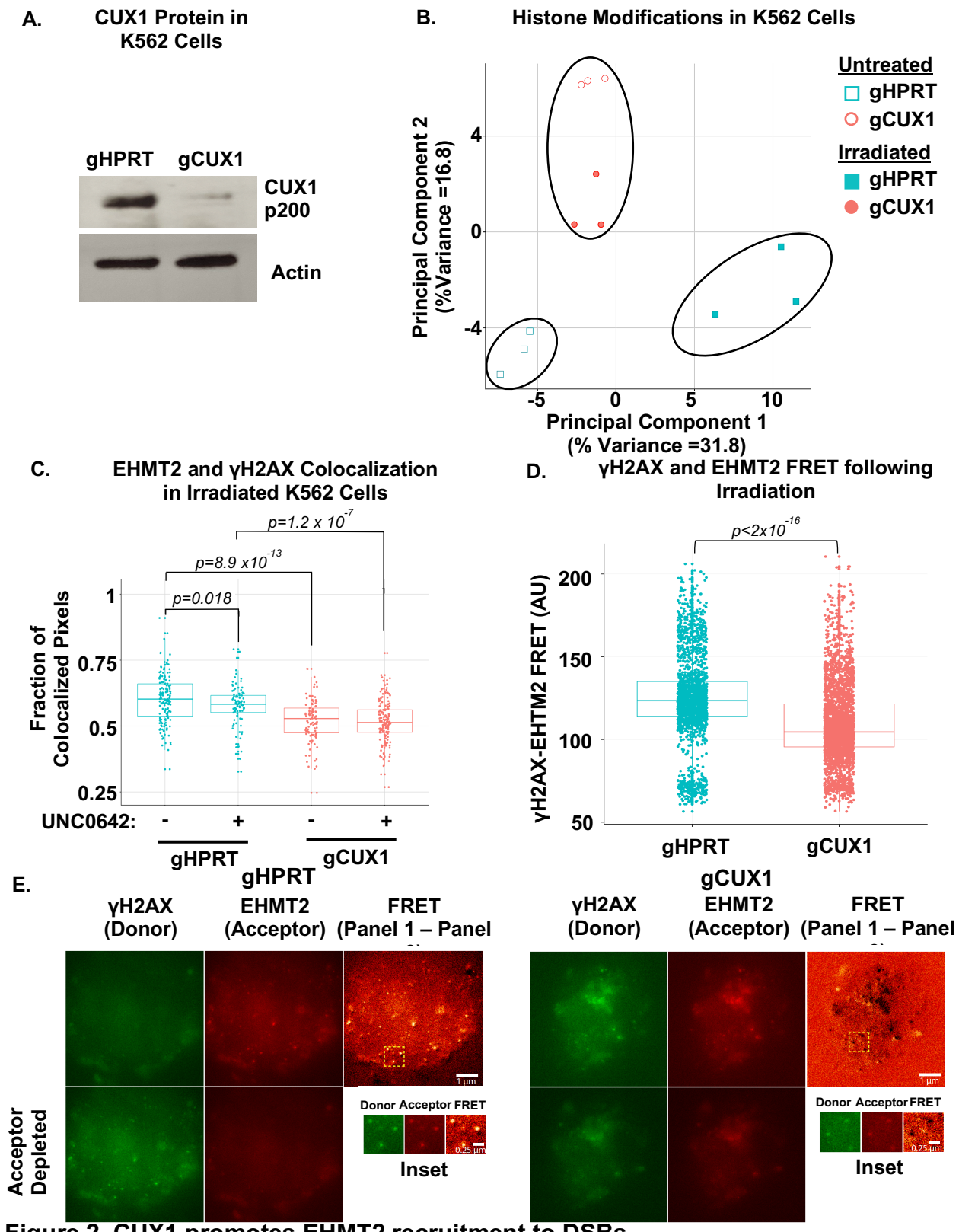


Figure 2. CUX1 promotes EHMT2 recruitment to DSBs.

A, Representative immunoblot for CUX1 protein in gHPRT and gCUX1 K562 cells (n=3)

Figure 2, continued

B, PCA analysis of the histone PTM matrix generated with EpiProfile analysis of histone PTMs in irradiated and mock-irradiate gHPRT and gCUX1 K562 cells. Histones were extracted 1 hour following irradiation (6 Gy). Results shown are derived from analysis of three independent samples. **C,** Immunofluorescence imaging for EHMT2 and γH2AX colocalization 1 hour after irradiation (6 Gy). Colocalization was quantified in gHPRT and gCUX1 K562 cells after irradiation with or without the addition of an EHMT2 inhibitor, UNC0642, 60 minutes prior to irradiation. The fraction of colocalized pixels was calculated per nucleus. Results shown are a composite of four independent experiments. **D,** GSD-FRET analysis of colocalization between γH2AX (donor) and EHMT2 (acceptor) in gHPRT and gCUX1 K562 cells (n=3). **E,** A representative image of FRET in gHPRT cells (left) and gCUX1 cells (right) is shown. Significance was determined with a Student *t* test between indicated samples.

Best recognized for dimethylating H3K9, EHMT2 can catalyze the mono- and dimethylation of H3K27[100,241–243]. EHMT2 also promotes H3K27 trimethylation through direct interaction with EZH2, a member of the Polycomb Repressive Complex 2 (PRC2); Mozzetta et al. reported that EHMT2 enzymatic activity is required to recruit EZH2 to common target genes, and loss of EHMT2 results in a global reduction in EZH2 binding and H3K27me3[244]. EHMT2 and EZH2 have also been reported to cooperate in gene regulation[245,246]. H3K27 and H3K9 methylation both play important roles in the early DDR[189,233,239,247]. To determine if impaired EHMT2 recruitment in CUX1-deficient cells attenuated damage-induced histone methylation, we examined our mass-spec proteomics data. One hour after irradiation, we observed decreased H3K9me2 and H3K9me3 post-irradiation in gCUX1 chromatin, although this did not achieve significance (p=0.11, p=0.13, **Figure 3A)**. H3K9me1 was increased after irradiation in both gHPRT and gCUX1 cells, with significantly more H3K9me1 in gCUX1 cells **(Figure 3A)**. As methylation of H3K9 to form H3K9me2/3 is upregulated in DNA damage repair[177], this increased H3K9me1 could be due to a failure to convert H3K9me1 to H3K9me2/3 after irradiation. On the other hand, H3K27me2 and H3K27me3 levels were significantly lower in gCUX1 cells compared to gHPRT cells, while H3K27me1 was upregulated appropriately after irradiation **(Figure 3B)**. The H3K27me2 phenotype was entirely damage-dependent, with significant differences in H3K27 dimethylation only appearing after irradiation **(Figure 3B)**. In contrast, H3K27me3 was significantly decreased both in irradiated and unirradiated cells after CUX1 loss. In summary, DNA damage-induced H3K9 and H3K27 methylation is disrupted by loss of CUX1, with more significant perturbation of H3K27 di- and tri-methylation.

Given that H3K27me3 was decreased in both untreated and irradiated gCUX1 cells, we next determined the basal level of H3K27me3 by chromatin immunoprecipitation (ChIP)-seq. Differential analysis revealed 848 loci with significantly decreased H3K27 trimethylation in gCUX1 K562 cells compared with just 130 sites that significantly gained H3K27Me3 in gCUX1 cells (10% FDR). H3K27me3 occupancy was also significantly decreased across all peaks (binomial p value=7.35 x 10^{-60}) **(Figure 3C-E, Table 1).** This global decrease in H3K27me3 in unirradiated gCUX1 cells corroborates our proteomics data **(Figure 3B)**, and suggests that CUX1 loss impairs H3K27 methylation. By RNA-seq, the expression of H3K27 methyltransferases, including the PRC2 complex members and *EHMT2*, was not reduced after CUX1 knockdown in $CD34^+$ HSPCs or K562 cells after CUX1 knockdown, nor was expression of H3K27 demethylases upregulated **(Figure 4A,B)** [94,96,248]. This finding implicates a non-transcriptional role for CUX1 in steady-state and DNA damage-induced H3K27me2/3 deposition.

CUX1 is necessary for DNA repair and foci formation

We next investigated whether the global decreases in H3K9 and H3K27 methylation seen after irradiation in CUX1-deficient cells were due to a loss of methylation specifically at sites of DNA damage. To investigate DSB-proximal histone methylation, we used immunofluorescence imaging to quantify methylation within γH2AX foci one hour after irradiation (6 Gy). Following irradiation, H3K9me1, H3K9me2 and H3K9me3 were significantly decreased at γH2AX foci in gCUX1 cells **(Figure 5)**. We found that H3K27 monomethylation was increased, while H3K27 di- and

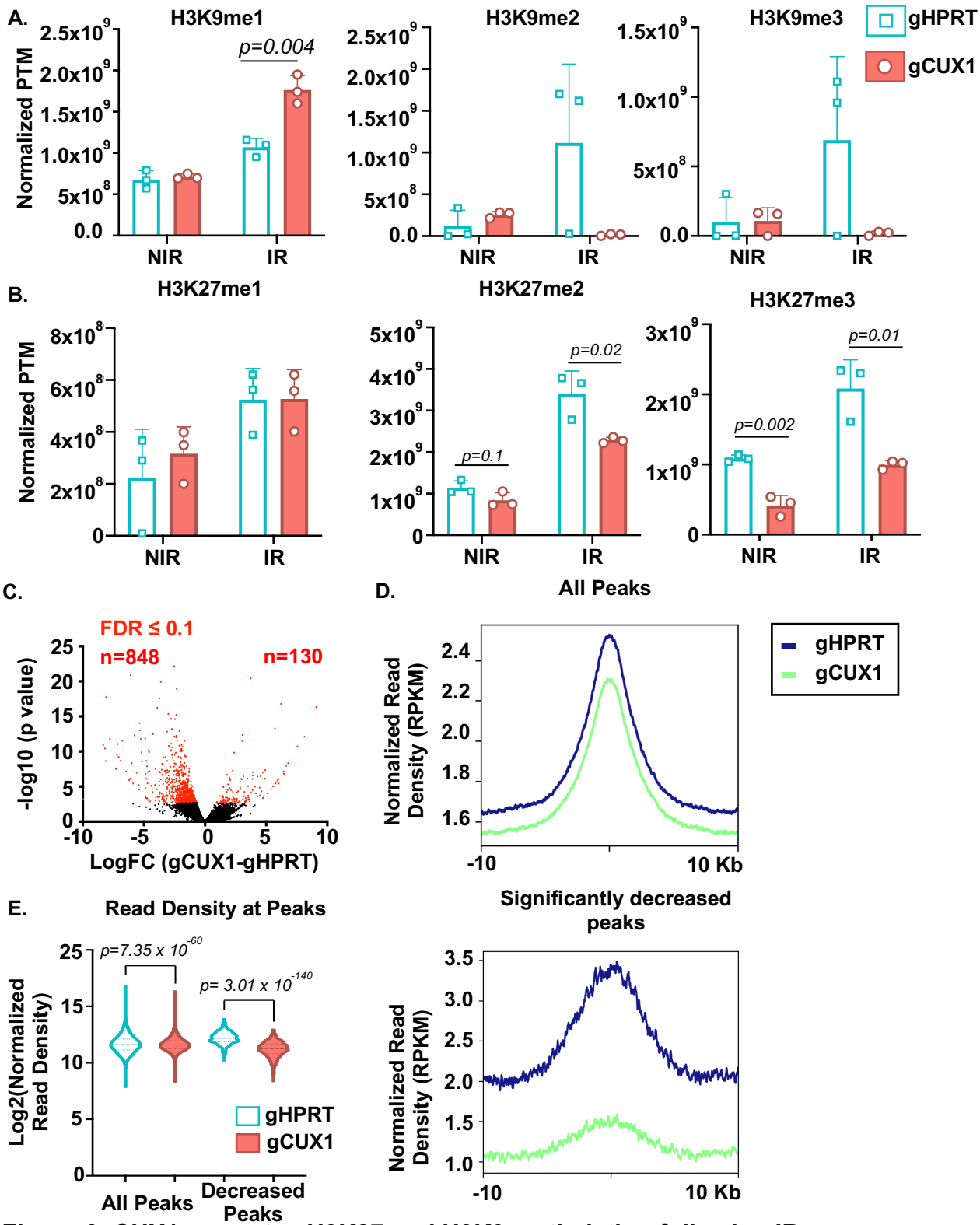


Figure 3. CUX1 promotes H3K27 and H3K9 methylation following IR.

A, EpiProfile analysis of H3K9 methylation in irradiated and mock-irradiated gHPRT and gCUX1 cells. **B,** EpiProfile analysis of H3K27 methylation in irradiated and mock-

Figure 3, continued
irradiated gHPRT and gCUX1 K562 cells. Histones were extracted 1 hour following irradiation (6 Gy). Significance was determined with a Student *t* test between indicated samples. Results shown are derived from analysis of three independent samples. **C,** ChIP-seq of H3K27me3 in K562 cells. Volcano plot showing differentially occupied ChIP-seq sites (n=2) between clonal gHPRT and gCUX1 K562 cell lines. Each point is the average of two replicates. DiffBind was used to identify significantly differentially occupied sites. Red points indicate significance ≤ 10% FDR. **D,** The panels depict a smooth line fit to the average column-wise read density for all differentially bound sites across the 20kb window. The top panel shows all H3K27me3 sites and the bottom shows only H3K27me3 sites significantly decreased in gCUX1 cells (10% FDR). **E,** The normalized read density is quantified at all H3K27me3 sites and at H3K27me3 sites significantly decreased in gCUX1 cells. A Wilcoxon signed-rank test was used to determine significance.

Table 1. ChIP-seq and RNA-seq Sequencing Reads Table

ChIP-seq (H3K27me3)	PF Clusters	Mapped reads (q30)
K562 gHPRT H3K27me3 ChIP-seq Rep 1	4.71E+07	3.60E+07
K562 gCUX1 H3K27me3 ChIP-seq Rep1	3.95E+07	3.07E+07
K562 gHPRT H3K27me3 ChIP-seq Rep 2	4.09E+07	2.59E+07
K562 gCUX1 H3K27me3 ChIP-seq Rep2	3.72E+07	3.01E+07
RNA-seq on Murine HSCs	**PF Clusters**	**Mapped Reads (q30)**
Renilla_HSC_Rep1	7.76E+07	2.06E+07
Renilla_HSC_Rep2	7.19E+07	4.69E+07
Renilla_HSC_Rep3	5.57E+07	4.56E+07
Cux1-low HSC Rep1	7.07E+07	1.69E+07
Cux1-low HSC Rep2	6.48E+07	5.12E+07
Cux1-low HSC Rep3	6.10E+07	4.98E+07

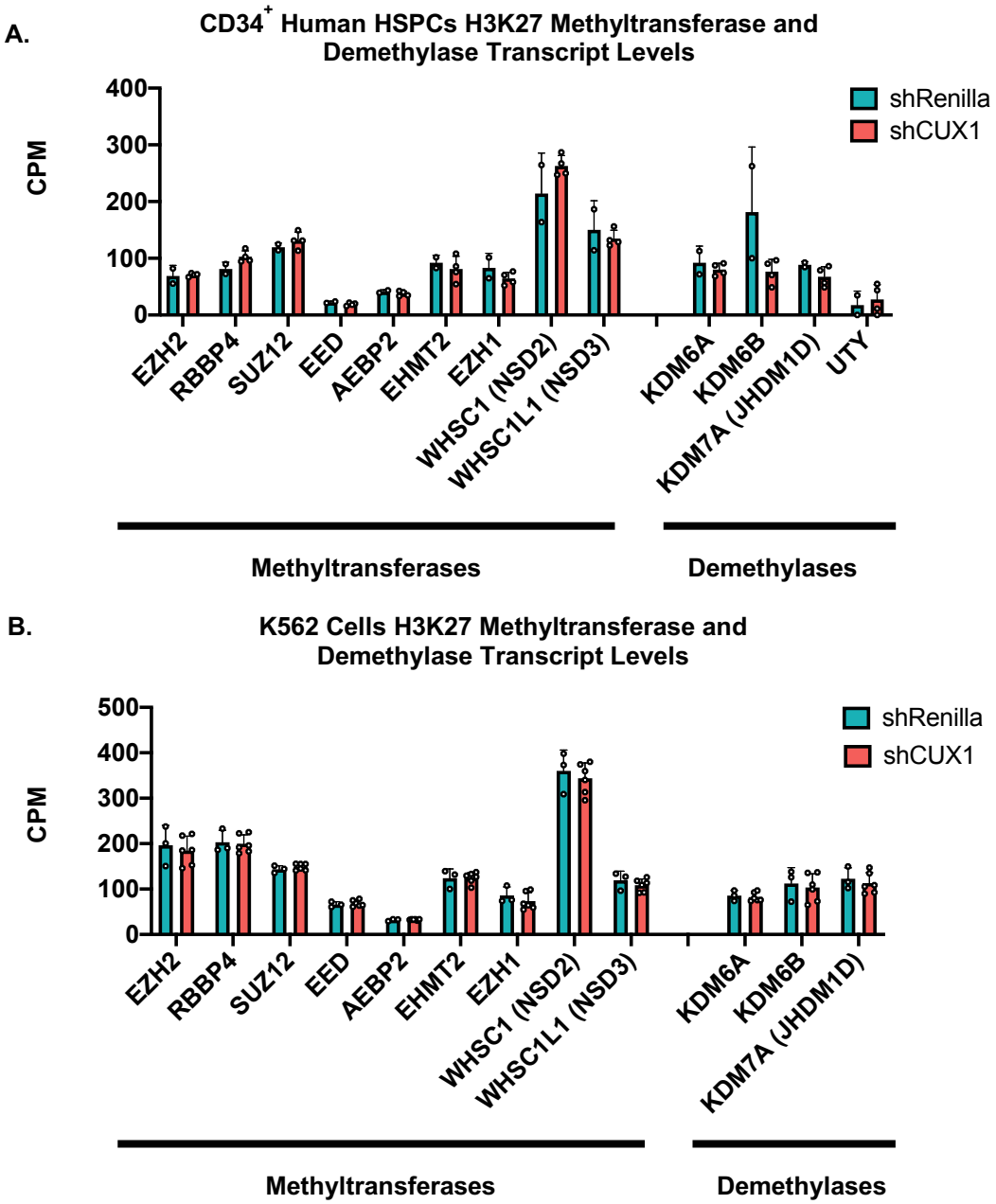


Figure 4. Methyltransferase and demethylase transcript levels are not decreased in CUX1-deficient cells.

Transcripts of H3K27 methyltransferases and demethylases in **A,** human CD34$^+$ HSPCs (An *et al.*, 2018) and **B,** K562 cells (Arthur *et al.*, 2017) after CUX1 knockdown. (Extracted from previously published RNA-seq data).

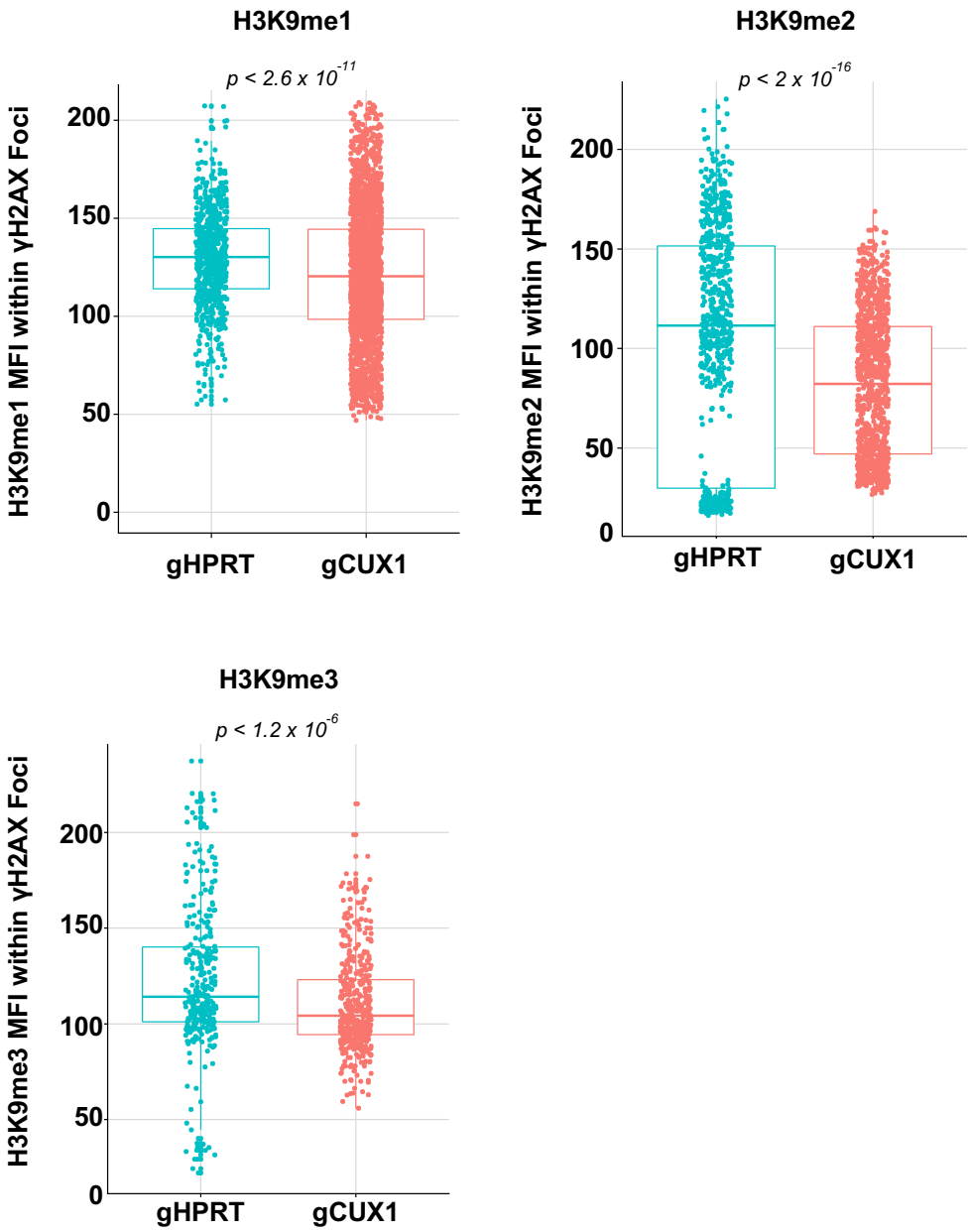


Figure 5. CUX1 knockdown leads to reduced H3K9 methylation at foci.

Cells were imaged for antibodies targeting γH2AX and H3K9 methylation 1 hour following irradiation. H3K9me1/2/3 MFI was quantified within each γH2AX foci. Significance was determined with a Student t test between indicated samples, with results displayed as a composite of three biological replicates.

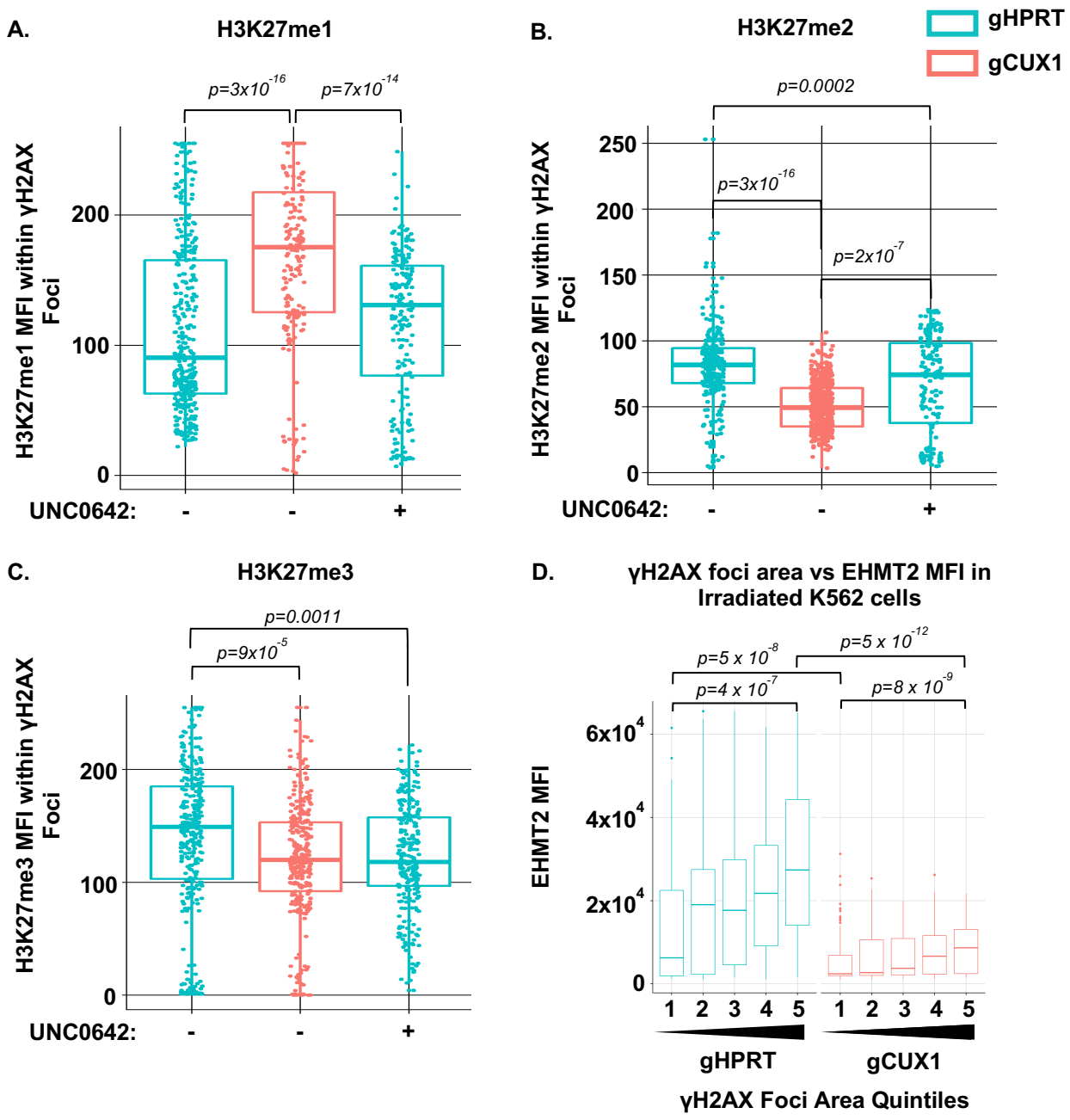


Figure 6. CUX1 loss inhibits H3K27 methylation at foci.

Cells were imaged for antibodies targeting γH2AX and H3K27 methylation. **A,** H3K27me1, **B,** H3K27me2 and **C,** H3K27me3 mean fluorescent intensity (MFI) were quantified within each γH2AX foci. **D,** γH2AX foci size was quantified and broken into quintiles by size, with Q1 containing the smallest foci, and Q5 the largest. The size of individual γH2AX foci was determined using a custom ImageJ macro. EHMT2 intensity was quantified by MFI within each γH2AX foci quintile. All plots are compiled from data derived from three independent biological replicates. Significance was determined with a Student t test between indicated samples.

trimethylation were significantly decreased at γH2AX foci after irradiation in gCUX1 K562 cells compared to gHPRT cells **(Figure 6A-C)**. Inhibition of EHMT2 using UNC0642 in gHPRT cells recapitulated the loss of CUX1, with significantly decreased H3K27me2 and H3K27me3 within γH2AX foci. **(Figure 6A-C)**. Thus, CUX1 is necessary for H3K9me1/2/3 and H3K27me2/3 deposition at sites of DNA damage.

Previously, EHMT2 was shown to be required for sustained retention of activated, phosphorylated ATM (pATM) at sites of DNA damage for signal amplification and foci expansion following DSBs[119]. To determine if CUX1 is required for EHMT2-mediated foci formation or spreading, we used immunofluorescence imaging to quantify the relationship between EHMT2 accumulation and γH2AX foci size one hour after irradiation (6 Gy). In gHPRT cells, EHMT2 accumulation correlates with increasing foci size, suggesting that EHMT2 recruitment is permissive for foci spreading **(Figure 6D)**. This correlation was maintained in gCUX1 cells, with increasing foci size corresponding to increased EHMT2, albeit with markedly decreased overall recruitment of EHMT2 **(Figure 6D)**. This led us to hypothesize that γH2AX foci would be smaller and less numerous in gCUX1 cells. We irradiated gHPRT and gCUX1 cells with 6 Gy gamma irradiation to induce DSBs. One hour after irradiation, the number of γH2AX foci was determined. Indeed, immunofluorescent staining for γH2AX revealed that loss of CUX1 in K562 cells led to significantly decreased γH2AX foci size **(Figure 7A)**, as well as decreased overall foci numbers **(Figure 7B)**. Similarly, treating gHPRT control cells with UNC0642 prior to irradiation led to decreased foci numbers, reducing γH2AX foci to the level seen in gCUX1 cells. UNC0642 treatment did not further reduce foci numbers in

gCUX1 cells **(Figure 7B)**. These data indicate that CUX1 is necessary early in the DNA repair process, upstream of H2AX phosphorylation and propagation.

To determine if decreased γH2AX foci size in gCUX1 cells was due to a failure to retain pATM at breaks, as seen in EHMT2-depleted cells[119], we performed immunofluorescence imaging for pATM after irradiation (6 Gy). ATM activation did occur in gCUX1 cells, with total nuclear pATM MFI elevated compared to gHPRT cells **(Figure 7C).** However, the pATM was not retained at γH2AX foci. pATM intensity within γH2AX foci was significantly decreased in gCUX1 cells compared to gHPRT cells after irradiation **(Figure 7D)**. EHMT2-depleted cells are similarly reported to show normal ATM phosphorylation coupled with a failure to accumulate pATM at sites of DNA damage[119]. As pATM retention at breaks is necessary for γH2AX foci spreading and downstream activation of DNA damage repair factors[120], we next examined repair factor recruitment. Both H3K27me2/3[189] and EHMT2[233] have been independently reported to be required for efficient recruitment of 53BP1, a critical component of DSB signaling and non-homologous end joining. We therefore performed immunofluorescent imaging for 53BP1 in irradiated CUX1-deficient cells and found that 53BP1 intensity at γH2AX foci was decreased in gCUX1 cells **(Figure 7E)**. In summary, CUX1-deficient cells fail to recruit EHMT2 to breaks and deposit H3K27 di- and trimethylation marks, leading to decreased γH2AX foci formation and spreading, decreased local pATM, and decreased localization of 53BP1 at sites of DNA damage.

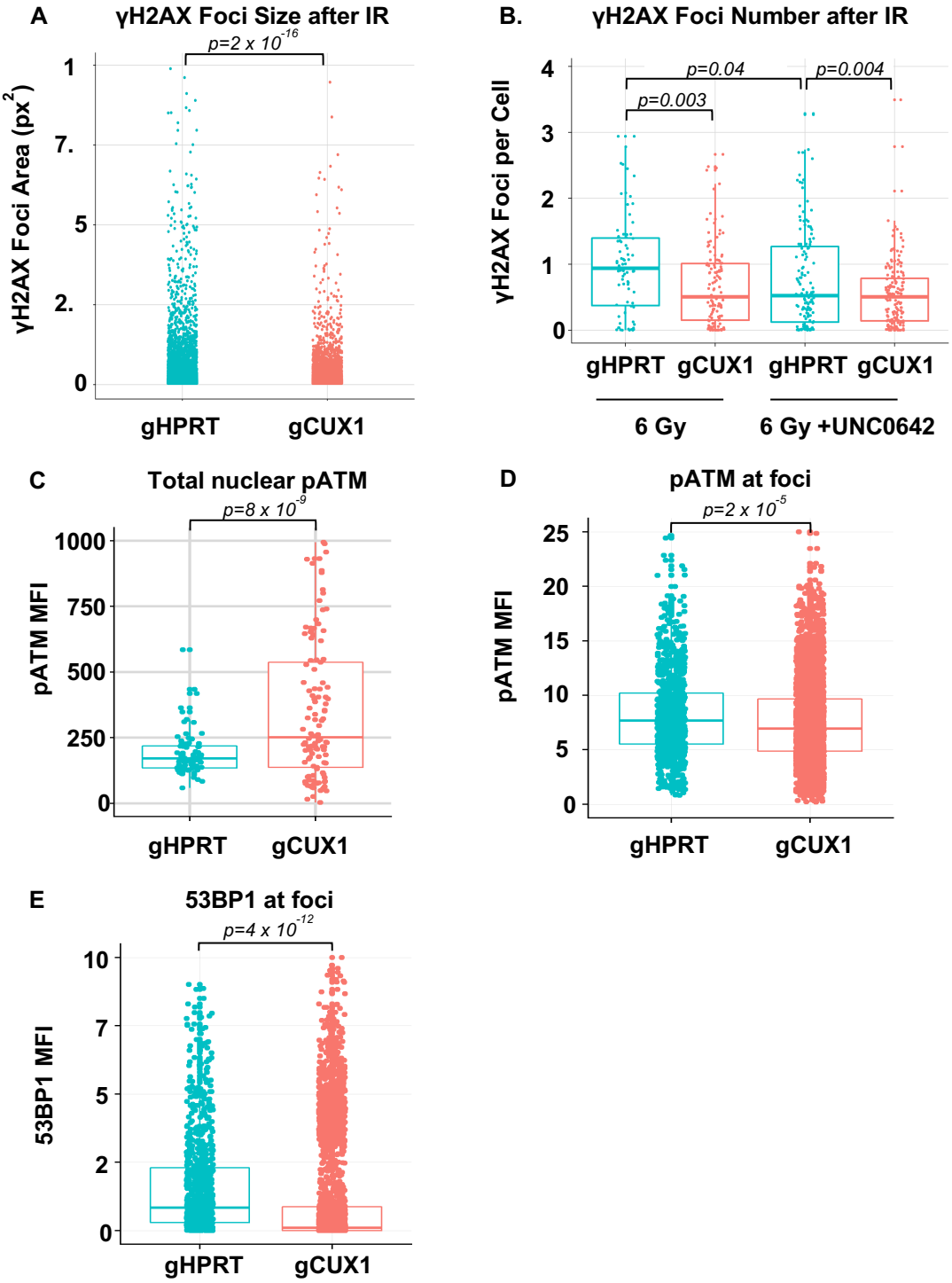


Figure 7. CUX1 loss impairs DNA damage recognition and foci formation.

K562 cells were irradiated (6 Gy) and imaged 1 hour post-irradiation. **A,** γH2AX foci size in gHPRT and gCUX1 cells **B,** Mean number of γH2AX foci per cell following irradiation with and without UNC0642. **C,** The intensity of total pATM (MFI) per nucleus was quantified after irradiation. **D,** The intensity of pATM within γH2AX foci. **E,** The intensity of 53BP1 within γH2AX foci. All plots are compiled from data derived from three independent biological replicates.

CUX1-deficient HSPCs have an impaired DNA damage response and unrepaired DNA damage *in vivo*

To determine if the DNA repair defects in CUX1-deficient K562 cells *in vitro* are also present in primary, CUX1-deficient hematopoietic cells *in vivo*, we used our two doxycycline-inducible shRNA transgenic mouse models[96]. Cux1^{mid} and Cux1^{low} lines express distinct shRNAs targeting *Cux1*[96]. Littermates expressing an shRNA targeting renilla luciferase were used as controls (Ren). Compared to Ren, Cux1^{mid} have 58% and Cux1^{low} have 42% residual *Cux1* expression in hematopoietic lineage^{-}/Sca-1^{+}/Kit^{+} cells (LSKs)[96]. We first assessed whether CUX1-deficient HSPCs exhibit the reduced γH2AX foci formation apparent in gCUX1 K562 cells. We treated Ren, Cux1^{mid} and Cux1^{low} mice with doxycycline for one week and collected whole bone marrow. We irradiated the bone marrow cells *ex vivo* (2 Gy) and performed intracellular flow cytometry to assess H2AX phosphorylation at 30 minutes, 1 hour, 4 hours and 6 hours post-irradiation. In agreement with our human cell line data, we found that CUX1-deficient HSPCs showed attenuated phosphorylation of H2AX. This was true in both LSKs and total lineage-negative cells (**Figure 8A).** These data indicate that CUX1 is necessary for recognition of DNA damage in primary, murine HSPCs.

To assess if CUX1 is required for break repair, in addition to break recognition, we performed neutral comet assays to measure DSBs in HSPCs[249]. In unirradiated cells, we did not detect increased DNA damage in CUX1-knockdown Kit^{+} cells with this assay (**Figure 8B**). However, following a single dose of whole-body gamma irradiation (6 Gy), Cux1^{mid} and Cux1^{low} HSPCs show significantly elevated levels of DSBs when isolated 6 hours post-irradiation **(Figure 8B).** The unrepaired breaks persisted 24 hours after

irradiation in Cux1^{low} HSPCs **(Figure 8B).** Thus, CUX1 deficiency leads to unrepaired DNA damage in HSPCs *in vivo* following irradiation. We find that, in both a human hematopoietic cell line and primary mouse HSPCs, CUX1 is required for H2AX phosphorylation and the resolution of DNA damage.

CUX1-deficient cells upregulate expression of genes involved in proliferation and DNA repair

Although we did not see an obvious role for CUX1 in the transcriptional control of key regulators of γH2AX foci formation, such as *ATM* or *ATR*, in our human RNA-seq data **(Figure 1D),** we sought to further assess a potential transcriptional mechanism for disrupted γH2AX foci formation in CUX1-knockdown HSPCs. To this end, we performed RNA-sequencing on Ren and Cux1^{low} HSCs (Lin^{-}, Kit^{+}, Sca1^{+}, CD135^{-}) after five days of continuous doxycycline. By RNA-seq, *Cux1* transcripts were ~50% decreased in Cux1^{low} HSCs **(Figure 9A)**. We identified 3,323 differentially expressed genes with a false discovery rate of 5%. 1,827 genes were upregulated after CUX1 knockdown, and 1,496 genes were downregulated **(Figure 9B).** As in human CD34^{+} HSPCs and K562 cells, CUX1 knockdown did not lead to decreased gene expression of H3K27 methyltransferases or increased transcription of demethylases **(Figure 10A).** Gene set enrichment analysis (GSEA) using the MSig Database Hallmarks gene set [250] showed that *Cux1* knockdown drives proliferative signatures, including genes activated by E2F and genes involved in progression through the G2M checkpoint, as well

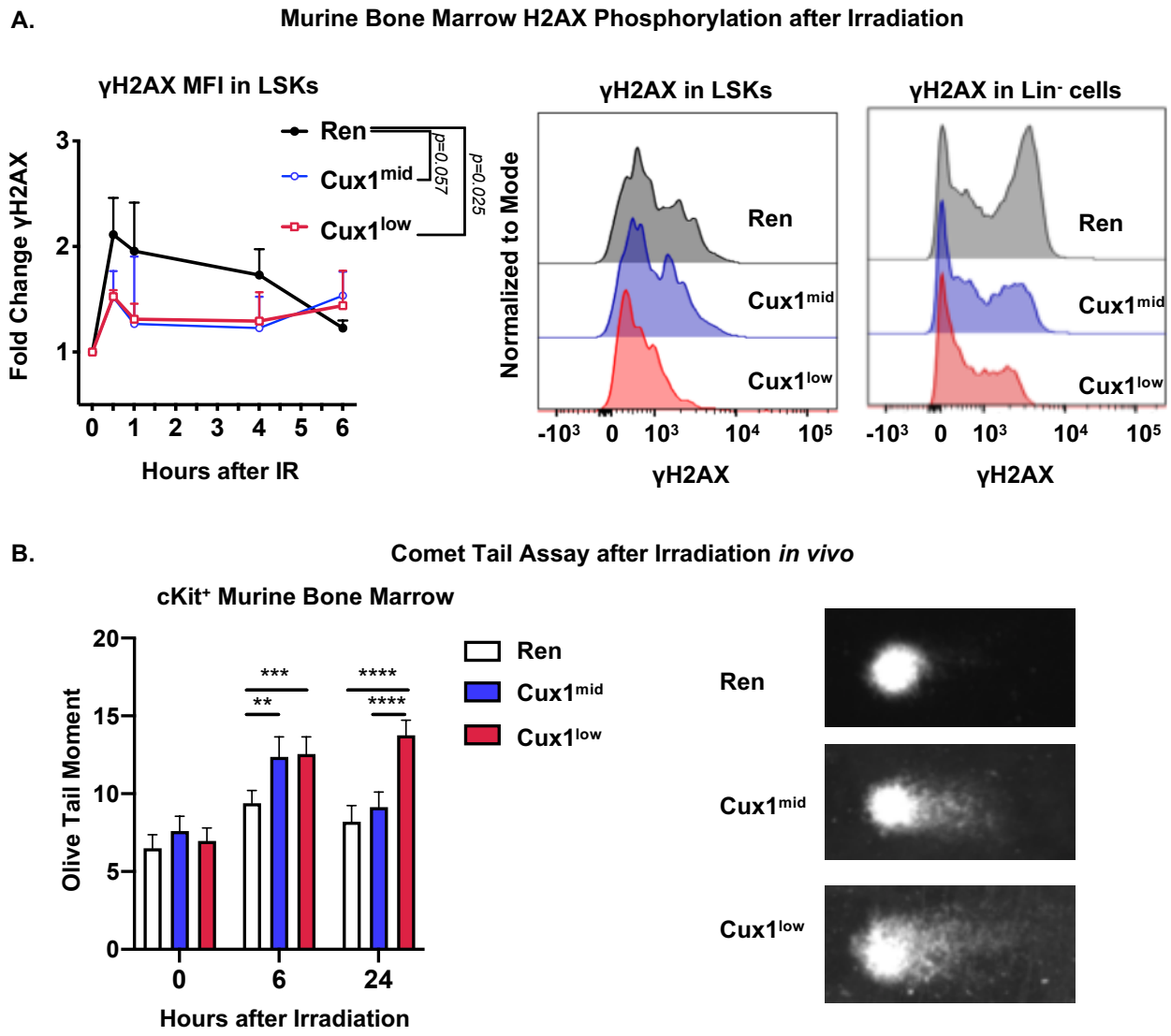


Figure 8. CUX1-deficient HSPCs have an impaired DDR and unrepaired DNA damage *in vivo*.

A, Bone marrow was collected from Ren, Cux1^{mid} and Cux1^{low} mice after treatment with doxycycline for seven days. The cells were irradiated *ex vivo* (2 Gy) and γH2AX induction was measured by intracellular flow cytometry at 30 minutes, 1 hour, 4 hours and 6 hours after irradiation. LSK cells were gated, and γH2AX MFI was normalized to the 0 hour timepoint from each experiment. Representative histograms of γH2AX staining one hour after irradiation in LSKs and total lineage-negative cells are shown. Plot is the result of three independent biological replicates. Data are shown as mean ± SD with p values from a two-way ANOVA. **(B)** Ren, Cux1^{mid} and Cux1^{low} mice were treated with doxycycline for 7 days and subsequently irradiated *in vivo* (6 Gy). Bone marrow was collected at 6 and 24 hours post-irradiation, and Kit^{+} cells were isolated for a neutral comet assay. Representative images are shown (right). Mean ± SEM is shown for three biological replicates. Mann-Whitney test, p>0.05; * p<0.05; ** p<0.01; *** p<0.001; **** p<0.0001

as targets of the pro-survival oncogene MYC **(Figure 9C)**. This is consistent with previous data reporting CUX1 as a regulator of cell cycle, proliferation and quiescence[96,230]. We did not find genes regulating the DDR downregulated (FC < -0.5) after *Cux1* knockdown and, in fact, we found an upregulation of genes involved in DNA. The Hallmark gene sets "DNA Repair" and "UV Response Up" were both upregulated in Cux1^{low} HSPCs. In agreement with the findings in human CD34^{+} HSPCs and K562 cells, transcription of *Atm* and *Atr* were unchanged after CUX1 knockdown **(Figure 10B)**. Our RNA-seq data from shCUX1 K562 cells also showed upregulation of the MSig Database Hallmarks gene sets involved in both proliferation and DNA repair **(Figure 9D)**[94]**.** repair, possibly reflecting a compensatory mechanism for unresolved DNA damage. The Thus, CUX1-knockdown in primary, murine HSCs leads to the upregulation of proliferation and DNA repair pathway genes.

Based on the impaired DNA damage recognition in both CUX1-deficient K562 cells (**Figure 7A,B)** and murine HSPCs **(Figure 8A),** and their simultaneous upregulation of genes involved in the cellular response to DNA damage and genes involved in proliferation **(Figure 9C,D)** we predicted that CUX1-deficient cells proliferate despite unrepaired damage. To test this, we treated gHPRT and gCUX1 K562 cells with irradiation (6 Gy) and measured BrdU incorporation 24 hours later. We found that gCUX1 cells exhibited increased proliferation after exposure to DNA damage compared to gHPRT cells **(Figure 11A).** There was not a significant change in cells undergoing apoptosis after irradiation, as measured by cleaved PARP **(Figure 11B).** In summary, we find that CUX1-deficient cells demonstrate enhanced proliferation in the presence of DNA damage.

Cux1^{low} cells aberrantly proliferate and expand following DNA-damaging alkylating agents

In patients, certain mutations have been shown to provide HSPCs a fitness advantage under the pressure of chemotherapy, enabling these clones to expand[33,56]. We hypothesized that the ability of CUX1-deficient cells to proliferate in the presence of DNA damage would provide a selective advantage under the pressure of chemotherapy. As alkylating agents are the most common chemotherapy exposure preceding t-MN[15], we used an alkylating agent, N-ethyl-N-nitrosourea (ENU), that is well-characterized in mouse models to recapitulate chemotherapy *in vivo*[14,196,251,252]. We performed mixed bone marrow chimera experiments, with Ren, Cux1^{mid} or Cux1^{low} donor bone marrow (CD45.2^{+}) transplanted at a 1:4 ratio with wildtype competitor bone marrow (CD45.1^{+}) into wildtype recipients (CD45.1^{+}). Doxycycline was administered continuously starting at the time of transplant. We allowed the transplants five weeks to engraft, then administered two doses of ENU (100 mg/kg), nine days apart[14], to half of each experimental group **(Figure 12A)**. Upon addition of ENU, Cux1^{low} cells exhibited a significantly increased contribution to the peripheral blood compared to either untreated Cux1^{low} or ENU-treated Ren cells **(Figure 12B).** At 16 weeks, we quantified the ENU-treated HSPCs. ENU-treated Cux1^{low} cells constituted a significantly higher percentage of the LSKs and MPs in the bone marrow and spleen compared to Ren **(Figure 12C, D)**. In the stem and progenitor cell compartments, this increase was largely due to an increase in multi-potent progenitors (MPPs). Cux1^{low} cells were found in increased frequency in the common myeloid progenitor population (CMPs) in the bone marrow and in all progenitor populations (CMPs, GMPs and MEPs) in the spleen **(Figure 12C,**

D). Unlike Cux1^{low}, Cux1^{mid} cells did not expand after ENU in this experiment, which is consistent with the generally milder phenotypes observed in Cux1^{mid} mice[96]. In summary, Cux1^{low} HSPCs have a competitive advantage in the transplant setting following ENU, characterized by an expanded progenitor population.

We tested whether the blunted DNA damage recognition in Cux1^{low} cells **(Figure 8A)** leads to a failure to halt proliferation post-DNA damage, as seen in gCUX1 K562 cells **(Figure 11A)**. We treated Ren and Cux1^{low} mice with two doses of ENU, 9 days apart, with BrdU administered after the second dose of ENU. Cux1^{low} mice showed increased BrdU incorporation in the 24 hours following treatment with ENU compared to control cells (**Figure 13A)**, without an increase in apoptosis **(Figure 13B).** Thus, we conclude that CUX1 deficiency drives a fitness advantage under the selective pressure of chemotherapy, characterized by persistent proliferation following DNA-damaging agents.

CUX1-deficient mice develop therapy-related myeloid neoplasms after alkylator chemotherapy exposure

Recent studies suggest that in many patients, pre-existing mutant HSPCs expand and transform to a t-MN after chemotherapy[54,56,225]. Therapy-induced CHIP is enriched for DNA damage response genes[33,56]. Thus, we investigated the link between defective DDR in CUX1-deficient cells and t-MN susceptibility. We treated adult Ren, Cux1^{mid} and Cux1^{low} mice continuously with doxycycline for one month to induce CUX1 knockdown, followed by acute chemotherapy exposure (ENU, 100 mg/kg) **(Figure 14A)**. A small number (n=2/12, 17%) of the ENU-treated control mice developed lymphoid disease,

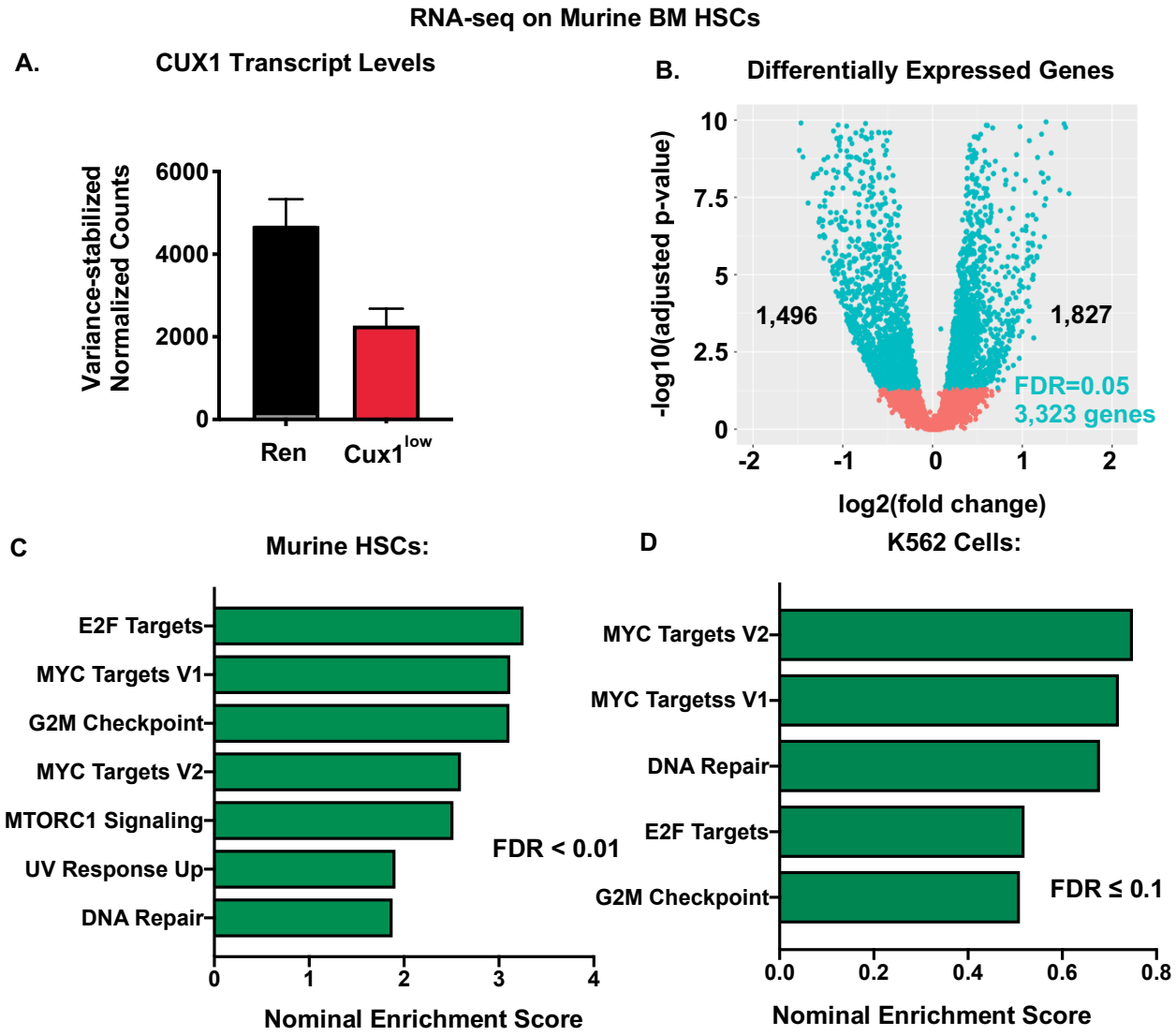


Figure 9. CUX1-deficient cells upregulate expression of genes involved in proliferation and DNA repair.

A, Ren and Cux1^{low} mice were treated with doxycycline for 5 days, and HSCs (lineage$^-$/cKit$^+$/Sca1$^+$/CD135$^-$) were sorted for RNA-sequencing, for a total of 3 biological replicates. *Cux1* transcript levels (excluding *Casp* isoforms) by RNA-seq are shown. **B,** Volcano plot showing gene expression changes in HSCs by RNA-seq after CUX1 knockdown. Blue color indicates differentially expressed genes with a false discovery rate (FDR) less than 5%. GSEA using the "Hallmarks" gene set from the MSig Database[250] of **C,** murine HSCs and **D,** shRen and shCUX1 K562 cells (previously published RNA-seq)[94]. Hallmark gene sets involved in proliferation and DNA damage repair with an FDR ≤ 0.1 are shown. Nominal enrichment score is plotted.

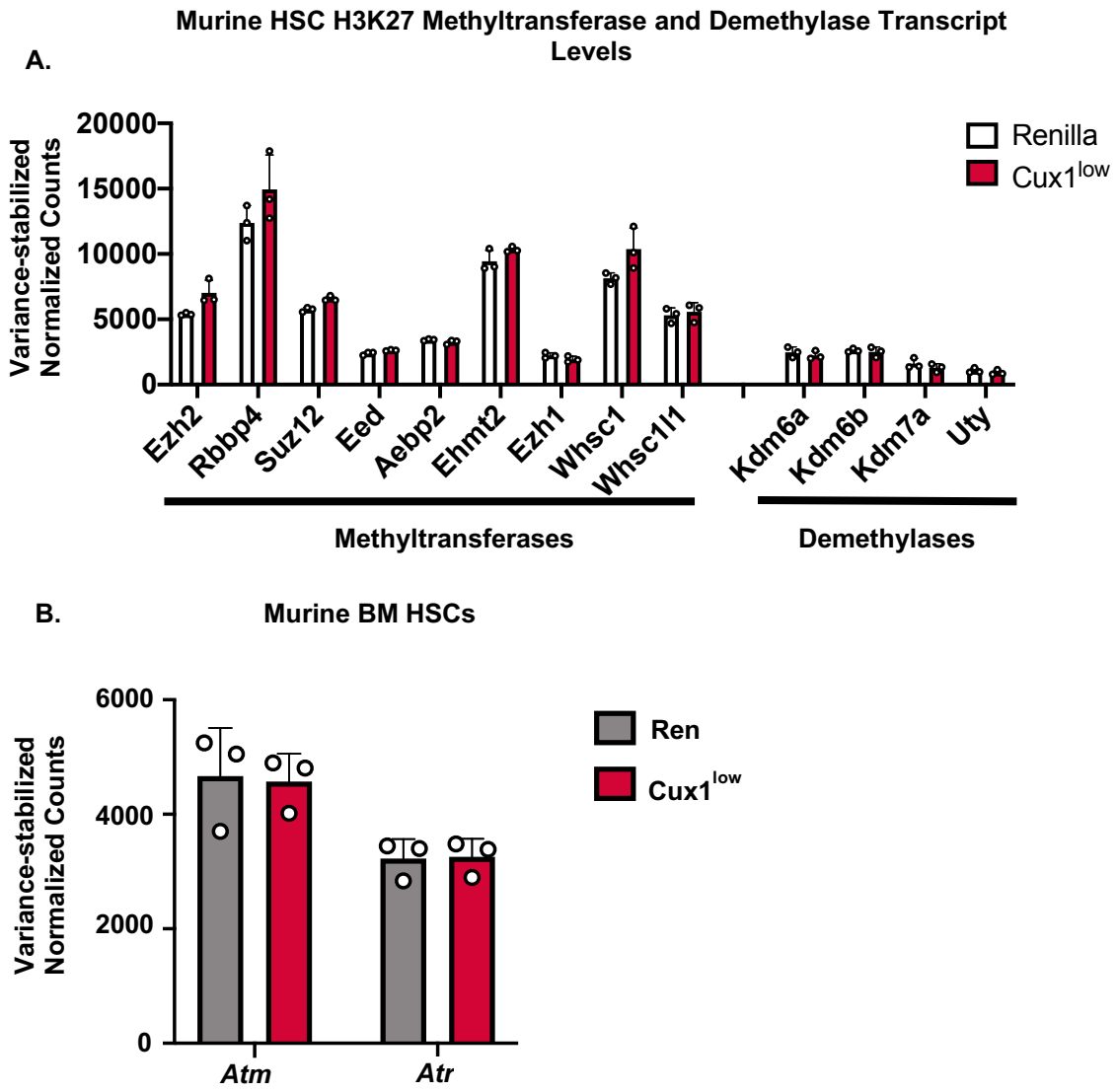


Figure 10. CUX1 does not transcriptionally regulate H3K27 methyltransferases and demethylases in murine HSCs.

A, Expression of H3K27 methyltransferases and demethylases in murine HSCs (lineage$^-$/cKit$^+$/Sca1$^+$/CD135$^-$) from RNA-seq data (n=3). **B,** *Atm* and *Atr* transcripts by RNA-seq from sorted murine HSCs**.**

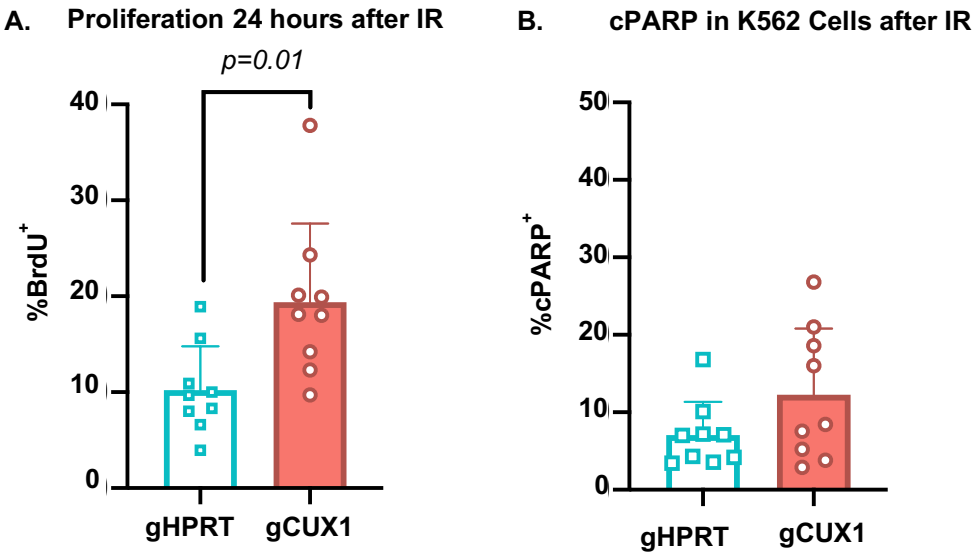


Figure 11. CUX1-deficient human K562 cells aberrantly proliferate following irradiation.

24 hours after irradiation (6 Gy), **A,** proliferation and **B,** apoptosis were assessed in gHPRT and gCUX1 K562 cells. Proliferation was measured via BrdU incorporation one hour before analysis. Apoptosis was measured via cleaved PARP (cPARP). Mean ± SD is shown for three biological replicates. Significance was determined with a Student *t* test between indicated samples.

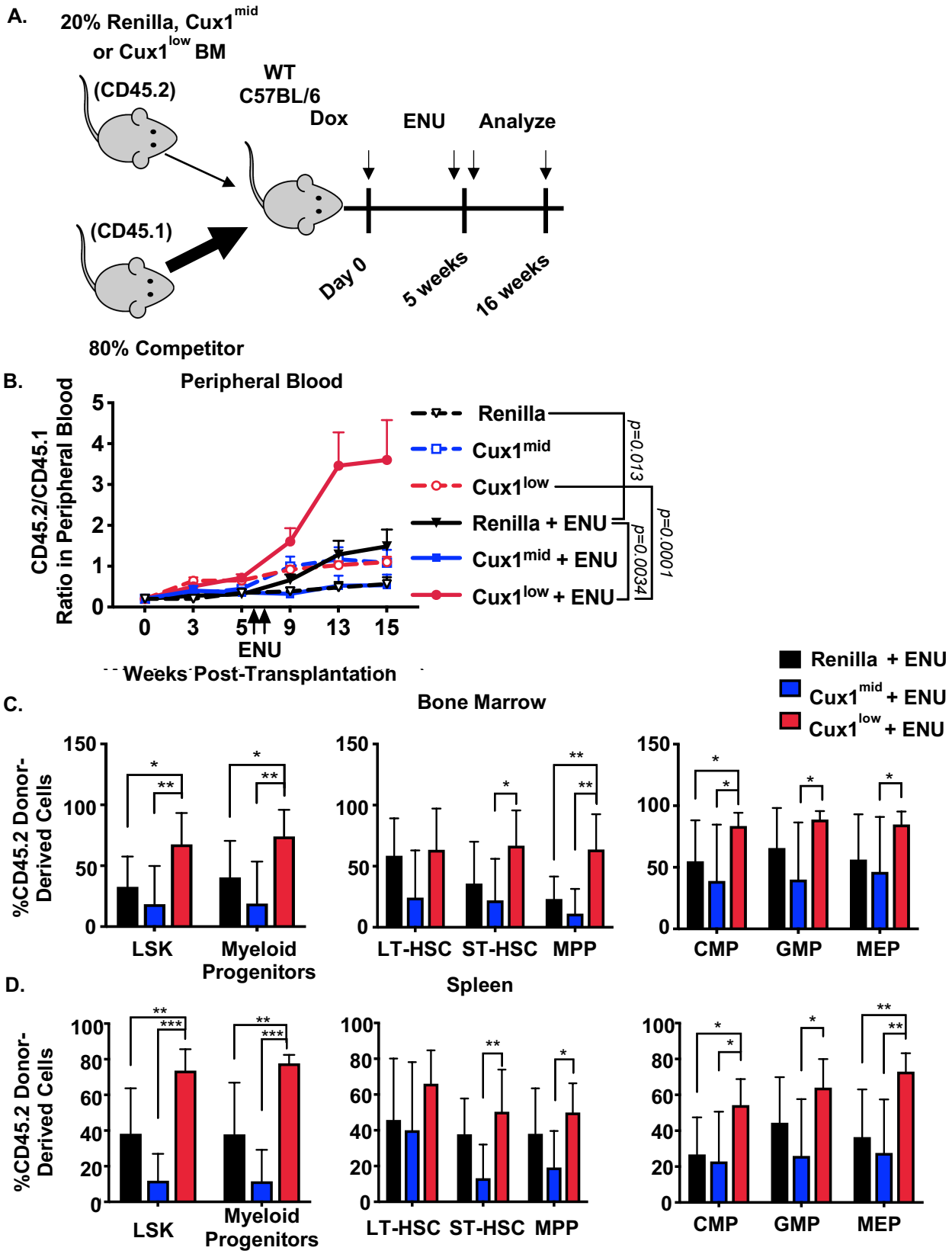


Figure 12. Cux1^{low} cells aberrantly proliferate and expand following DNA-damaging alkylating agents

Figure 12, continued
A, Bone marrow from Ren, Cux1^{mid} and Cux1^{low} mice was transplanted at a 1:4 ratio with competitor bone marrow and recipients were treated continuously with doxycycline beginning the day of transplant. Two doses of ENU (100 mg/kg) were administered 9 days apart, starting five weeks after transplant. **B,** The contributions of Ren (n=9), Cux1^{mid} (n=8) and Cux1^{low} (n=9) cells to the peripheral blood were monitored by flow cytometry. The ratio of Ren, Cux1^{mid} or Cux1^{low} cells (CD45.2) to competitor cells (CD45.1) is shown. The mean ± SEM is shown. A mixed-effects analysis with the Geisser-Greenhouse correction is shown. Two independent biological replicates were performed (n=4-5 mice per replicate per genotype). At 16 weeks, the mice were sacrificed and the contributions of Ren, Cux1^{mid} and Cux1^{low} (CD45.2) to the hematopoietic stem and progenitor populations were measured by flow cytometry in the **C,** bone marrow and **D,** spleen. LSK (Lin^{-}/Sca1^{+}/c-Kit^{+}) cells and myeloid progenitors (Lin^{-}/Sca1^{-}/c-Kit^{+}) are shown (left). LSK cells were further gated for LT-HSC (CD150^{+}/CD48^{-}), ST-HSC (CD48^{-}/CD150^{-}), and MPP (CD48^{+}/CD150^{-}) (center). Within the progenitor population, cells were separated into CMP (CD34^{+}/CD16/32^{low}), GMP (CD34^{+}/CD16/32^{high}), and MEP (CD34^{-}/CD16/32^{-}) (right). The mean ± SD and Student *t* test p values are shown. Two independent biological replicates were performed. p>0.05; * p<0.05; ** p<0.01; *** p<0.001; **** p<0.0001.

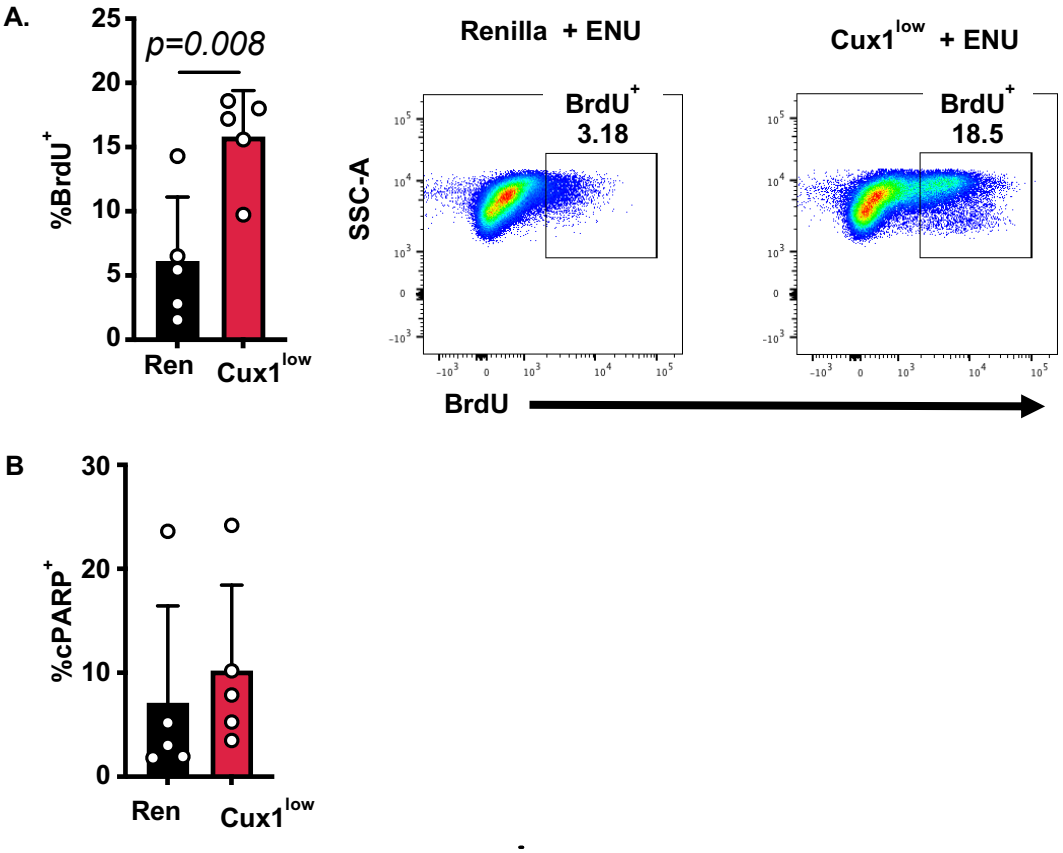


Figure 13. CUX1-deficient cells aberrantly proliferate following alkylator chemotherapy.

A, Proliferation was measured in Ren and Cux1^{low} mice after ENU administration. Mice were given two doses of ENU, 9 days apart. Six hours after the second dose of ENU, BrdU was administered. BrdU^{+} cells were measured by flow cytometry 12 hours after BrdU injection in the bone marrow HPSC population (Lin^{-}). Representative flow plots are shown. The mean ± SD and Student *t* test p value is shown. **B,** Apoptosis was measured in the same cells by flow cytometry using antibodies for cleaved PARP (cPARP). Three independent biological replicates were performed.

consistent with a prior report[196], but the majority of Ren mice had a normal lifespan. In the absence of chemotherapy, Cux1^{mid} mice spontaneously develop MDS but do not have decreased survival[96]. In contrast, ENU-exposed Cux1^{mid} mice have a significantly shortened lifespan (median survival 160 days). Untreated Cux1^{low} mice succumb to MDS/MPNs (275 days)[96]. Upon exposure to ENU, Cux1^{low} survival time is reduced by more than half (median survival 124 days) (**Figure 14B**). We used the Bethesda criteria to identify myeloid disease after alkylator chemotherapy[253]. None of the Ren mice treated with ENU developed a t-MN, consistent with prior work[196]. In stark contrast, 38% (3/8, $p = 0.049$) of Cux1^{mid} and 83% (10/12, $p < 0.0001$) of Cux1^{low} mice developed myeloid disease, while the remaining presented with lymphoid disease (**Figure 14C,D**). Of note, Cux1^{low} mice had accelerated onset ($p=0.002$) and increased penetrance ($p=0.035$) of t-MN compared to Cux1^{mid}. These results demonstrate that CUX1 deficiency sensitizes mice to therapy-induced myeloid disease and in a dosage-dependent manner.

After ENU, Cux1^{mid} and Cux1^{low} mice display myeloid skewing, similar to aged CUX1-deficient mice[96]. At the time of euthanasia for disease, most Cux1^{mid} and Cux1^{low} mice did not show significant changes in total white blood cell counts in the peripheral blood, although the percentage of monocytes was increased. Cux1^{low} mice also showed increased platelet counts **(Figure 15A).** By flow cytometry, granulocytes (CD11b^{+}/Gr1^{+}) are increased in the peripheral blood of ENU-treated Cux1^{low} mice, while B cells (B220^{+}) are significantly decreased. T cells (CD3e^{-}) are largely unchanged **(Figure 15B).** In Cux1^{low} mice, mature myeloid cells were significantly expanded in the white blood cell

(CD45^{+}) subset in the spleen and bone marrow, with Cux1^{mid} mice trending in the same direction **(Figure 15C,D)**.

In distinction to the MDS and MDS/MPN that develop in aged CUX1-deficient mice[96], ENU-treated CUX1-deficient mice develop acute erythroleukemia. Following ENU treatment, red blood cell counts progressively declined in both Cux1^{mid} and Cux1^{low} mice, leading to anemia at autopsy (**Figure 16A,B)**. This anemia was accompanied by an elevated red cell distribution width (RDW) **(Figure 16C)**. Both Cux1^{mid} and Cux1^{low} mice display splenomegaly with a total effacement of splenic architecture at autopsy (**Figure 16D, 17A**) The splenomegaly in both Cux1^{mid} and Cux1^{low} mice was primarily driven by a marked expansion of erythroid precursors in the spleen, illustrated by intense and pervasive GATA1 immunohistochemical staining and accompanied by a significant expansion of megakaryocyte-erythroid progenitors (MEPs, Lin^{-}/CD34^{-}/FcγR^{low}/Kit^{+}/Sca-1^{-}) in the spleen of Cux1^{low} mice **(Figure 16E-F, 17B)**. Normally, GATA1 predominates in scattered, early erythroid forms, as seen in the Ren spleen (**Figure 17B**). In pure erythroid leukemias in patients, GATA1 staining is uniformly intense, while other AML subtypes remain negative[254]. We further characterized this erythroid expansion by flow cytometry. CUX1 knockdown led to decreased mature erythroblasts (RIV, orthochromatophilic, CD71^{-}, Ter119^{+}) in the spleen and bone marrow. The expanded erythroblast population in the spleen was mainly comprised of immature RI (proerythroblasts, CD71^{+}, Ter119^{mid}) and RII (basophilic, CD71^{+}, Ter119^{+}) populations. The RI population was also increased significantly in the bone marrow **(Figure 17C, Figure 15E).** We observed infiltration of these immature erythroid populations in non-hematopoietic tissues, including the liver,

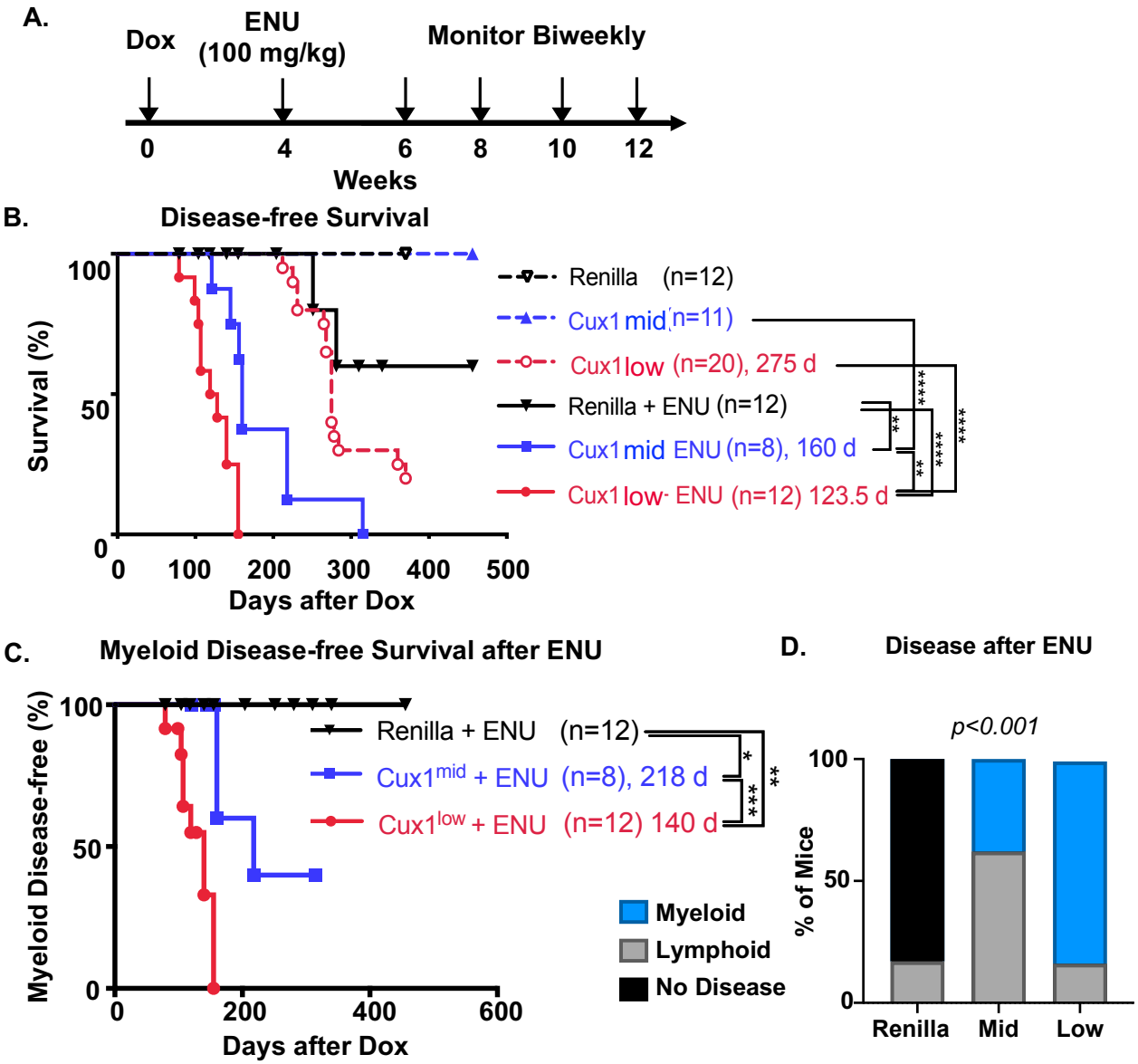


Figure 14. CUX1 deficiency prior to chemotherapy predisposes mice to t-MN.

A, Cux1^{mid}, Cux1^{low} and littermate Ren mice were treated continuously with doxycycline to induce CUX1 knockdown. At one month, mice were treated with an alkylating agent, ENU. Peripheral blood was monitored on a biweekly basis. **B,** Kaplan-Meier plot showing decreased survival (all-cause) for Cux1^{mid} (n=8) and Cux1^{low} (n=12) mice treated with ENU compared to Ren mice treated with ENU (n=12). Median survival data shown for Ren, Cux1^{mid} and Cux1^{low} mice without the addition of ENU (dashed lines) was previously published (An *et al.*, 2018). **C,** Kaplan-Meier plot showing significantly increased myeloid disease incidence for Cux1^{mid} and Cux1^{low} mice treated with ENU compared to Ren mice treated with ENU. Results are shown from two independent experiments (n=4-6 mice per replicate). **p < .01, *** p < .001, Log-rank test. Median survival is shown. **D,** Histologic classification of diseases arising in the mice. 2/12 Renilla mice develop lymphoid disease; 3/8 Cux1^{mid} mice develop myeloid and 5/8 develop lymphoid disease; 10/12 Cux1^{low} mice develop myeloid and 2/12 develop lymphoid disease. Chi-square test.

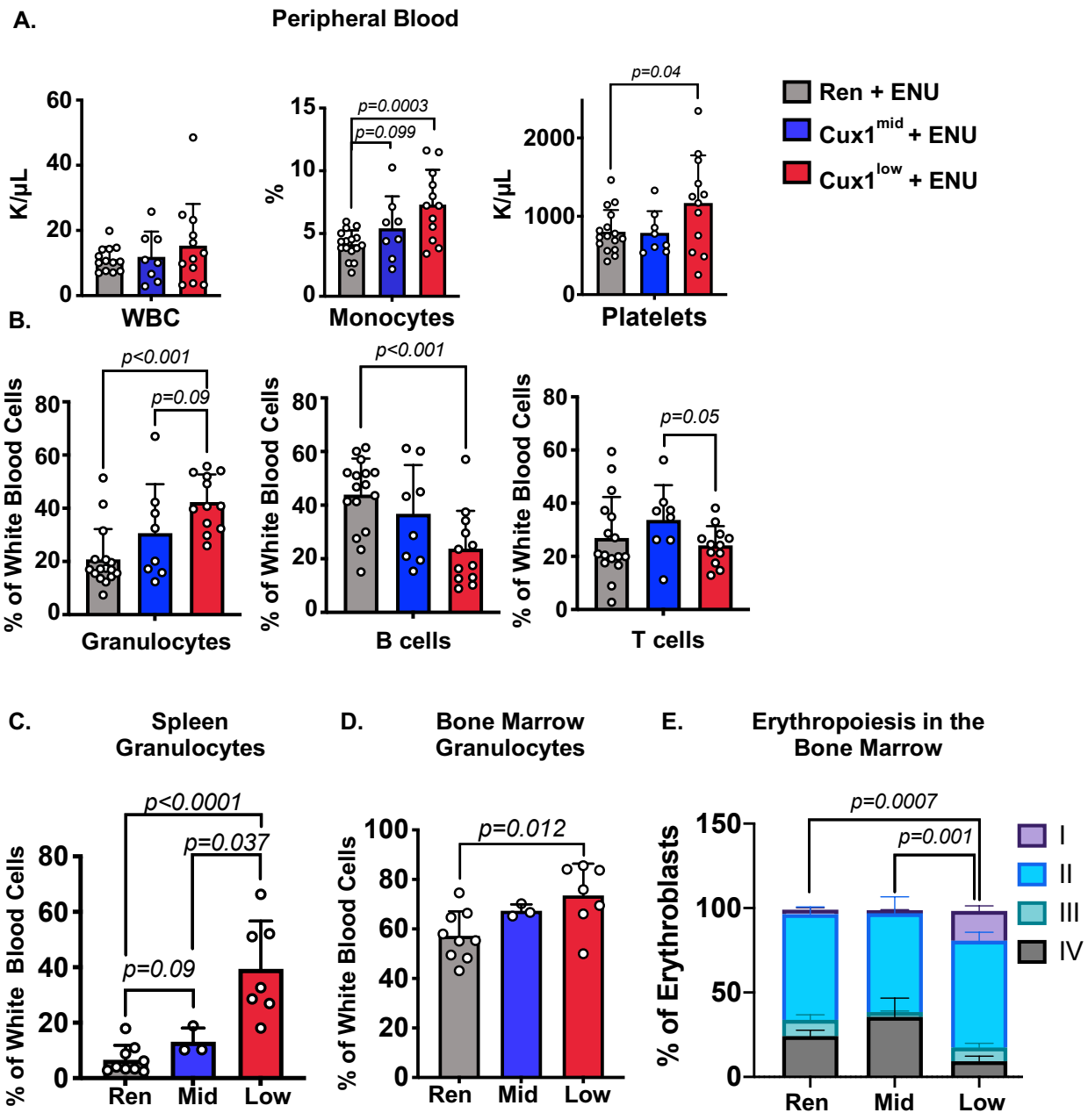


Figure 15. CUX1 deficiency leads to an expansion of myeloid cells.

A, Complete blood counts of the peripheral blood of Ren, Cux1^{mid} and Cux1^{low} mice at autopsy. White blood cell counts (WBC), percent monocytes and platelet counts are shown. **B,** Flow cytometry analysis of the peripheral blood at autopsy for granulocytes (Gr1^{+}/CD11b^{+}), B cells (B220^{+}) and T cells (CD3e^{+}). Flow cytometry of the **C,** spleen and **D,** bone marrow at autopsy**.** Granulocytes are quantified as a percentage of white blood cells (CD45^{+}) in mice with non-lymphoid disease. The mean ± SD and Student *t* test p values are shown. **E,** RI-RIV erythroid precursor populations in the bone marrow. Populations are quantified as percentage of erythroblasts (CD71^{+} or Ter119^{+}) in mice with non-lymphoid disease. An ordinary two-way ANOVA was performed, p values are shown.

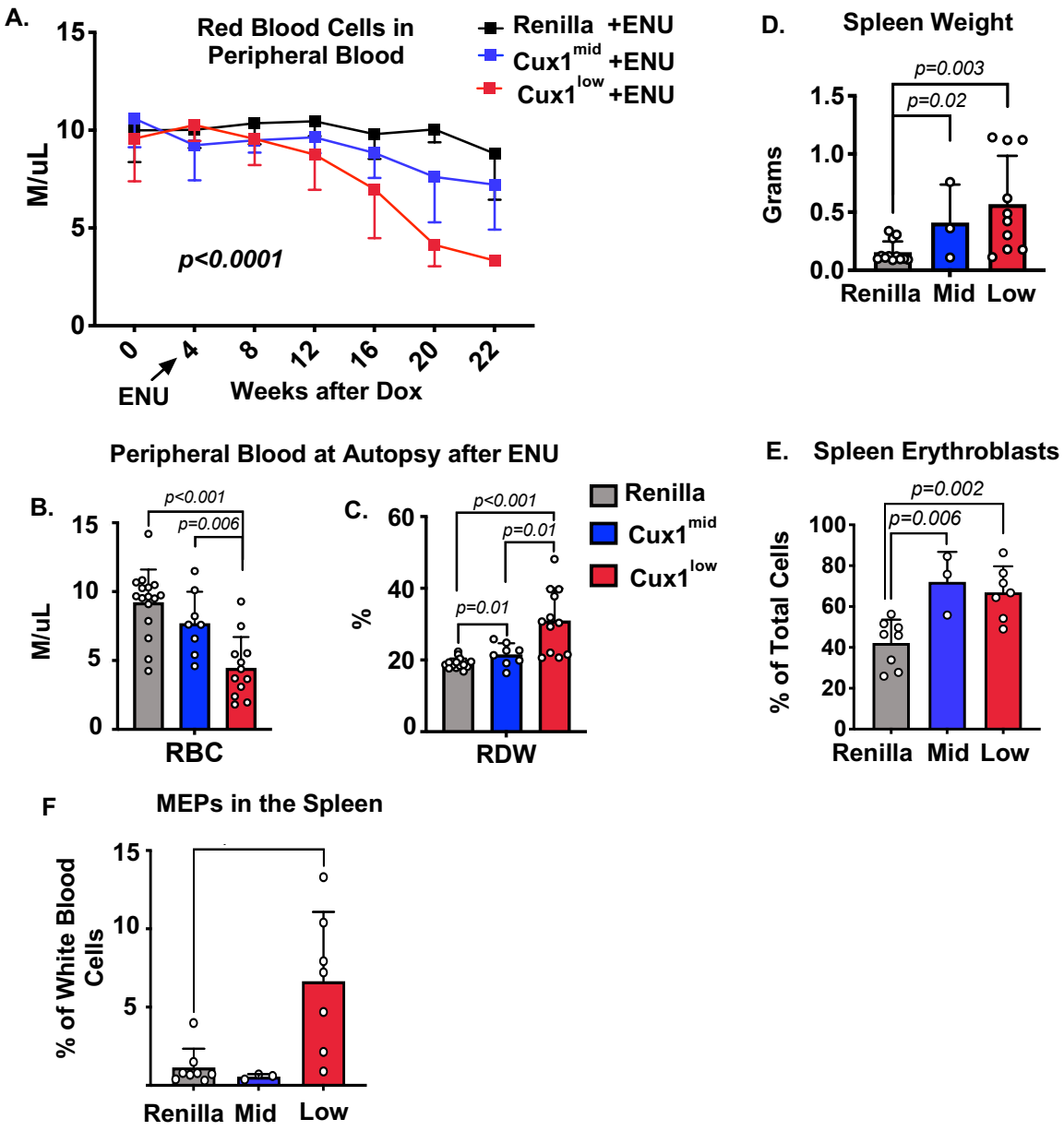


Figure 16. CUX1-deficient mice develop t-MN after alkylator chemotherapy.

A, Complete blood count analysis showing decreased red blood cell counts following ENU treatment in Cux1^{mid} and Cux1^{low} mice compared to Ren. The mean ± SD is shown. A mixed-effects analysis with the Geisser-Greenhouse correction was performed. **B,** Red blood cell counts (RBC) and **C,** red blood cell distribution width (RDW) from complete blood count analysis at autopsy. **D,** The spleen weight at autopsy for Ren, Cux1^{mid} and Cux1^{low} mice. **E,** Erythroblasts (CD71^{+} or Ter119^{+}) in the spleen. **F,** Megakaryocyte and erythrocyte progenitors in the spleen. The mean ± SD and Student *t* test p values are shown.

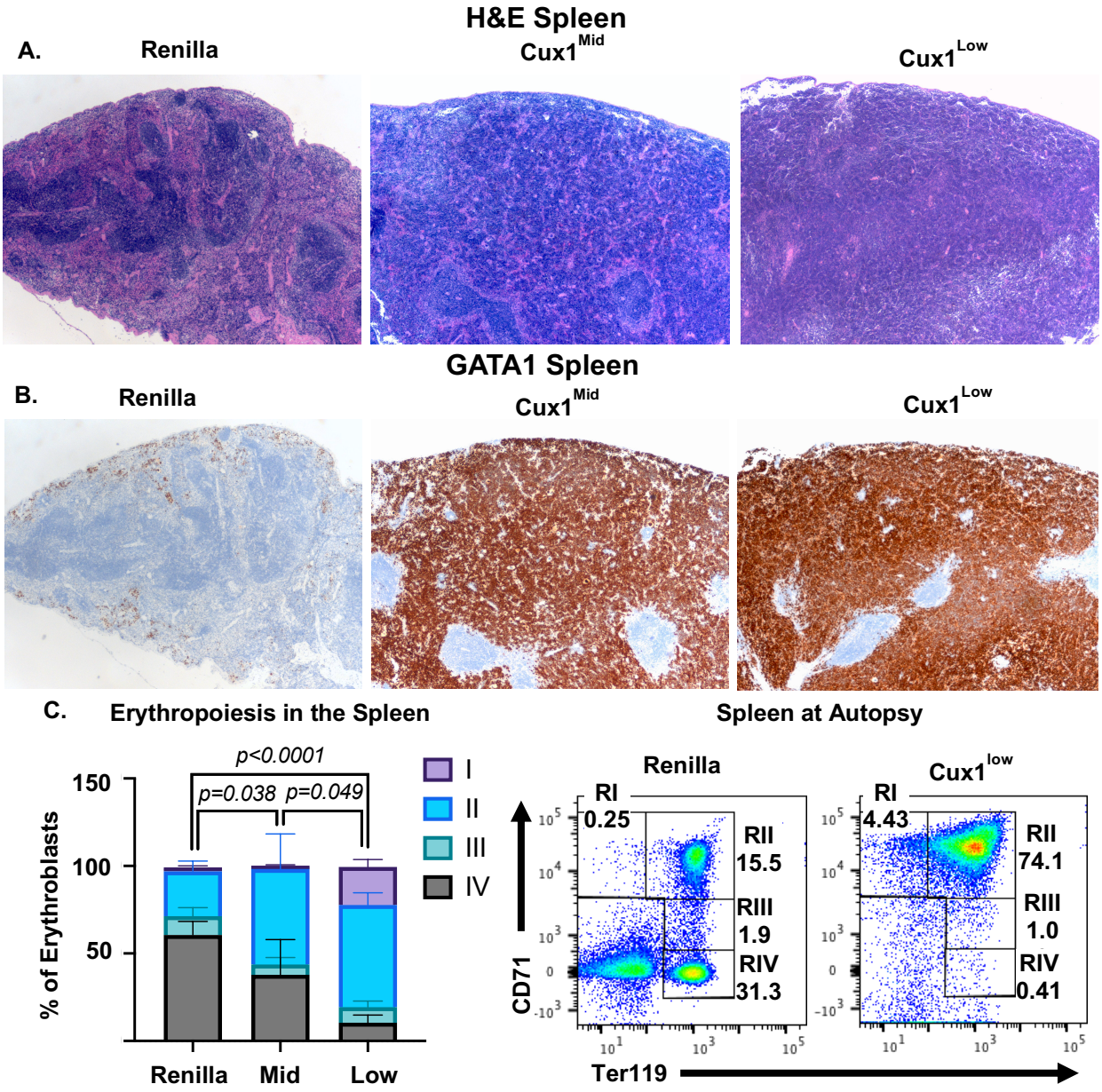


Figure 17. CUX1-deficient mice develop erythroleukemia following alkylator chemotherapy.

A, Representative images from Ren, Cux1^{mid} and Cux1^{low} spleens stained with hematoxylin and eosin (H&E) are shown. **B,** Representative Ren, Cux1^{mid} and Cux1^{low} spleens stained for an immature erythroid marker, GATA1. **C,** RI-RIV erythroid precursor populations quantified as a percentage of erythroblasts in the spleen. p values were calculated using a two-way ANOVA. Representative flow plots for the erythroblast markers CD71 and Ter119 are shown. The mean ± SD and Student *t* test p values are shown.

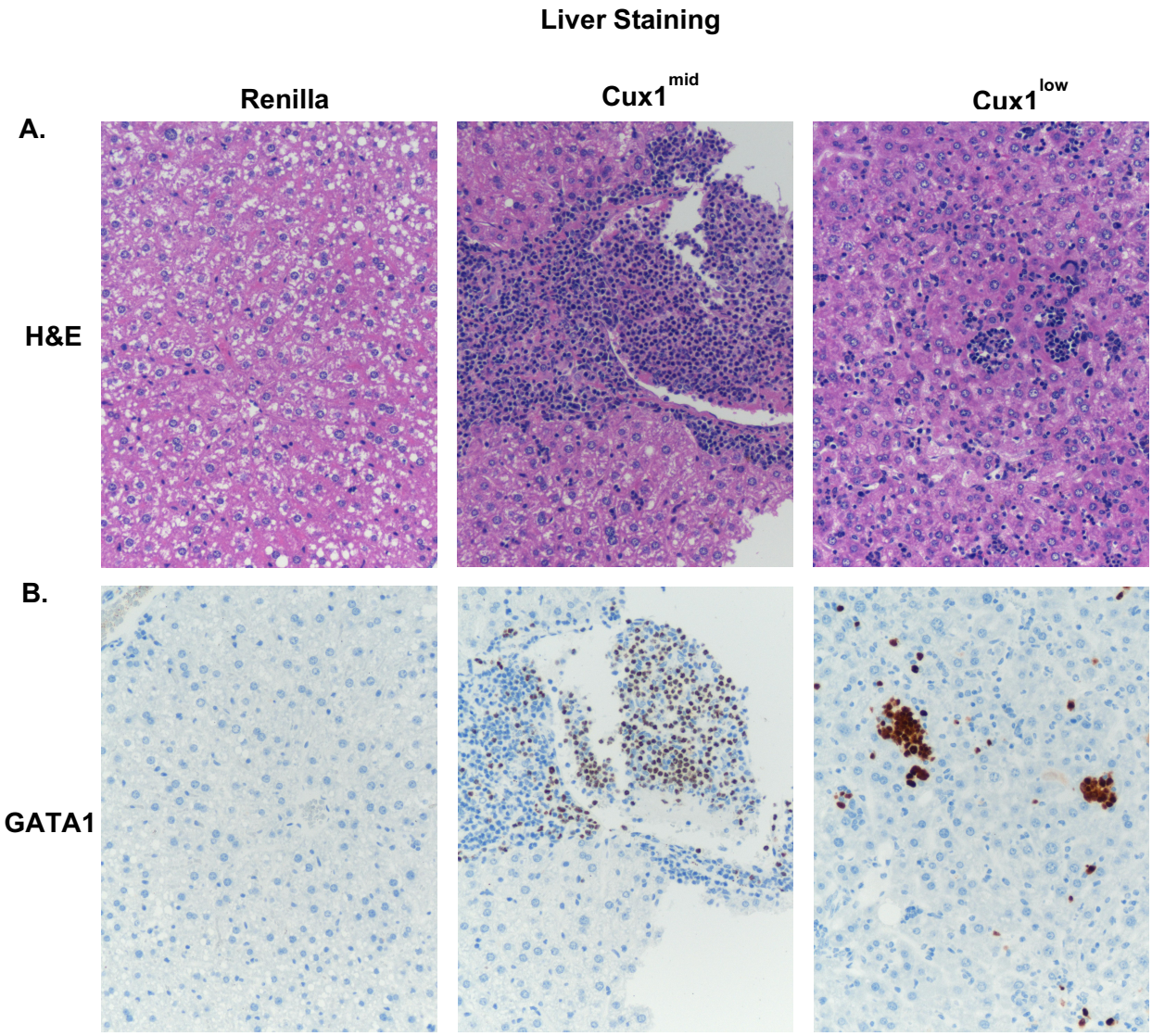


Figure 18. Erythroblasts infiltrate non-hematopoietic tissues in CUX1-deficient mice following alkylator chemotherapy.

A, Representative images of Renilla, Cux1^{mid} and Cux1^{low} liver H&E stains. **B,** Representative images of Renilla, Cux1^{mid} and Cux1^{low} liver stained for GATA1

with varying penetrance **(Figure 18A,B).** The anemia, dramatic expansion of immature erythroid precursors, infiltration into the liver, and rapid onset of disease led us to characterize the disease in both Cux1^{mid} and Cux1^{low} mice as a therapy-related erythroleukemia[253]. Of note, erythroleukemia in patients is often associated with prior chemotherapy as well as -7/del(7q)[255,256]. In summary, we find CUX1 deficiency predisposes mice to an aggressive t-MN, specifically an erythroleukemia.

Discussion

t-MN remains an inherently treatment-resistant cancer. While identifying novel drugs and drug targets is of paramount importance, equal, if not greater, emphasis should be placed on prevention. The field is now equipped with emerging biomarkers, including germline risk alleles and somatic CHIP mutations. Determining how these genetic changes interact with environmental exposures is the missing link in understanding and preventing the evolution of t-MN.

A common theme manifesting in t-MN genetics is the importance of intact DNA repair machinery. 21% of t-MN patients harbor inherited mutations in genes involved in the DDR[16]. CHIP mutations in DDR genes are particularly associated with t-MN[16–18,33,56,257]. *TP53* is a well-described example of this paradigm, in the contexts of both inherited and CHIP mutations[14,166]. However, TP53 inactivation accounts for less than 30% of t-MN patients[16,258].

-7/del(7q), on the other hand, is present in nearly half of t-MN patients. Among 7q-encoded genes, *CUX1* and *EZH2* are the only that are recurrently mutated in myeloid malignancies and CHIP[40,53,66,72,95,96,228,229]. Both genes are also mutated in solid tumors, although *EZH2* mutations are oncogenic in this context[259,260]. Loss of EZH2

alone does not lead to myeloid malignancies in mice[82] whereas loss of CUX1 does[96]. Thus, in the present study, we focused our attention on CUX1. We show that CUX1-deficient cells have impaired DNA damage foci formation, proliferate despite damage and demonstrate a significant fitness advantage in competitive transplants under the selective pressure of chemotherapy. The clonal expansion of Cux1^{low} cells following chemotherapy appears to be driven by an increased output of progenitor cells, specifically MPPs and CMPs in the bone marrow and CMPs and MEPs in the spleen. This corresponds with the dramatic expansion of MEPs seen in the spleens of Cux1^{low} mice that developed t-MN. We propose a model wherein CUX1-deficient HSPCs fail to recognize and repair DNA damage, clonally expand and transform to a t-MN **(Figure 19A)**. We demonstrate that CUX1 deficiency leads to a blunted γH2AX response to DNA damage in both murine and human hematopoietic cells, resulting in persistent DSBs. We show that these CUX1-deficient hematopoietic cells then aberrantly proliferate after chemotherapy and irradiation compared to wild type cells. Furthermore, we find that the loss of this single 7q gene predisposes mice to a lethal, highly-penetrant myeloid neoplasm after chemotherapy. Thus, we report the first model of -7/del(7q)-driven t-MN.

A unique and unexpected finding in our studies is the predominance of erythroleukemia. Few examples of pure erythroleukemia exist in mice[261–264]. To our knowledge, we report the first *in vivo* model of therapy-induced erythroleukemia, despite the fact that ~40% of cases of pure erythroleukemia are therapy-related[256]. Erythroleukemia is associated with complex karyotypes, including 7q abnormalities[255,256] and becomes more frequent with aging[265]. As the median survival time for acute

erythroleukemia is 3-9 months[266], our murine model will prove valuable for preclinical studies.

Of note, deficient DNA repair may not be sufficient to cause t-MN. $Tp53^{+/-}$ mice do not have increased incidence of alkylator-induced myeloid disease[197,267,268], without additional haploinsufficiency of two 5q genes, *Egr1* and *Apc*[197,269]. Upon transformation, the *Tp53, Egr1,* and *Apc* combinatorial model acquired somatic mutations in DNA damage response genes, underscoring the importance of defective DNA repair in t-MN[29]. Mutations in another key regulator of the DNA damage response, *PPM1D,* appear to promote a modest survival advantage under the pressure of chemotherapy, although it is unclear whether these mutations contribute to leukemogenesis[57,58]. By nature of its role in multiple facets of tumorigenesis, i.e., differentiation, proliferation, and DNA repair, CUX1 appears to be a particularly potent tumor suppressor gene and driver of t-MN. Nonetheless, perhaps the prominence of defective DDR is also a vulnerability. It is conceivable that t-MN could be therapeutically prevented in patients with DDR CHIP mutations via prophylactic treatment with a synthetic lethal DDR inhibitor, akin to poly(ADP-ribose) polymerase inhibitors in tumors deficient in homologous recombination[270].

Recent studies have indicated that EHMT2 plays a key role in promoting local DNA damage repair. EHMT2 catalyzes methylation of histones surrounding DSBs and methylation of MDC1 to promote pATM stabilization at breaks[119,233,271]. These modifications enlist critical downstream repair factors, including 53BP1[119,189,233]. Furthermore, in our data in human K562 cells, EHMT2 accumulation is positively correlated with γH2AX foci size, and EHMT2 inhibition reduces γH2AX foci numbers

and H3K27me2/3 at DSBs. The factor responsible for recruiting EHMT2 to sites of DNA damage was previously unknown[119,244] – we report a novel function for CUX1 in this role. With CUX1 loss, EHMT2 at DNA damage foci is reduced to the level of cells treated with an EHMT2 inhibitor, and γH2AX foci numbers are significantly diminished as a result. The decreased H2AX phosphorylation we see in gCUX1 K562 and Cux1-deficient murine HSPCs is in agreement with a previous study reporting a blunted γH2AX response in CUX1-deficient non-hematopoietic cells[99]. While Vadnais *et. al.* attributed the attenuated DDR to transcriptional changes, we did not see downregulation of DDR genes in human or murine hematopoietic cells; instead, we propose that CUX1 recruitment of EHMT2 to sites of DNA damage drives this phenotype[99]. In support of this premise, the same group later reported localization of CUX1 to sites of DNA damage[105]. Moreover, we observed decreased pATM stabilization at foci following CUX1 loss, but not impaired ATM activation, which phenocopies loss of EHMT2[119]. In agreement with the reports of roles for EHMT2 and H3K27me3 in non-homologous end joining[189,233], we observe that CUX1 is required for the recruitment of the downstream repair factor 53BP1. This provokes a model wherein CUX1 recruits EHMT2 to breaks, stabilizes pATM and promotes spreading of H2AX phosphorylation, foci formation and the localization of repair factors **(Figure 19B).** The loss of CUX1 impairs histone methylation and γH2AX foci formation, leading to a failure to efficiently recognize and repair breaks **(Figure 19C)**. In support of this model, it was recently reported that patient-derived bone marrow mononuclear cells with CUX1 mutations have an increased mutational burden, although only three patient samples were analyzed[198]. It is also possible that CUX1 deficiency allows cells to escape

chemotherapy, however, CUX1-deficient cells with a high mutational burden may be eliminated following chemotherapy. In this case, CUX1-deficient cells could still escape chemotherapy and expand without a high mutational burden.

Although the lost EHTM2 recruitment following CUX1 loss provides a compelling explanation for the DDR phenotypes reported here, other mechanisms may also contribute. CUX1 may participate in removal of the oxidative DNA damage lesion 7,8-dihydro-8-oxoguanine (8-oxoG), as reported in non-hematopoietic cells *in vitro*[105–107]. However, this lesion is primarily introduced through reactive oxygen species rather than alkylation[272,273]. Those same studies also conclude that CUX1 is oncogenic, which is inconsistent with our work and the frequently-observed *CUX1* loss-of-function mutations in human myeloid malignancies and solid tumors[40,53,66,79,95,96,228,229]. Additionally, EHMT2 also deposits methyl marks on H3K9, and we observed a trend towards decreased H3K9me1/2/3 after irradiation in gCUX1 cells. Our studies do not preclude an additional role for CUX1 in impacting the DDR response via H3K9 methylation.

Of note, the HSC DDR declines with age[172,274–276], as do CUX1 levels[277,278]. The combination may be particularly conducive for myeloid transformation. This may also explain the milder, and age-related phenotype in Cux1^{mid} mice (An *et al.*, 2018, **Figure 12**); i.e., with age, CUX1 levels drop past a critical threshold in Cux1^{mid} mice that is eventually permissive for malignant phenotypes. We speculate that in patients, loss of one allele of *CUX1* has more deleterious consequences in an aged HSC. Perhaps this partly explains why -7/del(7q) myeloid malignancies increase with age[9,15,279].

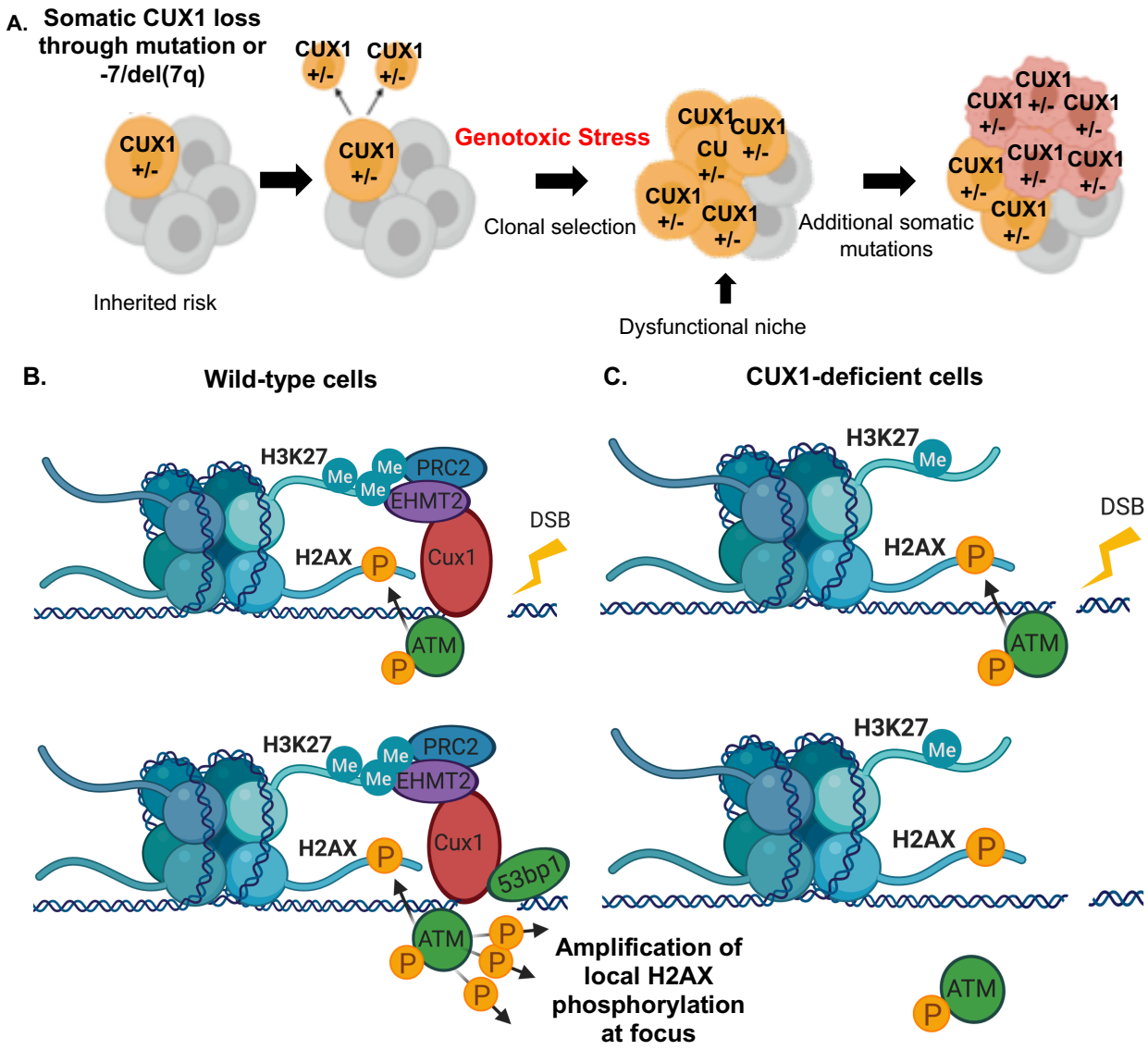


Figure 19. Model for CUX1 loss in therapy-related myeloid neoplasms

A, Some patients may be at increased risk of developing CHIP and t-MN due to somatic loss of CUX1, through mutation or -7/del(7q). Patients may also have inherited genetic risk[16]. CUX1 loss drives clonal hematopoiesis prior to chemotherapy. CUX1-deficient clones then have increased "fitness" under the pressure of genotoxic stress and are primed for transformation to a therapy-related myeloid neoplasm. Although not tested in the current study, others have shown that genotoxic stressors may also drive transformation by creating a dysfunctional niche and selecting for clones with additional mutations[29]. **B,** CUX1 recruits EHMT2 to sites of DNA damage, where EHMT2 promotes H3K27 methylation, likely through interactions with PRC2. pATM is stabilized at breaks to phosphorylate H2AX. The H2AX phosphorylation signal is amplified in foci spreading. 53BP1 is recruited for DNA repair. **C,** In the absence of CUX1, EHMT2 is not recruited efficiently to breaks and fails to methylate H3K27. pATM is not retained at breaks, and, as a result, γH2AX signal is not amplified, leading to impaired downstream recognition of DNA damage by DNA repair machinery, including 53BP1, and sustained DNA damage as a consequence.

Like CUX1, EZH2 plays a dual role in epigenetic regulation of gene expression and DNA damage repair [280], and *EZH2* mutations are associated with a poor-prognosis[72]. EZH2 is recruited to a subset of genes by EHMT2, and we now report CUX1 functions upstream of EHMT2 recruitment in DNA damage. As *EZH2* and *CUX1* are often lost together in -7/del(7q), it stands to reason that loss of both further impairs the DDR and drives treatment resistance, analogous to *TP53* inactivation[14,281]. Future studies are warranted to test this supposition. By identifying the critical genes associated with clonal selection and their mechanistic role in transformation, our work paves the way for identifying patients at risk for t-MN, such as those with pre-existing *CUX1* mutations or del(7q). Our hope is that treatment of patients with primary cancers can be tailored to decrease the onset of secondary malignancies for at-risk patients[282].

DISCUSSION

Overview

In this work, we examined the role of CUX1 in several stages of t-MN development. We find that during cytotoxic therapy, CUX1 is recruited to DSBs to promote histone methylation and γH2AX foci formation. CUX1-deficient cells are then unable to efficiently repair DSBs, and CUX1-deficient HSPCs proliferate and expand following therapy, despite unrepaired damage. Finally, CUX1-deficient cells are primed for transformation to an acute erythroleukemia. These findings challenge current paradigms about the function of CUX1 in hematopoietic cells and present a potential biomarker for t-MN development. Furthermore, this development of a mouse model of -7/del(7q)-driven t-MN creates opportunities for future preclinical drug studies for the prevention and treatment of t-MN.

Using several orthogonal approaches, including GSD-FRET, immunofluorescent imaging, mass spectrometry and ChIP, we find that CUX1 loss alters global and local histone modifications following DNA damage. In contrast to a previous report, we find that the role of CUX1 in responding to DNA damage is non-transcriptional, and we report CUX1 as the unknown factor responsible for recruiting EHMT2 to breaks. We find that both H3K9 and H3K27 methylation are reduced at breaks following irradiation, and CUX1 deficiency leads to reduced pATM at breaks, smaller γH2AX foci and impaired 53BP1 recruitment. Overall, this leads to sustained DNA damage following cytotoxic therapy in CUX1-deficient mice, and both human cell lines and murine HSPCs exhibit aberrant, elevated proliferation following DNA damage. CUX1-deficient cells are then able to out-compete wild type cells *in vivo* following irradiation. Finally, CUX1 deficiency

preceding treatment with alkylating agents leads to a rapidly lethal t-MN with features of an acute erythroleukemia. These finding position CUX1 as a novel epigenetic regulator of the DDR in hematopoietic cells and a key driver of t-MN in patients with -7/del(7q).

CUX1 plays a non-transcriptional role in the local DNA damage response

Previously, CUX1 was reported to regulate the DNA damage response via transcriptional activation of ATM and ATR[99]. CUX1 has also been reported to localize to sites of DNA damage to function as an ancillary factor for the base excision repair factor OGG1 in non-hematopoietic cells[107]. Here, we find a novel role for CUX1 in foci formation at DSBs. Following MDC1 recruitment to γH2AX, EHMT2 methylates and stabilizes MDC1 at breaks to promote foci spreading[119]. Methylation marks induced by EHMT2, including H3K9 and H3K27 methylation, are also induced locally at sites of DNA damage[177,189]. Loss of EHMT2 or MDC1 leads to impaired accumulation of pATM at foci, while total pATM levels are either unchanged[119] or elevated[120], and MDC1 knockout leads to impaired γH2AX foci formation[120]. Loss of CUX1 recapitulated many of the features of MDC1/EHMT2 loss, including reduced methylation at breaks, pATM accumulation, γH2AX foci formation and 53BP1 recruitment. Furthermore, the addition of an EHMT2 inhibitor reduced EHMT2 recruitment to breaks and γH2AX foci numbers to the levels seen in CUX1-deficient cells. While it was previously reported that CUX1 recruited EHMT2 to one locus to repress transcription[100], this is the first report of CUX1 recruiting EHMT2 to sites of DNA damage. It is possible that CUX1 also functions in base excision repair in hematopoietic cells, although this function appears to be oncogenic, rather than tumor suppressive. Furthermore, as DSBs are the most potent

form of DNA damage, it is likely that any disruption to the DSB response would be the most detrimental effect of CUX1 loss.

Synthetic lethal pathways in cells with an impaired DDR have become promising targets in cancer therapy. The best-known example of this is PARP inhibition in cells with BRCA1 deficiency. PARP plays a key role in base excision repair and the repair of single strand breaks, and PARP inhibition leads to unrepaired damage, collapsed replication forks and replication-induced DSBs. Cells then employ HR to repair these DSBs and, as a consequence, cells deficient in HR are hypersensitive to inhibition of PARP. In HR-deficient cells, DSBs are repaired by NHEJ or single strand annealing, which can lead to genomic instability[283]. NHEJ function is essential to the synthetic lethality of PARP inhibition in HR-deficient cells, and loss of 53BP1 renders HR-deficient cells resistant to PARP inhibition[284]. An important feature of PARP inhibitors is their specificity for cancer cells, as cells with functional HR are not killed by PARP inhibition[283]. It may also be possible to target HR in cancer cells with wild type BRCA1 in order to induce susceptibility to PARP inhibition. CUX1 deficiency leads to reduced 53BP1 recruitment, as does inhibition of *EHMT2* or *MDC1*. In this case, the loss of 53BP1 may render cells resistant to PARP inhibitors, however, it might be possible to inhibit homologous recombination to induce apoptosis. Moreover, CUX1 loss leads to a loss of quiescence and increased cycling in HSCs[96]. Cycling HSCs are more dependent on HR, and inhibiting HR may lead to genomic instability and apoptosis in CUX1-deficient cells that already have impaired NHEJ[125]. Future studies to investigate potentially synthetic lethal pathways in CUX1-deficient cells that exploit the ineffective DNA repair in these cells are warranted.

Although the use of PARP inhibitors and the concept of targeting synthetic lethal DDR pathways have yielded very promising results, recent studies have elucidated a potential pitfall of this strategy. Patients treated with PARP inhibitors have an increased risk of developing clonal hematopoiesis following therapy, specifically clonal hematopoiesis with mutations in DDR genes[285]. Given the association between DDR genes and t-MN[14,16,33], this could present a significant future risk to patients. It is possible that therapies that specifically induce death through DDR pathways may inadvertently select for cells that do not respond appropriately to damage. However, given the lifesaving potential of these inhibitors, strategies may have to be developed to treat t-MN developing after patients are treated with DDR-inhibiting drugs, rather than forgo them. Another possibility is developing therapies that can be used in conjunction with PARP inhibitors to prevent outgrowth of DDR-impaired clones. CUX1-deficient mice may be a useful model to test preclinical therapies to prevent CHIP and treat t-MN.

A particularly carcinogenic outcome of an impaired DDR is a failure to activate cell cycle checkpoints. Cells deficient in *ATM, H2AX or 53BP1* fail to arrest in G2 following irradiation[286]. This failure to arrest results in cells with unrepaired damage proceeding through mitosis, leading to genomic instability. The most frequently-mutated gene in human cancers is p53, a critical cell cycle checkpoint effector in the response to DSBs[143,287]. In studies of normal, neoplastic and pre-neoplastic lung, skin, bladder, breast and colon tissue, signs of an active DNA damage response were observed in both the pre-neoplastic and neoplastic tissue, but not normal tissue. However, the neoplastic tissue showed decreased cell cycle checkpoint activation and decreased apoptosis compared to the pre-neoplastic tissue, suggesting that the transformation to

neoplasia occurs when cells with DNA damage circumvent cell cycle checkpoints and proliferate with unrepaired damage[288,289]. Pre-neoplastic Cux1^{low} cells exhibit an active DNA damage response at baseline, as shown by RNA-seq. Following DNA damage, these cells exhibit a failure to arrest following genotoxic insult. The functions of CUX1 in regulating both the local DNA damage response and proliferation present a compelling explanation for the rapid onset of t-MN following cytotoxic therapy. Future studies are needed to uncover the specific stage of cell cycling that CUX1 loss may be impacting, and to elucidate any possible downstream transcriptional changes affecting cell cycling in response to damage.

Cell cycle checkpoint failure has been proposed as a therapeutic vulnerability in cancer cells. Specifically, several groups have investigated the viability of targeting CDKs and cyclins, as these genes are often upregulated in cancer[290]. Inhibiting CDKs and cyclins can be used to halt proliferation in cancer cells, or to induce apoptosis[290]. They may also be able to resensitize cells to DNA damage signals[291]. As CUX1-deficient cells are able to proliferate following chemotherapy, it is likely that cell cycle checkpoints are being overridden to allow for sustained outgrowth of clones with DNA damage, and inhibiting CDKs or cyclins could restore these checkpoints. Conversely, eliminating cell cycle checkpoints in cancer cells could also be a viable strategy. Removing cell cycle checkpoints can promote selective apoptosis in neoplastic cells by pushing these cells towards extreme genomic instability. Mutations in *SETD2*, an epigenetic tumor suppressor, lead to chemoresistance by ablating S and G2/M cell cycle checkpoints. Following chemotherapy, murine *Setd2*-mutant cells inappropriately exit S phase and progress to G2/M. Treating these cells with S and G2/M cell cycle

checkpoint inhibitors in addition to standard chemotherapy resensitizes these cells by inducing replication collapse, mitotic catastrophe and cell death[193]. Targeting cell cycle checkpoints may be a useful strategy, either in conjunction with traditional cytotoxic therapy to prevent or treat CUX1-deficient t-MN.

CUX1 promotes H3K9 and H3K27 methylation

Prior to this work, the role of CUX1 in promoting epigenetic modifications was limited to its role in recruiting EHMT2 to the *CDKN1A* promoter. We find that CUX1 loss in K562 cells alters global histone methylation as well as damage-associated methylation at DSBs. At sites of DNA damage, CUX1-deficient cells lack damage-associated H3K27 and H3K9 methylation. While EHMT2 is best-known for promoting H3K9me1/2 and H3K27me1/2, it has also been reported to bind EZH2 to promote H3K27me2/3. With this in mind, the role of CUX1 in recruiting EHMT2 to breaks could explain the reduced H3K27me3 at sites of DNA damage. This is supported by the reduced H3K27me2/3 observed at DSBs following both CUX1 loss and EHMT2 inhibition. The importance of epigenetic modifiers has been widely reported in CHIP, as has the importance of an intact DDR in preventing t-MN[15,40,44,45]. This unexpected connection between CUX1 and DNA damage-induced methylation may be a key insight into the types of clones most likely to be pathogenic following therapy.

CUX1 and EZH2 have both been reported as key tumor suppressor genes encoded on 7q. EZH2 mutations have been reported to co-occur with CUX1 mutations, as have mutations in EED and SUZ12, other PRC2 complex members[198]. It is possible that the reduction of these two genes in tandem, whether through mutations or del(7q),

leads to a more severe DNA damage repair defect. Here we see a reduction in both H3K9 and H3K27 methylation, both of which independently play roles in the local DNA damage response. Loss of H3K9me2/3 leads to a failure to active ATM signaling, genomic instability and a defective DDR[177]. Loss of H3K27me2/3 has been reported to significantly decrease 53BP1 recruitment and NHEJ[189]. In CUX1-deficient cells, we observed a loss of 53BP1 recruitment, indicating that NHEJ is inhibited, although we have not ruled out the possibility that HR is also impacted by CUX1 deficiency. NHEJ is the most important DDR pathway in quiescent HSCs, however, cycling HSCs employ HR as well[125]. Future experiments will be necessary to describe the DDR pathway(s) disrupted in CUX1-deficient cells, and whether pathway choice is affected following chemotherapy.

While EHMT2 has been reported to affect the DDR through MDC1 methylation[119] and H3K9me2[292], it is also possible that CUX1 recruitment of EHMT2 affects repair through H3K9me3. H3K9me3 is required at breaks to activate the acetyltransferase TIP60, which then acetylates and activates ATM. H3K9me3 is primarily deposited by SUV39H1, although SUV39H1 prefers mono- or dimethylated H3K9 as a substrate[293,294]. EHMT2 also complexes with SUV39H1[293]. We report here that local H3K9me3 is diminished at foci following irradiation in CUX1-deficient cells. Inactivation of SUV39H1, and loss of H3K9me2/3, diminishes HR without significantly impact NHEJ[177]. CUX1 may be an upstream factor necessary for both NHEJ and HR.

The finding that the transcription factor CUX1 is also involved in directing epigenetic modifications at sites of DNA damage has implications for other known CHIP genes. Epigenetic modifiers have been widely reported as frequently-mutated in CHIP.

Do these mutations similarly impact DNA damage repair? Or, does DNA damage repair efficiency explain the difference between clones that expand following aging and transplantation compared to cytotoxic therapy? For example, DNMT3A mutations are selected for with aging and following transplantation, whereas clones with mutations in two DDR factors, TP53 and PPM1D, preferentially expand following cytotoxic therapy[33,56]. As deeper sequencing is performed in patients before and after therapy, and following t-MN diagnoses, it is possible that genes with previously unknown roles in the DDR will be uncovered.

CUX1-deficient clones expand following cytotoxic therapy

Previously, An *et. al.* reported that CUX1-deficient HSPCs expand in competitive transplants. This expansion was modest and primarily driven by an expansion of myeloid cells[96]. Following cytotoxic therapy, $Cux1^{low}$ cells dramatically outcompete their wildtype counterparts. $Cux1^{mid}$ HSPCs, however, did not significantly expand compared to ENU-treated wild type or untreated $Cux1^{mid}$ HSPCs. These differing phenotypes suggest that there is a gene dosage effect of CUX1 in CHIP, and that a lower level of CUX1 is required to generate a fitness advantage following therapy. With aging, CUX1 levels decline[277,278]. We hypothesize that naturally decreasing levels of CUX1, in combination with the inflammation and accumulation of environmental exposures associated with aging, prime HSPCs for transformation and clonal expansion.

In $Cux1^{low}$ mice, CHIP following ENU appears to be driven by an expansion of progenitor cells. Transformation of progenitor cells has been seen following the loss of tumor suppressor genes. In mice, loss of *Jarid2* allows MPPs to self-renew and

transform through loss of PRC2 recruitment to self-renewal gene neworks[295]. MLL-fusion proteins can similarly transform either HSCs or GMPs[296–298]. In t-MN in Cux1^{low} mice, the most dramatically expanded cell population is the MEP population in the spleen. CUX1 loss may be most pathogenic in progenitor cells, leading to an expansion of this population and transformation to a myeloid neoplasm. Alternatively, CUX1-deficient HSCs may be pushed to generate more progeny, leading to increased production of myeloid and erythroid progenitor cells. Lu *et. al.* used HSCs tagged with unique molecular barcodes to demonstrate that not all HSCs contribute equally to blood cell production[299], and it is possible certain mutations in HSCs make them more productive.

Several mechanisms have been proposed to explain CHIP following cytotoxic therapy. Alterations in the microenvironment, through inflammation or aging-associated senescence, have been proposed to drive CHIP[29,31,300]. *PPM1D* mutations have both been reported to help HSCs evade apoptosis and alter cell cycling in response to cytotoxic therapy[57,58]. TP53 mutations alter many processes downstream of cell damage, including apoptosis, cell cycling and cell-extrinsic competition[32,33,166,301]. CUX1-deficient cells exhibit increased proliferation, without any concomitant increase in apoptosis. Mutations in *TP53*, *PPM1D* and *CUX1* all lead to an impaired DDR[57,150]. Intriguingly, *TP53*, *PPM1D* and *CUX1* mutations were recently reported to predict poor overall survival in MDS patients following allogeneic transplant[302]. Whether some of the defects seen in *PPM1D* and *TP53*-mutant clones, such as lost cell cycle checkpoints or cell-extrinsic competition, occur in CUX1-deficient clones remains to be investigated.

Although -7 and del(7q) occur in CHIP, thus far these events have not been frequently detected[19,22,55]. In addition to being lost prior to chemotherapy in HSCs, -7/(del(7q) may also be a consequence of cytotoxic therapy. In cells with an impaired DNA damage response, the accumulation of extensive unrepaired DNA damage in response to therapy could lead to chromosomal losses or translocations. Following stochastic -7/del(7q), the resulting reduction in *CUX1* and other 7q tumor suppressor genes would then provide these cells a fitness advantage under the ongoing pressure of chemotherapy, allowing them to preferentially expand. CUX1 mutations have been seen in CHIP in healthy individuals and following cytotoxic therapy, and it is possible that CUX1 mutations occur more frequently in CHIP than -7/del(7q)[33,40,53,228,229]. Deeper sequencing of patients before and after chemotherapy may help elucidate the order of events.

CHIP in non-hematopoietic tissues

While clonal hematopoiesis has been best-characterized in hematopoietic tissues, growing evidence suggests that clonal expansions of stem cells carrying somatic mutations exist in nearly all tissues[35]. Somatic mutations can be induced by the spontaneous deamination of 6-methylcytosine to thymine, leading to point mutations[303]. They can also be introduced by small insertions and deletions following errors in NHEJ[304]. A third common mechanism is the introduction of mutations through replication errors by DNA polymerase, leading to base substitutions or small insertions and deletions[305]. Finally, large structural variations, such as chromosomal loss, chromosomal rearrangements, large insertions or deletions can occur[19]. All of these

types of mutations are associated with aging[163,306,307]. Most mutations do not confer a survival advantage to stem cells[308]. However, certain mutations confer a fitness advantage, allowing a stem cell to clonally expand, as has been widely observed in CHIP. The three tissues that have been reported to accumulate the largest number of somatic mutations are sun-exposed skin, esophagus mucosa and lung[35]. The location of these tissues suggests that environmental mutagens, in addition to age, are a driving force of somatic mutations. The initiation and progression of cancer remain elusive, despite extensive, decades-long research into these questions. These new studies indicating that precancerous populations of somatically-mutated stem cells exist in almost every tissue in the body opens a promising avenue of study.

Therapy-related neoplasms present a model for studying the evolution from clonal populations of stem cells with somatic mutations to malignancy. In most patients, aging likely provides the selective pressure leading to the expansion of somatically-mutated stem cells. In t-MN, alkylating agents appear to induce a similar selective pressure, allowing certain populations to escape apoptotic forces such as inflammation, DNA damage and reactive oxygen species. Therapy-related malignancies can develop in other tissues besides the hematopoietic compartment, and it is possible that the pressure of chemotherapy similarly selects for certain stem cell clones in these tissues, leading to transformation. The association between radiation exposure and thyroid cancer has been well-documented[309–311]. Following radiation therapy for primary neoplasms, bone and soft-tissue sarcomas can occur in the margins of the radiation field, as well as skin, brain, thyroid and breast cancers. Although AML is the most common therapy-associated leukemia, therapy-related acute lymphocytic leukemia and

chronic myelogenous leukemia have been observed[312]. Clonal stem cell expansions in otherwise healthy patients have been observed in the majority of tissues[35], and it is possible that these somatic mutations could contribute to risk of secondary cancer in these non-hematopoietic tissues. Many advances in oncology are discovered first in the hematopoietic system, from the first chemotherapy to the observation that chromosomal abnormalities can cause cancer[59,313], and models in the hematopoietic system of clonal stem cell expansion preceding neoplasia can inform future studies in other tissues. Furthermore, understanding the types of mutations that are pathogenic, and their mechanism of action, could help prevent and treat resulting therapy-related neoplasms.

In addition to conferring an increased risk of hematologic malignancy, CHIP is linked to increased all-cause mortality. This has been mainly attributed to higher cardiovascular motality[40]. Individuals with CHIP have a higher risk of ischemic stroke and coronary heart disease, and the risk associated with CHIP depends in part on the mutations detected. For example, carrying CHIP with a mutation in *DNMT3A, TET2* or *ASXL1* led to 2x the risk for coronary heart disease compared to individuals without CHIP, whereas a *JAK2* mutation led to 12x increased risk[51]. Studies like the one presented in this thesis, investigating the pathogenic risk for individual mutations, can help elucidate which individuals may benefit from intervention. Such screening may prove beneficial in preventing t-MN, myeloid transformation and cardiovascular disease.

CUX1 loss predisposes mice to t-MN

Mouse models of both inherited and acquired risk for t-MN have previously been reported. Graubert *et. al.* treated a selection of inbred mouse strains with ENU, and

found that certain strains exhibit a higher propensity to develop a myeloid neoplasm following alkylator chemotherapy. Quantitative trait loci analysis implicated genes involved in the DNA damage response and apoptosis in this increased suceptibility[196]. Genes encoded on 5q, including *Apc* and *Egr1*, have also been shown to cooperate with *Tp53* reduction to promote t-MN development following ENU treatment[269]. Mice expressing *RUX1/ETO* or *CBFβ-MYH11,* two oncogenic fusion genes commonly seen in human AML, are similarly predisposed to develop t-MN[314,315]. However, prior to this study, no mouse model of -7/del(7q)-driven t-MN existed, despite this chromosomal abnormality occurring in approximately half of all t-MN. Furthermore, we present the first mouse model of a mutation that provides both a clonal advantage following acute chemotherapy exposure and predisposition to t-MN *in vivo.*

In addition to modeling t-MN, CUX1-deficient mice are also the first mouse model of therapy-related erythroleukemia, and the first model of -7/del(7q)-driven erythroleukemia. The median survival for erythroleukemia is very poor, at 3-9 months[266]. When intensive chemotherapy is used, median overall survival ranges between 7.6 and 9 months. Hypomethylating agents slightly extend median overall survival in patients with high-risk cytogenetics, such as -7/del(7q), compared to intensive chemotherapy, however, the median survival is still dismal at 13.3 months[266]. The rarity of acute erythroleukemia, comprising between 2 and 5% of all leukemias, leads to few studies reporting on solely this subtype,[266] and may explain why traditional AML therapies are ineffective. CUX1-deficient mice can provide a preclinical model to test targeted therapies and extend survival. The DDR defects seen in CUX1-deficient cells may be driving the erythroleukemia subtype of t-MN observed in CUX1-deficient mice. For

example, H2AX deficiency in mice leads to erythroid dysplasia, cell-autonomous anemia and loss of HSPC quiescence[316], all of which are also seen in CUX1-deficient mice[96]. It is possible that the loss of γH2AX seen in CUX1-deficient cells drives the anemia and dyserythropoiesis seen in CUX1-deficient mice, and that this aspect of the DDR could be targeted in -7/del(7q) erythroleukemia.

T-MN has been reported to have similar outcomes and cytogenetic profiles to *de novo* AML in the elderly, including increased prevalence of -7/del(7q), suggesting that common pathways may be driving pathogenesis[9,15,279]. CUX1-deficient mice develop MDS and MDS/MPN, however, they occur after significant aging. CUX1-deficient mice develop t-MN much more rapidly, and the myeloid disease is lethal in $Cux1^{mid}$ mice treated with ENU, but not in aged $Cux1^{mid}$ mice. However, there are several similarities between the aged CUX1-deficient mice and the therapy-treated mice. Both models develop anemia with an elevated RDW, a myeloid expansion, increased platelets, a loss of B cells and splenomegaly. It was recently reported that alkylating agents induce senescence, a phenomena associated with aging, in the bone marrow microenvironment[29]. Inflammation is induced by aging[317] and alkylating agent exposure[318], and inflammation promotes clonal hematopoiesis[31]. It is possible that the CUX1-deficient transformation to myeloid neoplasia is dependent on an inflammatory milieu, which in patients can occur after aging or therapy. The relationship between inflammation and CUX1 deficiency in transformation may also be proportional, such that with less inflammation you need a lower level of CUX1 to proceed to neoplasia, whereas with more inflammation a more modest reduction in CUX1 can drive disease. Advanced aging and higher doses of chemotherapy would both be associated with

higher levels of inflammation. This would account for the observation that Cux1^{low} mice develop myeloid disease at a younger age than Cux1^{mid} mice, and that fewer Cux1^{mid} mice than Cux1^{low} mice develop myeloid disease after a single dose of ENU. Future experiments could examine this relationship by treating Cux1^{mid} and Cux1^{low} mice with an agent to induce inflammation, such as lipopolysaccharide, with and without chemotherapy and/or aging. It might be hypothesized that all CUX1-deficient mice would develop myeloid disease much more quickly and with higher penetrance in these settings. Furthermore, inhibitors of inflammation could potentially prevent CHIP, if administered alongside standard chemotherapies, or be used to treat t-MN.

In addition to the inflammation that chemotherapy induces, the widespread cytotoxicity of chemotherapy induces emergency hematopoiesis to replenish blood cells. This increased cycling following therapy may have several consequences. HSCs have very controlled cycling patterns, and cycling influences the mutational load of stem cells[307]. HSCs with mutations in DDR genes may be particularly vulnerable to acquiring mutations. Mice deficient in caspase-9 have increased DNA damage and an increased mutational burden following treatment with ENU[251]. Or, cells with an impaired DDR may be particularly adept at competing with cells that appropriately respond to DNA damage, as was seen in HSPCs deficient in p53[32]. The increased cycling following alkylator chemotherapy may also influence the DDR. HSCs primarily rely on NHEJ during quiescence, however, upon re-entry into cell cycle it has been reported that HSCs upregulate almost all repair pathways to repair DSBs accumulated during quiescence[163]. We similarly observed a transcriptional upregulation of DDR pathways in

proliferative CUX1-deficient HSCs, and it may be especially crucial to have a functional DDR following an induction to cycling.

The observation that CUX1-deficient HSPCs have both a survival advantage following chemotherapy and are capable of transforming to a t-MN has wide-ranging implications for cancer research. Although this model has been previously proposed following observations of mutational patterns in human samples[14], we are the first to demonstrate this concept in a mouse model. Previous mouse models of t-MN have either only demonstrated a clonal advantage following therapy, such as *Ppm1d* mutations[57,58], or have only demonstrated the capacity for cells to transform following ENU treatment, as is the case with *Egr1/Apc/Tp53*-deficient mice. In previous studies of CHIP following cytotoxic therapy, DDR genes have been implicated. Here, our data presenting a novel role for CUX1 in DDR, as well as in CHIP and t-MN, supports the hypothesis that mutations in genes in this pathway are pathogenic in the context of cytotoxic therapy.

Conclusions

Therapy-induced malignancies constitute a major failing of the treatments we have developed to combat cancer. Until we have developed more targeted therapies, patients will continue to suffer from this devastating late-effect of the treatments used to save their lives. The pathogenesis, and risk factors, of these malignancies remain poorly understood. The role -7/del(7q), found in half of all t-MN patients, in driving t-MN similarly remains an enigma for the field. Here, we present CUX1, a gene encoded on 7q, as a crucial myeloid tumor suppressor gene in CHIP and t-MN. CUX1 loss in

HSPCs is able to drive CHIP following chemotherapy and predispose mice to t-MN in a dosage-dependent manner. We find this is due to the ability of CUX1-deficient cells to proliferate despite unrepaired DNA damage. We then investigated the role of CUX1 in promoting efficient DDR, uncovering a novel role for CUX1 in the local DNA damage response. We find that CUX1 is an epigenetic regulator of DNA damage repair, recruiting EHMT2 to breaks to promote histone methylation, pATM stabilization, γH2AX foci formation and 53BP1 recruitment. CUX1 knockdown leads to a global loss of H3K27me3, and focal loss of damage-dependent H3K9me2/3 and H3K27me2/3. This role in the DDR positions CUX1 as a key regulator of the HSPC response to cytotoxic therapy. This mouse model of t-MN provides a proof-of-concept for clonal stem cell expansions preceding therapy and predisposing to therapy-related disease. This model may open future avenues for developing treatments for t-MN and modeling premalignant transformation following therapy in other tissues. Even more promising is the potential to develop therapies that prevent t-MN, by screening for pathogenic mutations and chromosomal abnormalities prior to chemotherapy, possibly altering therapy class or intensity for individual patients. CUX1 mutations and -7/del(7q) could be used as novel biomarkers for malignant CHIP preceding t-MN. With these studies, we conclude that CUX1 is a key myeloid tumor suppressor gene, promoting effective DNA damage repair and protecting against therapy-related myeloid neoplasms.

Future Directions

1. Which DDR pathways are affected by CUX1 loss? Although reduced 53BP1 recruitment indicates that NHEJ efficiency is impaired, it is possible that HR is

also impacted. Understanding the pathways affected by CUX1 deficiency may point to synthetic lethal drug targets to prevent CHIP and t-MN.

2. What other cytotoxic therapies induce CUX1-deficient CHIP and t-MN? Are the observed *in vivo* consequences of CUX1 deficiency specific to ENU treatment, or does irradiation also induce clonal expansion and t-MN? Do other alkylating agents, or other classes of chemotherapy, such as platinum-based agents or antimetabolites? Could combination therapies targeting synthetic lethal pathways protect mice from therapy-induced CHIP and t-MN?
3. How does CUX1 affect EZH2 recruitment and function? The loss of H3K27me2/3 at breaks, and H3K27me3 globally, indicates that EZH2 function is reduced at breaks. Whether this is due solely to the loss of EHMT2, or points to a more direct interaction with CUX1, remains unknown. Furthermore, interaction of these two 7q genes independent of DNA damage could play a role in -7/del(7q)-driven myeloid disease.
4. What role does CUX1 recruitment of EHMT2 play in gene expression? Do EHMT2 and CUX1 colocalize at promoters and enhancers, in addition to the *CDKN1A* promoter and sites of DNA damage? Could this methylation promote lymphoid and erythroid differentiation?
5. Does CUX1 loss increase the mutational burden of HSPCs? Are cooperating mutations necessary for transformation to an erythroleukemia?
6. What differentiation pathways are perturbed following CUX1 loss in HSPCs that drive the resulting erythroleukemia?

7. What differentiates the Cux1^{mid} mice that develop therapy-related myeloid as opposed to lymphoid disease? Do cooperating mutations play a role?

REFERENCES

1. Hulegårdh, E. *et al.* Characterization and prognostic features of secondary acute myeloid leukemia in a population-based setting: A report from the Swedish Acute Leukemia Registry. *Am. J. Hematol.* **90**, 208–214 (2015).

2. De Roos, A. J. *et al.* Incidence of myelodysplastic syndromes within a nonprofit healthcare system in western Washington state, 2005-2006. *Am. J. Hematol.* **85**, 765–770 (2010).

3. de Moor, J. S. *et al.* Cancer survivors in the United States: prevalence across the survivorship trajectory and implications for care. *Cancer Epidemiol. Biomarkers Prev.* **22**, 561–570 (2013).

4. Granfeldt Østgård, L. S. *et al.* Epidemiology and Clinical Significance of Secondary and Therapy-Related Acute Myeloid Leukemia: A National Population-Based Cohort Study. *J. Clin. Oncol.* **33**, 3641–3649 (2015).

5. Fianchi, L. *et al.* Characteristics and outcome of therapy-related myeloid neoplasms: Report from the Italian network on secondary leukemias. *Am. J. Hematol.* **90**, E80–E85 (2015).

6. Wolff, A. C. *et al.* Risk of marrow neoplasms after adjuvant breast cancer therapy: The national comprehensive cancer network experience. *J. Clin. Oncol.* **33**, 340–348 (2015).

7. Morton, L. M. *et al.* Evolving risk of therapy-related acute myeloid leukemia following cancer chemotherapy among adults in the United States, 1975-2008. *Blood* **121**, 2996–3004 (2013).

8. Radivoyevitch, T. *et al.* Defining AML and MDS second cancer risk dynamics after diagnoses of first cancers treated or not with radiation. *Leukemia* **30**, 285–94 (2015).

9. Smith, S. M. *et al.* Clinical-cytogenetic associations in 306 patients with therapy-related myelodysplasia and myeloid leukemia: the University of Chicago series. *Blood* **102**, 43–52 (2003).

10. Mahgoub, N. *et al.* Myeloid malignancies induced by alkylating agents in Nf1 mice. *Blood* **93**, 3617–23 (1999).

11. Kondo, N. *et al.* DNA ligase IV as a new molecular target for temozolomide. *Biochem. Biophys. Res. Commun.* **387**, 656–660 (2009).

12. Roos, W. P. *et al.* Brca2/Xrcc2 dependent HR, but not NHEJ, is required for protection against O6-methylguanine triggered apoptosis, DSBs and chromosomal aberrations by a process leading to SCEs. *DNA Repair (Amst).* **8**, 72–86 (2009).

13. Zahid, M. F., Parnes, A., Savani, B. N., Litzow, M. R. & Hashmi, S. K. Therapy-related myeloid neoplasms - what have we learned so far? *World J. Stem Cells* **8**, 231–42 (2016).

14. Wong, T. N. *et al.* Role of TP53 mutations in the origin and evolution of therapy-related acute myeloid leukaemia. *Nature* **518**, 552–555 (2014).

15. McNerney, M. E., Godley, L. A. & Le Beau, M. M. Therapy-related myeloid neoplasms: when genetics and environment collide. *Nat. Rev. Cancer* **17**, 513–527 (2017).

16. Churpek, J. Inherited mutations in cancer susceptibility genes are common among survivors of breast cancer who develop therapy-related leukemia. *Cancer* **122**, 304–311 (2016).

17. Schulz, E. Germline mutations in the DNA damage response genes BRCA1, BRCA2, BARD1 and TP53 in patients with therapy related myeloid neoplasms. *J. Med. Genet.* **49**, 422–428 (2012).

18. Voso, M. Fanconi anemia gene variants in therapy-related myeloid neoplasms. *Blood Cancer J.* **5**, e323 (2015).

19. Laurie, C. C. *et al.* Detectable clonal mosaicism from birth to old age and its relationship to cancer. *Nat. Genet.* **44**, 642–650 (2012).

20. Rodríguez-Santiago, B. *et al.* Mosaic Uniparental Disomies and Aneuploidies as Large Structural Variants of the Human Genome. *Am. J. Hum. Genet.* **87**, 129–138 (2010).

21. Forsberg, L. A. *et al.* Age-Related Somatic Structural Changes in the Nuclear Genome of Human Blood Cells. *Am. J. Hum. Genet.* **90**, 217–228 (2012).

22. Jacobs, K. B. *et al.* Detectable clonal mosaicism and its relationship to aging and cancer. *Nat. Genet.* **44**, 651–658 (2012).

23. Schick, U. M. *et al.* Confirmation of the reported association of clonal chromosomal mosaicism with an increased risk of incident hematologic cancer. *PLoS One* **8**, e59823 (2013).

24. Kode, A. *et al.* Leukaemogenesis induced by an activating β-catenin mutation in osteoblasts. *Nature* **506**, 240–244 (2014).

25. Medyouf, H. *et al.* Myelodysplastic cells in patients reprogram mesenchymal

stromal cells to establish a transplantable stem cell niche disease unit. *Cell Stem Cell* **14**, 824–837 (2014).

26. Raaijmakers, M. H. G. P. *et al.* Bone progenitor dysfunction induces myelodysplasia and secondary leukaemia. *Nature* **464**, 852–857 (2010).

27. Stoddart, A. *et al.* Inhibition of WNT signaling in the bone marrow niche prevents the development of MDS in the Apcdel/+ MDS mouse model. *Blood* **129**, 2959–2970 (2017).

28. Mattiucci, D., Maurizi, G., Leoni, P. & Poloni, A. Aging- and Senescence-associated Changes of Mesenchymal Stromal Cells in Myelodysplastic Syndromes. *Cell Transplantation* **27**, 754–764 (2018).

29. Stoddart, A. *et al.* Cytotoxic therapy-induced effects on both hematopoietic and marrow stromal cells promotes therapy-related myeloid neoplasms. *Blood Cancer Discov* 1–16 (2020). doi:10.1158/2643-3230.BCD-19-0028

30. Zambetti, N. A. *et al.* Mesenchymal Inflammation Drives Genotoxic Stress in Hematopoietic Stem Cells and Predicts Disease Evolution in Human Pre-leukemia. *Cell Stem Cell* **19**, 613–627 (2016).

31. Meisel, M. *et al.* Microbial signals drive pre-leukaemic myeloproliferation in a Tet2-deficient host. *Nature* **557**, 580–584 (2018).

32. Bondar, T. & Medzhitov, R. p53-Mediated Hematopoietic Stem and Progenitor Cell Competition. *Cell Stem Cell* **6**, 309–322 (2010).

33. Wong, T. N. *et al.* Cellular stressors contribute to the expansion of hematopoietic clones of varying leukemic potential. *Nat. Commun.* **9**, 455 (2018).

34. Bowman, R. L., Busque, L. & Levine, R. L. Clonal hematopoiesis and evolution to hematopoietic malignancies. *Cell Stem Cell* **22**, 157–170 (2018).

35. Yizhak, K. *et al.* RNA sequence analysis reveals macroscopic somatic clonal expansion across normal tissues. *Science (80-.).* **364**, (2019).

36. Young, A. L., Challen, G. A., Birmann, B. M. & Druley, T. E. Clonal haematopoiesis harbouring AML-associated mutations is ubiquitous in healthy adults. *Nat. Commun.* **7**, 12484 (2016).

37. Steensma, D. P. *et al.* Clonal hematopoiesis of indeterminate potential and its distinction from myelodysplastic syndromes. *Blood* **126**, 9–16 (2015).

38. Genovese, G. *et al.* Clonal hematopoiesis and blood-cancer risk inferred from blood DNA sequence. *N. Engl. J. Med.* **371**, 2477–2487 (2014).

39. Xie, M. *et al.* Age-related mutations associated with clonal hematopoietic

expansion and malignancies. *Nat. Med.* **20**, 1472–1478 (2014).

40. Jaiswal, S. *et al.* Age-related clonal hematopoiesis associated with adverse outcomes. **371**, 2488–2498 (2014).

41. Champion, K. M., Gilbert, J. G. R., Asimakopoulos, F. A., Hinshelwood, S. & Green, A. R. Clonal haemopoiesis in normal elderly women: Implications for the myeloproliferative disorders and myelodysplastic syndromes. *Br. J. Haematol.* **97**, 920–926 (1997).

42. Loh, P. R. *et al.* Insights into clonal haematopoiesis from 8,342 mosaic chromosomal alterations. *Nature* **559**, 350–355 (2018).

43. Bonnefond, A. *et al.* Association between large detectable clonal mosaicism and type 2 diabetes with vascular complications. *Nat. Genet.* **45**, 1040–1043 (2013).

44. Challen, G. A. *et al.* Dnmt3a is essential for hematopoietic stem cell differentiation. *Nat. Genet.* **44**, 23–31 (2012).

45. Moran-Crusio, K. *et al.* Tet2 Loss Leads to Increased Hematopoietic Stem Cell Self-Renewal and Myeloid Transformation. *Cancer Cell* **20**, 11–24 (2011).

46. Abelson, S. *et al.* Prediction of acute myeloid leukaemia risk in healthy individuals. *Nature* **559**, 400–404 (2018).

47. Ko, M. *et al.* Ten-eleven-translocation 2 (TET2) negatively regulates homeostasis and differentiation of hematopoietic stem cells in mice. *Proc. Natl. Acad. Sci. U. S. A.* **108**, 14566–14571 (2011).

48. Sano, S. *et al.* CRISPR-mediated gene editing to assess the roles of TET2 and DNMT3A in clonal hematopoiesis and cardiovascular disease. *Circ. Res.* **123**, 335–341 (2018).

49. Cull, A. H., Snetsinger, B., Buckstein, R., Wells, R. A. & Rauh, M. J. Tet2 restrains inflammatory gene expression in macrophages. *Exp. Hematol.* **55**, 56-70.e13 (2017).

50. Leoni, C. *et al.* Dnmt3a restrains mast cell inflammatory responses. *Proc. Natl. Acad. Sci. U. S. A.* **114**, E1490–E1499 (2017).

51. Jaiswal, S. *et al.* Clonal Hematopoiesis and risk of atherosclerotic cardiovascular disease. *N. Engl. J. Med.* **377**, 111–121 (2017).

52. Fuster, J. J. *et al.* Clonal hematopoiesis associated with TET2 deficiency accelerates atherosclerosis development in mice. *Science (80-.).* **355**, 842–847 (2017).

53. Gibson, C. J. *et al.* Clonal hematopoiesis associated with adverse outcomes after

autologous stem-cell transplantation for lymphoma. *J. Clin. Oncol.* **35**, 1598–1605 (2017).

54. Gillis, N. K. *et al.* Clonal haemopoiesis and therapy-related myeloid malignancies in elderly patients: a proof-of-concept, case-control study. *Lancet Oncol.* **18**, 112–121 (2017).

55. Takahashi, K. *et al.* Copy number alterations detected as clonal hematopoiesis of indeterminate potential. *Blood Adv.* **1**, 1031–1036 (2017).

56. Bolton, K. L. *et al.* Oncologic therapy shapes the fitness landscape of clonal hematopoiesis. *bioRxiv, https://doi.org/10.1101/848739* 848739 (2019). doi:10.1101/848739

57. Kahn, J. D. *et al.* PPM1D-truncating mutations confer resistance to chemotherapy and sensitivity to PPM1D inhibition in hematopoietic cells. *Blood* **132**, 1095–1105 (2018).

58. Hsu, J. I. *et al.* PPM1D mutations drive clonal hematopoiesis in response to cytotoxic chemotherapy. *Cell Stem Cell* **23**, 700–713 (2018).

59. Rowley, J. D. A new consistent chromosomal abnormality in chronic myelogenous leukaemia identified by quinacrine fluorescence and Giemsa staining. *Nature* **243**, 290–293 (1973).

60. Greenberg, P. *et al.* International scoring system for evaluating prognosis in myelodysplastic syndromes. *Blood* **89**, 2079–2088 (1997).

61. Luna-Fineman, S. *et al.* Myelodysplastic and myeloproliferative disorders of childhood: a study of 167 patients. *Blood* **93**, 459–466 (1999).

62. Luna-Fineman, S., Shannon, K. M. & Lange, B. J. Childhood monosomy 7: Epidemiology, biology, and mechanistic implications. *Blood* **85**, 1985–1999 (1995).

63. Bejar, R., Levine, R. & Ebert, B. L. Unraveling the molecular pathophysiology of myelodysplastic syndromes. *J. Clin. Oncol.* **29**, 504–515 (2011).

64. Pezeshki, A., Podder, S., Kamel, R. & Corey, S. J. Monosomy 7/del (7q) in inherited bone marrow failure syndromes: A systematic review. *Pediatr. Blood Cancer* **64**, (2017).

65. Dumitriu, B. *et al.* Telomere attrition and candidate gene mutations preceding monosomy 7 in aplastic anemia. *Blood* **125**, 706–9 (2015).

66. McNerney, M. E. *et al.* The spectrum of somatic mutations in high-risk acute myeloid leukaemia with -7/del(7q). *Br. J. Haematol.* **166**, 550–556 (2014).

67. Hussain, F. T. N. *et al.* Sole abnormalities of chromosome 7 in myeloid malignancies: Spectrum, histopathologic correlates, and prognostic implications. *Am. J. Hematol.* **87**, 684–686 (2012).

68. Rowley, J. D. Deletions of chromosome 7 in haematological disorders. *The Lancet* **302**, 1385–1386 (1973).

69. Knudson, A. G. Mutation and cancer: statistical study of retinoblastoma. *Proc. Natl. Acad. Sci. U. S. A.* **68**, 820–823 (1971).

70. Davoli, T. *et al.* Cumulative haploinsufficiency and triplosensitivity drive aneuploidy patterns and shape the cancer genome. *Cell* **155**, 948 (2013).

71. White, J. K. *et al.* Genome-wide generation and systematic phenotyping of knockout mice reveals new roles for many genes. *Cell* **154**, 452 (2013).

72. Zhang, Q. *et al.* Mutations in EZH2 are associated with poor prognosis for patients with myeloid neoplasms. *Genes Dis.* **6**, 276–281 (2019).

73. Ernst, T. *et al.* Inactivating mutations of the histone methyltransferase gene EZH2 in myeloid disorders. *Nat. Genet.* **42**, 722–726 (2010).

74. Schmickel, R. D. Contiguous gene syndromes: A component of recognizable syndromes. *J. Pediatr.* **109**, 231–241 (1986).

75. Wong, J. C. *et al.* Functional evidence implicating chromosome 7q22 haploinsufficiency in myelodysplastic syndrome pathogenesis. *Elife* **4**, (2015).

76. Beau, M. Le. Cytogenetic and molecular delineation of a region of chromosome 7 commonly deleted in malignant myeloid diseases. *Blood* **88**, 1930–1935 (1996).

77. Jerez, A. *et al.* Loss of heterozygosity in 7q myeloid disorders: clinical associations and genomic pathogenesis. *Blood* **119**, 6109–6117 (2012).

78. Döhner, K. *et al.* Molecular cytogenetic characterization of a critical region in bands 7q35-q36 commonly deleted in malignant myeloid disorders. *Blood* **92**, 4031–4035 (1998).

79. McNerney, M. E. *et al.* CUX1 is a haploinsufficient tumor suppressor gene on chromosome 7 frequently inactivated in acute myeloid leukemia. *Blood* **121**, 975–983 (2013).

80. Chen, C. MLL3 is a haploinsufficient 7q tumor suppressor in acute myeloid leukemia. *Cancer Cell* **25**, 652–665 (2014).

81. Sashida, G. *et al.* Ezh2 loss promotes development of myelodysplastic syndrome but attenuates its predisposition to leukaemic transformation. *Nat. Commun.* **5**, 1–14 (2014).

82. Shimizu, T. *et al.* Loss of Ezh2 synergizes with JAK2-V617F in initiating myeloproliferative neoplasms and promoting myelofibrosis. *J. Exp. Med.* **213**, 1479–1496 (2016).

83. Marti, A., Wirbelauer, C., Scheffner, M. & Krek, W. Interaction between ubiquitin-protein ligase SCFSKP2 and E2F-1 underlies the regulation of E2F-1 degradation. *Nat. Cell Biol.* **1**, 14–19 (1999).

84. Kipreos, E. T., Lander, L. E., Wing, J. P., He, W. W. & Hedgecock, E. M. cul-1 is required for cell cycle exit in C. elegans and identifies a novel gene family. *Cell* **85**, 829–839 (1996).

85. N Hosono, H Makishima, A Jerez, K Yoshida, B Przychodzen, S. M. *et al. Recurrent genetic defects on chromosome 7q in myeloid neoplasms*. *Leukemia* **28**, 1348–1351 (Nature Publishing Group, 2014).

86. Yoshida, K. *et al.* Frequent pathway mutations of splicing machinery in myelodysplasia. *Nature* **478**, 64–69 (2011).

87. A Nagamachi, H. M. H. A. Y. O. D. A. A. K. Haploinsufficiency of SAMD9L, an endosome fusion facilitator, causes myeloid malignancies in mice mimicking human diseases with monosomy 7. *Cancer Cell* **24**, 305–317 (2013).

88. Heuser, M. *et al.* Loss of MII5 results in pleiotropic hematopoietic defects, reduced neutrophil immune function, and extreme sensitivity to DNA demethylation. *Blood* **113**, 1432–1443 (2009).

89. Zhang, Y. *et al.* MII5 contributes to hematopoietic stem cell fitness and homeostasis. *Blood* **113**, 1455–1463 (2009).

90. Madan, V. *et al.* Impaired function of primitive hematopoietic cells in mice lacking the mixed-lineage-leukemia homolog MII5. *Blood* **113**, 1444–1454 (2009).

91. V Yajnik, C. P. R. S. A. M. M. S. D. W. DOCK4, a GTPase activator, is disrupted during tumorigenesis. *Cell* **112**, 672–684 (2003).

92. E Kjeldsen, C. V. DOCK4 deletion at 7q31.1 in a de novo acute myeloid leukemia with a normal karyotype. *Cell Oncol* **36**, 395–403 (2013).

93. Ramdzan, Z. M. & Nepveu, A. CUX1, a haploinsufficient tumour suppressor gene overexpressed in advanced cancers. *Nat. Rev. Cancer* **14**, 673–682 (2014).

94. Arthur, R. K., An, N., Khan, S. & McNerney, M. E. The haploinsufficient tumor suppressor, CUX1, acts as an analog transcriptional regulator that controls target genes through distal enhancers that loop to target promoters. *Nucleic Acids Res.* **45**, 6350–6361 (2017).

95. Wong, C. C. *et al.* Inactivating CUX1 mutations promote tumorigenesis. *Nat.*

Genet. **46**, 33–38 (2013).

96. An, N. *et al.* Gene dosage effect of CUX1 in a murine model disrupts HSC homeostasis and controls the severity and mortality of MDS. *Blood* **131**, 2682–2697 (2018).

97. Nepveu, A. Role of the multifunctional CDP/Cut/Cux homeodomain transcription factor in regulating differentiation, cell growth and development. *Gene* **270**, 1–15 (2001).

98. Blochlinger, K., Jan, L. Y. & Jan, Y. N. Transformation of sensory organ identity by ectopic expression of Cut in Drosophila. *Genes Dev.* **5**, 1124–35 (1991).

99. Vadnais, C. *et al.* CUX1 transcription factor is required for optimal ATM/ATR-mediated responses to DNA damage. *Nucleic Acids Res.* **40**, 4483–95 (2012).

100. Nishio, H. & Walsh, M. J. CCAAT displacement protein/cut homolog recruits G9a histone lysine methyltransferase to repress transcription. *Proc. Natl. Acad. Sci. U. S. A.* **101**, 11257–62 (2004).

101. Ikeda, T. *et al.* Transforming growth factor-β-induced CUX1 isoforms are associated with fibrosis in systemic sclerosis lung fibroblasts. *Biochem. Biophys. Reports* **7**, 246–252 (2016).

102. Ripka, S. *et al.* CUX1: Target of Akt signalling and mediator of resistance to apoptosis in pancreatic cancer. *Gut* **59**, 1101–1110 (2010).

103. Lindahl, T. Instability and decay of the primary structure of DNA. *Nature* **362**, 709–715 (1993).

104. Krokan, H. E. & Bjørås, M. Base excision repair. *Cold Spring Harb. Perspect. Biol.* **5**, 1–22 (2013).

105. Ramdzan, Z. M. *et al.* The DNA repair function of CUX1 contributes to radioresistance. *Oncotarget* **8**, 19021–19038 (2017).

106. Ramdzan, Z. M. *et al.* RAS transformation requires CUX1-dependent repair of oxidative DNA damage. *PLoS Biol.* **12**, e1001807 (2014).

107. Ramdzan, Z. M. *et al.* The function of CUX1 in oxidative DNA damage repair is needed to prevent premature senescence of mouse embryo fibroblasts. *Oncotarget* **6**, 3613–26 (2015).

108. Gillingham, A. K., Pfeifer, A. C. & Munro, S. CASP, the alternatively spliced product of the gene encoding the CCAAT-displacement protein transcription factor, is a Golgi membrane protein related to giantin. *Mol. Biol. Cell* **13**, 3761–3774 (2002).

109. Sinclair, A. M. *et al.* Lymphoid apoptosis and myeloid hyperplasia in CCAAT displacement protein mutant mice. *Blood* **98**, 3658–67 (2001).

110. Ellis, T. *et al.* The transcriptional repressor CDP (Cutl1) is essential for epithelial cell differentiation of the lung and the hair follicle. *Genes Dev.* **15**, 2307–19 (2001).

111. Tufarelli, C., Fujiwara, Y., Zappulla, D. C. & Neufeld, E. J. Hair defects and pup loss in mice with targeted deletion of the first cut repeat domain of the Cux/CDP homeoprotein gene. *Dev. Biol.* **200**, 69–81 (1998).

112. Luong, M. X. *et al.* Genetic Ablation of the CDP/Cux Protein C Terminus Results in Hair Cycle Defects and Reduced Male Fertility. *Mol. Cell. Biol.* **22**, 1424–1437 (2002).

113. O'Kane, G. M., Connor, A. A. & Gallinger, S. Characterization, Detection, and Treatment Approaches for Homologous Recombination Deficiency in Cancer. (2017). doi:10.1016/j.molmed.2017.10.007

114. Yuan, J., Adamski, R. & Chen, J. Focus on histone variant H2AX: To be or not to be. *FEBS Letters* **584**, 3717–3724 (2010).

115. Singleton, W. R. Actions of radiations on living cells. *J. Hered.* **47**, 34–35 (1956).

116. Saleh-Gohari, N. *et al.* Spontaneous Homologous Recombination Is Induced by Collapsed Replication Forks That Are Caused by Endogenous DNA Single-Strand Breaks. *Mol. Cell. Biol.* **25**, 7158–7169 (2005).

117. Sun, Y. *et al.* Histone H3 methylation links DNA damage detection to activation of the tumour suppressor Tip60. *Nat. Cell Biol.* **11**, 1376–1382 (2009).

118. Sun, Y., Jiang, X., Chen, S., Fernandes, N. & Price, B. D. A role for the Tip60 histone acetyltransferase in the acetylation and activation of ATM . **102**, 13182–13187 (2005).

119. Watanabe, S. *et al.* MDC1 methylation mediated by lysine methyltransferases EHMT1 and EHMT2 regulates active ATM accumulation flanking DNA damage sites. *Sci. Rep.* **8**, 1–10 (2018).

120. Lou, Z. *et al.* MDC1 maintains genomic stability by participating in the amplification of ATM-dependent DNA damage signals. *Mol. Cell* **21**, 187–200 (2006).

121. Nimonkar, A. V. *et al.* BLM-DNA2-RPA-MRN and EXO1-BLM-RPA-MRN constitute two DNA end resection machineries for human DNA break repair. *Genes Dev.* **25**, 350–362 (2011).

122. Ma, C. J., Gibb, B., Kwon, Y., Sung, P. & Greene, E. C. Protein dynamics of

human RPA and RAD51 on ssDNA during assembly and disassembly of the RAD51 filament. *Nucleic Acids Res.* **45**, 749–761 (2016).

123. Hustedt, N. & Durocher, D. The control of DNA repair by the cell cycle. *Nature Cell Biology* **19**, 1–9 (2017).

124. Bétermier, M., Bertrand, P. & Lopez, B. S. Is Non-Homologous End-Joining Really an Inherently Error-Prone Process? *PLoS Genetics* **10**, e1004086 (2014).

125. Mohrin, M. *et al.* Hematopoietic stem cell quiescence promotes error-prone DNA repair and mutagenesis. *Cell Stem Cell* **7**, 174–185 (2010).

126. Lieber, M. R. The Mechanism of Double-Strand DNA Break Repair by the Nonhomologous DNA End-Joining Pathway. *Annu. Rev. Biochem.* **79**, 181–211 (2010).

127. Wyatt, D. W. *et al.* Essential Roles for Polymerase θ-Mediated End Joining in the Repair of Chromosome Breaks. *Mol. Cell* **63**, 662–673 (2016).

128. Mateos-Gomez, P. A. *et al.* Mammalian polymerase θ promotes alternative NHEJ and suppresses recombination. *Nature* **518**, 254–257 (2015).

129. Ceccaldi, R. *et al.* Homologous-recombination-deficient tumours are dependent on Polθ -mediated repair. *Nature* **518**, 258–262 (2015).

130. Bakker, S. T. & Passegué, E. Resilient and resourceful: Genome maintenance strategies in hematopoietic stem cells. *Experimental Hematology* **41**, 915–923 (2013).

131. Reese, J. S., Liu, L. & Gerson, S. L. Repopulating defect of mismatch repair-deficient hematopoietic stem cells. *Blood* **102**, 1626–1633 (2003).

132. Gillet, L. C. J. & Schärer, O. D. Molecular mechanisms of mammalian global genome nucleotide excision repair. *Chemical Reviews* **106**, 253–276 (2006).

133. Friedberg, E., Walker, G., Siede, W. & Wood, R. *DNA repair and mutagenesis*. (ASM Press, 2005).

134. Martín-Pardillos, A. *et al.* Genomic and functional integrity of the hematopoietic system requires tolerance of oxidative DNA lesions. *Blood* **130**, 1523–1534 (2017).

135. Fischer, J. L. *et al.* The Xpc gene markedly affects cell survival in mouse bone marrow. *Mutagenesis* **24**, 309–316 (2009).

136. Di Leonardo, A., Linke, S. P., Clarkin, K. & Wahl, G. M. DNA damage triggers a prolonged p53-dependent G1 arrest and long-term induction of Cip1 in normal human fibroblasts. *Genes Dev.* **8**, 2540–2551 (1994).

137. Nakamura, A. J. *et al.* Both telomeric and non-telomeric DNA damage are determinants of mammalian cellular senescence. *Epigenetics Chromatin* **1**, (2008).

138. Shao, L. *et al.* Total body irradiation causes long-term mouse BM injury via induction of HSC premature senescence in an Ink4a- and Arf-independent manner. *Blood* **123**, 3105–3115 (2014).

139. Cuadrado, M. *et al.* ATM regulates ATR chromatin loading in response to DNA double-strand breaks. *J. Exp. Med.* **203**, 297–303 (2006).

140. Jazayeri, A. *et al.* ATM- and cell cycle-dependent regulation of ATR in response to DNA double-strand breaks. *Nat. Cell Biol.* **8**, 37–45 (2006).

141. Matsuoka, S. *et al.* Ataxia telangiectasia-mutated phosphorylates Chk2 in vivo and in vitro. *Proc. Natl. Acad. Sci. U. S. A.* **97**, 10389–10394 (2000).

142. Bartek, J. & Lukas, J. Chk1 and Chk2 kinases in checkpoint control and cancer. *Cancer Cell* **3**, 421–429 (2003).

143. Kastan, M. B. & Bartek, J. Cell-cycle checkpoints and cancer. *Nature* **432**, 316–323 (2004).

144. Reinhardt, H. C. & Yaffe, M. B. Kinases that control the cell cycle in response to DNA damage: Chk1, Chk2, and MK2. *Current Opinion in Cell Biology* **21**, 245–255 (2009).

145. Squire, C. J., Dickson, J. M., Ivanovic, I. & Baker, E. N. Structure and inhibition of the human cell cycle checkpoint kinase, Wee1A kinase: An atypical tyrosine kinase with a key role in CDK1 regulation. *Structure* **13**, 541–550 (2005).

146. Xiao, Z., Xue, J., Sowin, T. J. & Zhang, H. Differential roles of checkpoint kinase 1, checkpoint kinase 2, and mitogen-activated protein kinase-activated protein kinase 2 in mediating DNA damage-induced cell cycle arrest: Implications for cancer therapy. *Mol. Cancer Ther.* **5**, 1935–1943 (2006).

147. Thanasoula, M., Escandell, J. M., Suwaki, N. & Tarsounas, M. ATM/ATR checkpoint activation downregulates CDC25C to prevent mitotic entry with uncapped telomeres. *EMBO J.* **31**, 3398–3410 (2012).

148. Chehab, N. H., Malikzay, A., Appel, M. & Halazonetis, T. D. Chk2/hCds1 functions as a DNA damage checkpoint in G1 by stabilizing p53. *Genes Dev.* **14**, 278–288 (2000).

149. Vousden, K. H. & Prives, C. Blinded by the Light: The Growing Complexity of p53. *Cell* **137**, 413–431 (2009).

150. Senturk, E. & Manfredi, J. J. p53 and Cell Cycle Effects After DNA Damage. in

Methods in molecular biology (Clifton, N.J.) **962**, 49–61 (NIH Public Access, 2013).

151. Agarwal, M. L., Agarwal, A., Taylor, W. R. & Stark, G. R. p53 controls both the G2/M and the G1 cell cycle checkpoints and mediates reversible growth arrest in human fibroblasts. *Proc. Natl. Acad. Sci. U. S. A.* **92**, 8493–8497 (1995).

152. Flatt, P. M., Tang, L. J., Scatena, C. D., Szak, S. T. & Pietenpol, J. A. p53 Regulation of G2 Checkpoint Is Retinoblastoma Protein Dependent. *Mol. Cell. Biol.* **20**, 4210–4223 (2000).

153. Taylor, W. R. *et al.* Mechanisms of G2 arrest in response to overexpression of p53. *Mol. Biol. Cell* **10**, 3607–3622 (1999).

154. Bunz, F. *et al.* Requirement for p53 and p21 to sustain G2 arrest after DNA damage. *Science (80-.).* **282**, 1497–1501 (1998).

155. Chan, T. A., Hermeking, H., Lengauer, C., Kinzler, K. W. & Vogelstein, B. 14-3-3σ is required to prevent mitotic catastrophe after DNA damage. *Nature* **401**, 616–620 (1999).

156. Kastan, M. B. *et al.* A mammalian cell cycle checkpoint pathway utilizing p53 and GADD45 is defective in ataxia-telangiectasia. *Cell* **71**, 587–597 (1992).

157. Doulatov, S., Notta, F., Laurenti, E. & Dick, J. E. Hematopoiesis: A human perspective. *Cell Stem Cell* **10**, 120–136 (2012).

158. Wilson, A. *et al.* Hematopoietic Stem Cells Reversibly Switch from Dormancy to Self-Renewal during Homeostasis and Repair. *Cell* **135**, 1118–1129 (2008).

159. Ishikawa, E. T. *et al.* Connexin-43 prevents hematopoietic stem cell senescence through transfer of reactive oxygen species to bone marrow stromal cells. *Proc. Natl. Acad. Sci. U. S. A.* **109**, 9071–9076 (2012).

160. Wang, J. *et al.* A differentiation checkpoint limits hematopoietic stem cell self-renewal in response to DNA damage. *Cell* **148**, 1001–1014 (2012).

161. Akala, O. O. *et al.* Long-term haematopoietic reconstitution by Trp53-/-p16 Ink4a-/-p19Arf-/- multipotent progenitors. *Nature* **453**, 228–232 (2008).

162. Moehrle, B. M. *et al.* Stem Cell-Specific Mechanisms Ensure Genomic Fidelity within HSCs and upon Aging of HSCs. *Cell Rep.* **13**, 2412–2424 (2015).

163. Beerman, I., Seita, J., Inlay, M. A., Weissman, I. L. & Rossi, D. J. Quiescent hematopoietic stem cells accumulate DNA damage during aging that is repaired upon entry into cell cycle. *Cell Stem Cell* **15**, 37–50 (2014).

164. Rübe, C. E. *et al.* Accumulation of DNA damage in hematopoietic stem and

progenitor cells during human aging. *PLoS One* **6**, (2011).

165. Meijne, E. I. *et al.* The effects of x-irradiation on hematopoietic stem cell compartments in the mouse. *Exp. Hematol.* **19**, 617–23 (1991).

166. Marusyk, A., Porter, C. C., Zaberezhnyy, V. & DeGregori, J. Irradiation selects for p53-deficient hematopoietic progenitors. *PLoS Biol.* **8**, e1000324 (2010).

167. Blanpain, C., Mohrin, M., Sotiropoulou, P. A. & Passegué, E. DNA-damage response in tissue-specific and cancer stem cells. *Cell Stem Cell* **8**, 16–29 (2011).

168. Bakker, S. T., De Winter, J. P. & Te Riele, H. Learning from a paradox: Recent insights into Fanconi anaemia through studying mouse models. *DMM Disease Models and Mechanisms* **6**, 40–47 (2013).

169. Kottemann, M. C. & Smogorzewska, A. Fanconi anaemia and the repair of Watson and Crick DNA crosslinks. *Nature* **493**, 356–363 (2013).

170. Bender, C. F. *et al.* Cancer predisposition and hematopoietic failure in Rad50S/S mice. *Genes Dev.* **16**, 2237–2251 (2002).

171. Navarro, S. *et al.* Hematopoietic Dysfunction in a Mouse Model for Fanconi Anemia Group D1. *Mol. Ther.* **14**, 525–535 (2006).

172. Rossi, D. J. *et al.* Deficiencies in DNA damage repair limit the function of haematopoietic stem cells with age. *Nature* **447**, 725–729 (2007).

173. Nijnik, A. *et al.* DNA repair is limiting for haematopoietic stem cells during ageing. *Nature* **447**, 686–690 (2007).

174. Biechonski, S., Yassin, M. & Milyavsky, M. DNA-damage response in hematopoietic stem cells: an evolutionary trade-off between blood regeneration and leukemia suppression. *Carcinogenesis* **38**, 367–377 (2017).

175. Rossetto, D., Truman, A. W., Kron, S. J. & Côté, J. Epigenetic modifications in double-strand break DNA damage signaling and repair. *Clinical Cancer Research* **16**, 4543–4552 (2010).

176. Mariotti, L. G. *et al.* Use of the γ-H2AX assay to investigate DNA repair dynamics following multiple radiation exposures. *PLoS One* **8**, e79541 (2013).

177. Ayrapetov, M. K., Gursoy-Yuzugullu, O., Xu, C., Xu, Y. & Price, B. D. DNA double-strand breaks promote methylation of histone H3 on lysine 9 and transient formation of repressive chromatin. *Proc. Natl. Acad. Sci. U. S. A.* **111**, 9169–9174 (2014).

178. Fnu, S. *et al.* Methylation of histone H3 lysine 36 enhances DNA repair by nonhomologous end-joining. *Proc. Natl. Acad. Sci. U. S. A.* **108**, 540–545 (2011).

179. Chou, D. M. *et al.* A chromatin localization screen reveals poly (ADP ribose)-regulated recruitment of the repressive polycomb and NuRD complexes to sites of DNA damage. *Proc. Natl. Acad. Sci. U. S. A.* **107**, 18475–18480 (2010).

180. Savic, V. *et al.* Formation of dynamic γ-H2AX domains along broken DNA Strands is distinctly regulated by ATM and MDC1 and dependent upon H2AX densities in chromatin. *Mol. Cell* **34**, 298–310 (2009).

181. Paull, T. T. *et al.* A critical role for histone H2AX in recruitment of repair factors to nuclear foci after DNA damage. *Curr. Biol.* **10**, 886–895 (2000).

182. Celeste, A. *et al.* Genomic instability in mice lacking histone H2AX. *Science (80-.).* **296**, 922–927 (2002).

183. Bassing, C. H. *et al.* Increased ionizing radiation sensitivity and genomic instability in the absence of histone H2AX. *Proc. Natl. Acad. Sci. U. S. A.* **99**, 8173–8178 (2002).

184. Ogiwara, H. *et al.* Histone acetylation by CBP and p300 at double-strand break sites facilitates SWI/SNF chromatin remodeling and the recruitment of non-homologous end joining factors. *Oncogene* **30**, 2135–2146 (2011).

185. Ayoub, N., Jeyasekharan, A. D., Bernal, J. A. & Venkitaraman, A. R. HP1-β mobilization promotes chromatin changes that initiate the DNA damage response. *Nature* **453**, 682–686 (2008).

186. Panier, S. & Boulton, S. J. Double-strand break repair: 53BP1 comes into focus. *Nature Reviews Molecular Cell Biology* **15**, 7–18 (2014).

187. Paquin, K. L. & Howlett, N. G. Understanding the histone DNA repair code: H4K20me2 makes its mark. *Molecular Cancer Research* **16**, 1335–1345 (2018).

188. Huyen, Y. *et al.* Methylated lysine 79 of histone H3 targets 53BP1 to DNA double-strand breaks. *Nature* **432**, 406–411 (2004).

189. Zhang, Y. *et al.* Histone H3K27 methylation is required for NHEJ and genome stability by modulating the dynamics of FANCD2 on chromatin. **131**, 215525 (2018).

190. Bothmer, A. *et al.* Regulation of DNA End Joining, Resection, and Immunoglobulin Class Switch Recombination by 53BP1. *Mol. Cell* **42**, 319–329 (2011).

191. Fradet-Turcotte, A. *et al.* 53BP1 is a reader of the DNA-damage-induced H2A Lys 15 ubiquitin mark. *Nature* **499**, 50–54 (2013).

192. Paquin, K. L. *et al.* FANCD2 Binding to H4K20me2 via a Methyl-Binding Domain Is Essential for Efficient DNA Cross-Link Repair. *Mol. Cell. Biol.* **39**, (2019).

193. Pfister, S. X. *et al.* SETD2-Dependent Histone H3K36 Trimethylation Is Required for Homologous Recombination Repair and Genome Stability. *Cell Rep.* **7**, 2006–2018 (2014).

194. Hsiao, K.-Y. & Mizzen, C. A. Histone H4 deacetylation facilitates 53BP1 DNA damage signaling and double-strand break repair. *J. Mol. Cell Biol.* **5**, 157–65 (2013).

195. Wei, S. *et al.* Histone methylation in DNA repair and clinical practice: New findings during the past 5-years. *Journal of Cancer* **9**, 2072–2081 (2018).

196. Fenske, T. S. *et al.* Identification of candidate alkylator-induced cancer susceptibility genes by whole genome scanning in mice. *Cancer Res.* **66**, 5029–38 (2006).

197. Stoddart, A. *et al.* Haploinsufficiency of del(5q) genes, Egr1 and Apc, cooperate with Tp53 loss to induce acute myeloid leukemia in mice. *Blood* **123**, 1069–1078 (2014).

198. Aly, M. *et al.* Distinct clinical and biological implications of CUX1 in myeloid neoplasms. *Blood Adv.* **3**, 2164–2178 (2019).

199. Lindsley, R. C. *et al.* Prognostic mutations in myelodysplastic syndrome after stem-cell transplantation. *N. Engl. J. Med.* **376**, 536–547 (2017).

200. Gundry, M. C. *et al.* Highly efficient genome editing of murine and human hematopoietic progenitor cells by CRISPR/Cas9. *Cell Rep.* **17**, 1453–1461 (2016).

201. Brunetti, L., Gundry, M. C., Kitano, A., Nakada, D. & Goodell, M. A. Highly efficient gene disruption of murine and human hematopoietic progenitor cells by CRISPR/Cas9. *J. Vis. Exp.* **2018**, (2018).

202. Doench, J. G. *et al.* Optimized sgRNA design to maximize activity and minimize off-target effects of CRISPR-Cas9. *Nat. Biotechnol.* **34**, 184–191 (2016).

203. Yuan, Z. F. *et al.* pParse: A method for accurate determination of monoisotopic peaks in high-resolution mass spectra. *Proteomics* **12**, 226–235 (2012).

204. MATLAB. 9.7.0.1190202 (R2019b). (2018).

205. Yuan, Z.-F. *et al.* EpiProfile 2.0: A computational platform for processing Epi-proteomics mass spectrometry data. *J. Proteome Res.* **17**, 2533–2541 (2018).

206. Yuan, Z.-F. *et al.* EpiProfile quantifies histone peptides with modifications by extracting retention time and intensity in high-resolution Mass Spectra. *Mol. Cell. Proteomics* **14**, 1696–1707 (2015).

207. Tyanova, S. *et al.* The Perseus computational platform for comprehensive analysis of (prote)omics data. *Nat. Methods* **13**, 731–740 (2016).

208. Li, H. & Durbin, R. Fast and accurate short read alignment with Burrows-Wheeler transform. *Bioinformatics* **25**, 1754–1760 (2009).

209. Li, H. *et al.* The Sequence Alignment/Map format and SAMtools. *Bioinforma. Appl. Note* **25**, 2078–2079 (2009).

210. Zhang, Y. *et al.* Model-based analysis of ChIP-Seq (MACS). *Genome Biol.* **9**, R137 (2008).

211. Stark, R. & Brown, G. DiffBind: Differential binding analysis of ChIP-Seq peak data. (2011).

212. Ramírez, F. *et al.* deepTools2: a next generation web server for deep-sequencing data analysis. *Nucleic Acids Res.* **44**, W160-5 (2016).

213. Li, Q. *et al.* A Syntaxin 1, Gαo, and N-type calcium channel complex at a presynaptic nerve terminal: Analysis by quantitative immunocolocalization. *J. Neurosci.* **24**, 4070–4081 (2004).

214. Bolte, S. & Cordelières, F. P. A guided tour into subcellular colocalization analysis in light microscopy. *J. Microsc.* **224**, 213–232 (2006).

215. Ovesný, M., Křížek, P., Borkovec, J., Švindrych, Z. & Hagen, G. M. ThunderSTORM: a comprehensive ImageJ plug-in for PALM and STORM data analysis and super-resolution imaging. *Bioinformatics* **30**, 2389–2390 (2014).

216. Dobin, A. *et al.* Sequence analysis STAR: ultrafast universal RNA-seq aligner. **29**, 15–21 (2013).

217. Love, M. I., Huber, W. & Anders, S. Moderated estimation of fold change and dispersion for RNA-seq data with DESeq2. *Genome Biol.* **15**, 550 (2014).

218. Edgar, R., Domrachev, M. & Lash, A. E. Gene Expression Omnibus: NCBI gene expression and hybridization array data repository. *Nucleic Acids Res.* **30**, 207–210 (2002).

219. Gyori, B. M., Venkatachalam, G., Thiagarajan, P. S., Hsu, D. & Clement, M. V. OpenComet: An automated tool for comet assay image analysis. *Redox Biol.* **2**, 457–465 (2014).

220. R Core Team. R: A Language and Environment for Statistical Computing. (2019).

221. Kassambara, A. ggpubr: 'ggplot2' Based Publication Ready Plots. (2020).

222. Storey, J. D., Bass, A. J., Dabney, A. & Robinson, D. qvalue: Q-value estimation

for false discovery rate control. (2019).

223. Wickham, H. ggplot2: Elegant Graphics for Data Analysis. (2016).

224. Wilke, C. O. cowplot: Streamlined Plot Theme and Plot Annotations for 'ggplot2'. (2019).

225. Takahashi, K. *et al.* Preleukaemic clonal haemopoiesis and risk of therapy-related myeloid neoplasms: a case-control study. *Lancet Oncol.* **18**, 100–111 (2017).

226. Medeiros, B. C., Othus, M., Fang, M., Roulston, D. & Appelbaum, F. R. Prognostic impact of monosomal karyotype in young adult and elderly acute myeloid leukemia: The Southwest Oncology Group (SWOG) experience. *Blood* **116**, 2224–2228 (2010).

227. Dimitriou, M. *et al.* Perturbed hematopoietic stem and progenitor cell hierarchy in myelodysplastic syndromes patients with monosomy 7 as the sole cytogenetic abnormality. *Oncotarget* **7**, 72685–72698 (2016).

228. Zink, F. *et al.* Clonal hematopoiesis, with and without candidate driver mutations, is common in the elderly. *Blood* **130**, 742–752 (2017).

229. Yoshizato, T. *et al.* Somatic mutations and clonal hematopoiesis in aplastic anemia. *N. Engl. J. Med.* **373**, 35–47 (2015).

230. Seguin, L. *et al.* CUX1 and E2F1 regulate coordinated expression of the mitotic complex genes Ect2, MgcRacGAP, and MKLP1 in S phase. *Mol. Cell. Biol.* **29**, 570–581 (2009).

231. Shankar, S. R. *et al.* G9a, a multipotent regulator of gene expression. *Epigenetics* **8**, 16–22 (2013).

232. Chaturvedi, C. P. *et al.* Maintenance of gene silencing by the coordinate action of the H3K9 methyltransferase G9a/KMT1C and the H3K4 demethylase Jarid1a/KDM5A. *Proc. Natl. Acad. Sci. U. S. A.* **109**, 18845–18850 (2012).

233. Ginjala, V. *et al.* Protein-lysine methyltransferases G9a and GLP1 promote responses to DNA damage. *Sci. Rep.* **7**, 1–12 (2017).

234. Cuozzo, C. *et al.* DNA damage, homology-directed repair, and DNA methylation. *PLoS Genet.* **3**, 1144–1162 (2007).

235. Qin, S. & Parthun, M. R. Histone H3 and the histone acetyltransferase Hat1p contribute to DNA double-strand break repair. *Mol. Cell. Biol.* **22**, 8353–8365 (2002).

236. Giannattasio, M., Lazzaro, F., Plevani, P. & Muzi-Falconi, M. The DNA damage checkpoint response requires histone H2B ubiquitination by Rad6-Bre1 and H3

methylation by Dot1. *J. Biol. Chem.* **280**, 9879–9886 (2005).

237. Sanders, S. L. *et al.* Methylation of histone H4 lysine 20 controls recruitment of Crb2 to sites of DNA damage. *Cell* **119**, 603–614 (2004).

238. Van Attikum, H. & Gasser, S. M. The histone code at DNA breaks: A guide to repair? *Nature Reviews Molecular Cell Biology* **6**, 757–765 (2005).

239. Yang, Q. *et al.* G9a coordinates with the RPA complex to promote DNA damage repair and cell survival. *Proc. Natl. Acad. Sci. U. S. A.* **114**, E6054–E6063 (2017).

240. Liu, F. *et al.* Discovery of an in vivo chemical probe of the lysine methyltransferases G9a and GLP. *J. Med. Chem.* **56**, 8931–8942 (2013).

241. Kondo, Y. *et al.* Downregulation of histone H3 lysine 9 methyltransferase G9a induces centrosome disruption and chromosome instability in cancer cells. *PLoS One* **3**, e2037 (2008).

242. Wu, H. *et al.* Histone methyltransferase G9a contributes to H3K27 methylation in vivo. *Cell Res.* **21**, 365–367 (2011).

243. Tachibana, M., Sugimoto, K., Fukushima, T. & Shinkai, Y. SET domain-containing protein, G9a, is a novel lysine-preferring mammalian histone methyltransferase with hyperactivity and specific selectivity to lysines 9 and 27 of histone H3. *J. Biol. Chem.* **276**, 25309–25317 (2001).

244. Mozzetta, C. *et al.* The Histone H3 Lysine 9 Methyltransferases G9a and GLP Regulate Polycomb Repressive Complex 2-Mediated Gene Silencing. *Mol. Cell* **53**, 277–289 (2014).

245. Curry, E. *et al.* Dual EZH2 and EHMT2 histone methyltransferase inhibition increases biological efficacy in breast cancer cells. *Clin. Epigenetics* **7**, (2015).

246. Bellamy, J. *et al.* Increased Efficacy of Histone Methyltransferase G9a Inhibitors Against MYCN-Amplified Neuroblastoma. *Front. Oncol.* **10**, 818 (2020).

247. Efimova, E. V. *et al.* Linking cancer metabolism to DNA repair and accelerated senescence. *Mol. Cancer Res.* **14**, 173–184 (2016).

248. Xu, Y. *et al.* WERAM: a database of writers, erasers and readers of histone acetylation and methylation in eukaryotes. *Nucleic Acids Res.* **45**, D264–D270 (2017).

249. Lu, Y., Liu, Y. & Yang, C. Evaluating in vitro DNA damage using comet assay. *J. Vis. Exp.* **128**, e56450 (2017).

250. Subramanian, A. *et al.* Gene set enrichment analysis: A knowledge-based approach for interpreting genome-wide expression profiles. *Proc. Natl. Acad. Sci.*

U. S. A. **102**, 15545–15550 (2005).

251. Lu, E. P. *et al.* Caspase-9 is required for normal hematopoietic development and protection from alkylator-induced DNA damage in mice. *Blood* **124**, 3887–95 (2014).

252. Quwailid, M. M. *et al.* A gene-driven ENU-based approach to generating an allelic series in any gene. *Mamm. Genome* **15**, 585–591 (2004).

253. Kogan, S. C. *et al.* Bethesda proposals for classification of nonlymphoid hematopoietic neoplasms in mice. *Blood* **100**, 238–245 (2002).

254. Lee, W. Y., Weinberg, O. K. & Pinkus, G. S. GATA1 is a sensitive and specific nuclear marker for erythroid and megakaryocytic lineages. *Am. J. Clin. Pathol.* **147**, 420–426 (2017).

255. Liu, W. *et al.* Pure erythroid leukemia: A reassessment of the entity using the 2008 World Health Organization classification. *Mod. Pathol.* **24**, 375–383 (2011).

256. Wong, E., Ling, V., Westerman, D., Morgan, S. & Juneja, S. How unique is pure erythroid leukaemia? A retrospective analysis of seven cases and review of the literature. *J. Clin. Pathol.* **68**, 301–305 (2015).

257. Bhatia, S. Genetic variation as a modifier of association between therapeutic exposure and subsequent malignant neoplasms in cancer survivors. *Cancer* **121**, 648–663 (2015).

258. Prokocimer, M., Molchadsky, A. & Rotter, V. Dysfunctional diversity of p53 proteins in adult acute myeloid leukemia: Projections on diagnostic workup and therapy. *Blood* **130**, 699–712 (2017).

259. Barsotti, A. M. *et al.* Epigenetic reprogramming by tumor-derived EZH2 gain-offunction mutations promotes aggressive 3D cell morphologies and enhances melanoma tumor growth. *Oncotarget* **6**, 2928–2938 (2015).

260. Harms, P. W. *et al.* Activating mutations of the oncogene EZH2 in cutaneous melanoma revealed by next generation sequencing. *Hum. Pathol. Case Reports* **1**, 21–28 (2014).

261. Moreau-Gachelin, F. *et al.* Spi-1/PU.1 transgenic mice develop multistep erythroleukemias. *Mol. Cell. Biol.* **16**, 2453–2463 (1996).

262. Friend, C. Cell-free transmission in adult Swiss mice of a disease having the character of a leukemia. *J. Exp. Med.* **105**, 307–318 (1957).

263. Thoene, S. *et al.* The ParaHox gene Cdx4 induces acute erythroid leukemia in mice. *Blood Adv.* **3**, 3729 (2019).

264. Iacobucci, I. *et al.* Genomic subtyping and therapeutic targeting of acute erythroleukemia. *Nat. Genet.* **51**, 694–704 (2019).

265. Wells, A. W. *et al.* Erythroleukaemia in the north of England: a population based study. *J. Clin. Pathol.* **54**, 608–612 (2001).

266. Almeida, A. M. *et al.* Clinical outcomes of 217 patients with acute erythroleukemia according to treatment type and line: A retrospective multinational study. *Int. J. Mol. Sci.* **18**, (2017).

267. Mitsumori, K. *et al.* Rapid induction of uterine tumors with p53 point mutations in heterozygous p53-deficient CBA mice given a single intraperitoneal administration of N-ethyl-N-nitrosourea. *Carcinogenesis* **21**, 1039–1042 (2000).

268. Harvey, M. *et al.* Spontaneous and carcinogen−induced tumorigenesis in p53−deficient mice. *Nat. Genet.* **5**, 225–229 (1993).

269. Stoddart, A. *et al.* Cell intrinsic and extrinsic factors synergize in mice with haploinsufficiency for Tp53, and two human del(5q) genes, Egr1 and Apc. *Blood* **123**, 228–238 (2014).

270. Ashworth, A. A synthetic lethal therapeutic approach: Poly(ADP) ribose polymerase inhibitors for the treatment of cancers deficient in DNA double-strand break repair. *Journal of Clinical Oncology* **26**, 3785–3790 (2008).

271. Agarwal, P. & Jackson, S. P. G9a inhibition potentiates the anti-tumour activity of DNA double-strand break inducing agents by impairing DNA repair independent of p53 status. *Cancer Lett.* **380**, 467–475 (2016).

272. Gruber, C. C. & Walker, G. C. Incomplete base excision repair contributes to cell death from antibiotics and other stresses. *DNA Repair* **71**, 108–117 (2018).

273. Kondo, N., Takahashi, A., Ono, K. & Ohnishi, T. DNA Damage Induced by Alkylating Agents and Repair Pathways. *J. Nucleic Acids* **2010**, 543531 (2010).

274. Park, Y. & Gerson, S. L. DNA repair defects in stem cell function and aging. *Annu. Rev. Med.* **56**, 495–508 (2005).

275. Sedelnikova, O. A. *et al.* Senescing human cells and ageing mice accumulate DNA lesions with unrepairable double-strand breaks. *Nat. Cell Biol.* **6**, 168–170 (2004).

276. Popp, H. D. *et al.* Increase of DNA damage and alteration of the DNA damage response in myelodysplastic syndromes and acute myeloid leukemias. *Leuk. Res.* **57**, 112–118 (2017).

277. Sun, D. *et al.* Epigenomic profiling of young and aged HSCs reveals concerted changes during aging that reinforce self-renewal. *Cell Stem Cell* **14**, 673–688

(2014).

278. Adelman, E. R. *et al.* Aging human hematopoietic stem cells manifest profound epigenetic reprogramming of enhancers that may predispose to leukemia. *Cancer Discov.* **9**, 1080–1101 (2019).

279. Appelbaum, F. R. *et al.* Age and acute myeloid leukemia. *Blood* **107**, 3481–3485 (2006).

280. Campbell, S., Ismail, I. H., Young, L. C., Poirier, G. G. & Hendzel, M. J. Polycomb repressive complex 2 contributes to DNA double-strand break repair. *Cell Cycle* **12**, 2675–2683 (2013).

281. Yan, B. *et al.* Low-frequency TP53 hotspot mutation contributes to chemoresistance through clonal expansion in acute myeloid leukemia. *Leukemia* **34**, 1816–1827 (2020).

282. Bolton, K. L. *et al.* Managing clonal hematopoiesis in patients with solid tumors. *J. Clin. Oncol.* **37**, 7–11 (2019).

283. Javle, M. & Curtin, N. J. The role of PARP in DNA repair and its therapeutic exploitation. *British Journal of Cancer* **105**, 1114–1122 (2011).

284. Bunting, S. F. *et al.* 53BP1 inhibits homologous recombination in brca1-deficient cells by blocking resection of DNA breaks. *Cell* **141**, 243–254 (2010).

285. Bolton, K. L. *et al.* The impact of poly ADP ribose polymerase (PARP) inhibitors on clonal hematopoiesis. *J. Clin. Oncol.* **38**, 1513–1513 (2020).

286. Fernandez-Capetillo, O. *et al.* DNA damage-induced G2-M checkpoint activation by histone H2AX and 53BP1. *Nat. Cell Biol.* **4**, 993–997 (2002).

287. Hollstein, M., Sidransky, D., Vogelstein, B. & Harris, C. C. p53 mutations in human cancers. *Science (80-.).* **253**, 49–53 (1991).

288. Gorgoulis, V. G. *et al.* Activation of the DNA damage checkpoint and genomic instability in human precancerous lesions. *Nature* **434**, 907–913 (2005).

289. Bartkova, J. *et al.* DNA damage response as a candidate anti-cancer barrier in early human tumorigenesis. *Nature* **434**, 864–870 (2005).

290. Schwartz, G. K. & Dickson, M. Development of Cell Cycle Inhibitors for Cancer Therapy. *Curr. Oncol.* **16**, 36 (2009).

291. Maude, S. L. & Enders, G. H. Cdk Inhibition in Human Cells Compromises Chk1 Function and Activates a DNA Damage Response. *Cancer Res.* **65**, (2005).

292. Wu, W. *et al.* Interaction of BARD1 and HP1 is required for BRCA1 retention at

sites of DNA damage. *Cancer Res.* **75**, 1311–1321 (2015).

293. Fritsch, L. *et al.* A Subset of the Histone H3 Lysine 9 Methyltransferases Suv39h1, G9a, GLP, and SETDB1 Participate in a Multimeric Complex. *Mol. Cell* **37**, 46–56 (2010).

294. Peters, A. H. F. M. *et al.* Partitioning and Plasticity of Repressive Histone Methylation States in Mammalian Chromatin. *Mol. Cell* **12**, 1577–1589 (2003).

295. Celik, H. *et al.* JARID2 Functions as a Tumor Suppressor in Myeloid Neoplasms by Repressing Self-Renewal in Hematopoietic Progenitor Cells. *Cancer Cell* **34**, 741-756.e8 (2018).

296. Krivtsov, A. V. *et al.* Cell of origin determines clinically relevant subtypes of MLL-rearranged AML. *Leukemia* **27**, 852–860 (2013).

297. Cozzio, A. *et al.* Similar MLL-associated leukemias arising from self-renewing stem cells and short-lived myeloid progenitors. *Genes Dev.* **17**, 3029–3035 (2003).

298. Krivtsov, A. V. *et al.* Transformation from committed progenitor to leukaemia stem cell initiated by MLL-AF9. *Nature* **442**, 818–822 (2006).

299. Lu, R., Neff, N. F., Quake, S. R. & Weissman, I. L. Tracking single hematopoietic stem cells in vivo using high-throughput sequencing in conjunction with viral genetic barcoding. *Nat. Biotechnol.* **29**, 928–934 (2011).

300. Park, S. J. & Bejar, R. Clonal Hematopoiesis in Aging. *Current Stem Cell Reports* **4**, 209–219 (2018).

301. Chen, S. *et al.* Genotoxic stresses promote clonal expansion of hematopoietic stem cells expressing mutant p53. *Leukemia* **32**, 850–854 (2018).

302. Nazha, A. *et al.* A Personalized Prediction Model for Outcomes after Allogeneic Hematopoietic Cell Transplant in Myelodysplastic Syndromes Patients. *Biol. Blood Marrow Transplant.* **0**, (2020).

303. Duncan, B. K. & Miller, J. H. Mutagenic deamination of cytosine residues in DNA. *Nature* **287**, 560–561 (1980).

304. Rodgers, K. & Mcvey, M. Error-Prone Repair of DNA Double-Strand Breaks. *Journal of Cellular Physiology* **231**, 15–24 (2016).

305. Kunkel, T. A. DNA Replication Fidelity. *Journal of Biological Chemistry* **279**, 16895–16898 (2004).

306. Alexandrov, L. B. *et al.* Signatures of mutational processes in human cancer. *Nature* **500**, 415–421 (2013).

307. Tomasetti, C. & Vogelstein, B. Variation in cancer risk among tissues can be explained by the number of stem cell divisions. *Science (80-.).* **347**, 78–81 (2015).

308. McFarland, C. D., Korolev, K. S., Kryukov, G. V., Sunyaev, S. R. & Mirny, L. A. Impact of deleterious passenger mutations on cancer progression. *Proc. Natl. Acad. Sci. U. S. A.* **110**, 2910–2915 (2013).

309. Baverstock, K., Egloff, B., Pinchera, A., Ruchti, C. & Williams, D. Thyroid cancer after Chernobyl. *Nature* **359**, 21–22 (1992).

310. Conard, R. A., Dobyns, B. M. & Sutow, W. W. Thyroid Neoplasia as Late Effect of Exposure to Radioactive Iodine in Fallout. *JAMA J. Am. Med. Assoc.* **214**, 316–324 (1970).

311. SOCOLOW, E. L., HASHIZUME, A., NERIISHI, S. & NIITANI, R. Thyroid carcinoma in man after exposure to ionizing radiation. A summary of the findings in Hiroshima and Nagasaki. *N. Engl. J. Med.* **268**, 406–410 (1963).

312. Rheingold, S. R., Neugut, A. I. & Meadows, A. T. Therapy-Related Secondary Cancers. (2003).

313. Gilman, A. The initial clinical trial of nitrogen mustard. *Am. J. Surg.* **105**, 574–578 (1963).

314. Higuchi, M. *et al.* Expression of a conditional AML1-ETO oncogene bypasses embryonic lethality and establishes a murine model of human t(8;21) acute myeloid leukemia. *Cancer Cell* **1**, 63–74 (2002).

315. Castilla, L. H. *et al.* The fusion gene Cbfb-MYH11 blocks myeloid differentiation and predisposes mice to acute myelomonocytic leukaemia. *Nature Genetics* **23**, 144–146 (1999).

316. Zhao, B. *et al.* H2AX deficiency is associated with erythroid dysplasia and compromised haematopoietic stem cell function. *Sci. Rep.* **6**, 1–12 (2016).

317. Chung, H. Y. *et al.* Redefining chronic inflammation in aging and age-related diseases: Proposal of the senoinflammation concept. *Aging and Disease* **10**, 367–382 (2019).

318. Zanotto-Filho, A. *et al.* Sorafenib improves alkylating therapy by blocking induced inflammation, invasion and angiogenesis in breast cancer cells. *Cancer Lett.* **425**, 101–115 (2018).